Studies in Models of Onset of Chaos

混沌運動發生之模型的研究

by

LO WAI SHUN

(勞維信)

A Thesis Submitted in Partial Fulfillment

of the Requirements for the Degree of

Master of Philosophy in Physics

The Chinese University of Hong Kong

May 1985

TABLE OF CONTENTS

ACKOWLEDGEMENT

I would like to express my deep gratitude to my supervisors, Dr. K. Young and Dr. K.L. Liu. Their patient guidance and advice are important and essential in preparing this thesis.

ABSTRACT

The various routes to chaos in dynamical systems with few degrees of freedom are reviewed. In particular, the use of renormalization group in the study of onset of chaos is studied. The dependence of the limiting function g(x) on the order of local maximum is studied and the existence of a generalized universal limiting function is proved numerically.

The onset of chaos in limit cycle oscillations is studied in details using autonomous maps driven by an external force with a commensurate integer period (e.g. 3 or 5). Various bifurcation diagrams and power spectra are obtained. There exists a transition from partial entrainment $\longrightarrow$ chaos $\longrightarrow$ full entrainment through a series of period doubling cascade-anticascade. A topological connection between full entrainment and a pre-existing resonant period is observed. The MSS sequence in the parameter space is also observed and the relation to the Farey sequence is investigated.

CHAPTER 1

Introduction

1.1 Chaos and turbulence

Chaos is an active field of scientific research, attracting the attention of many physicists, mathematicians, biologists and ecologists. With the development of more powerful computers, this field will undoubtedly become more and more important and attract more efforts from physicists in this decade.

What is chaos? Roughly speaking, chaos means randomness or irregular motion in systems described by deterministic equations. In classical physics, there are two types of descriptions for physical systems, deterministic and statistical. Celestial mechanics is probably the best example of deterministic descriptions in physics. Laplace is reputed to have said that once the initial conditions of all particles in the universe were given, he could calculate their orbits for any time in the future. However, when physical systems get more and more complicated, it is always easier to use a statistical description, such as the kinetic theory of gases. Furthermore, there are many nonlinear dissipative systems in physics, such as fluids described by the Navier-Stokes equations:

$$\frac{\partial \vec{v}}{\partial t} + (\vec{v}\cdot\vec{\nabla})\vec{v} = -\frac{1}{\rho}\vec{\nabla}P + \frac{\eta}{\rho}\nabla^2\vec{v} \qquad (1.1)$$

where $\vec{v}$ is the velocity field of a fluid. p, η and ρ are the pressure, viscosity and density respectively. These equations, together with appropriate boundary and initial conditions, are deterministic in nature. However, experiments show that patterns of hydrodynamic flow will become more and more erratic under certain conditions. These complicated patterns are usually described statistically.

Consider an obstacle in a stream of fluid. Define the Reynolds number

$$R = \frac{v \ell \rho}{\eta}$$

where ℓ is the characteristic length and v the velocity. R is a dimensionless number and is very important in describing the nature of the flow pattern. The fluid flows in a regular and time-independent pattern for very slow speeds, that is, small R (Fig. 1.1a). For larger speed, there are swirls but the motion is still time-independent (Fig. 1.1b). For still larger velocity, the swirls move downstream and break away to produce time-dependent flow pattern (Fig. 1.1c). As R is increased further, irregular internal swirls are induced. A very complicated velocity field (turbulence) is formed when R is raised further (Fig. 1.1d).

The onset of turbulence has been a long mystery for physicists. It is still unsolved today. The difficulty lies in the presence of many different length scales, large swirls containing smaller swirls down to very small sizes. One may ask whether the onset of turbulence can be described by the Navier-Stokes equations which are obtained from the exact

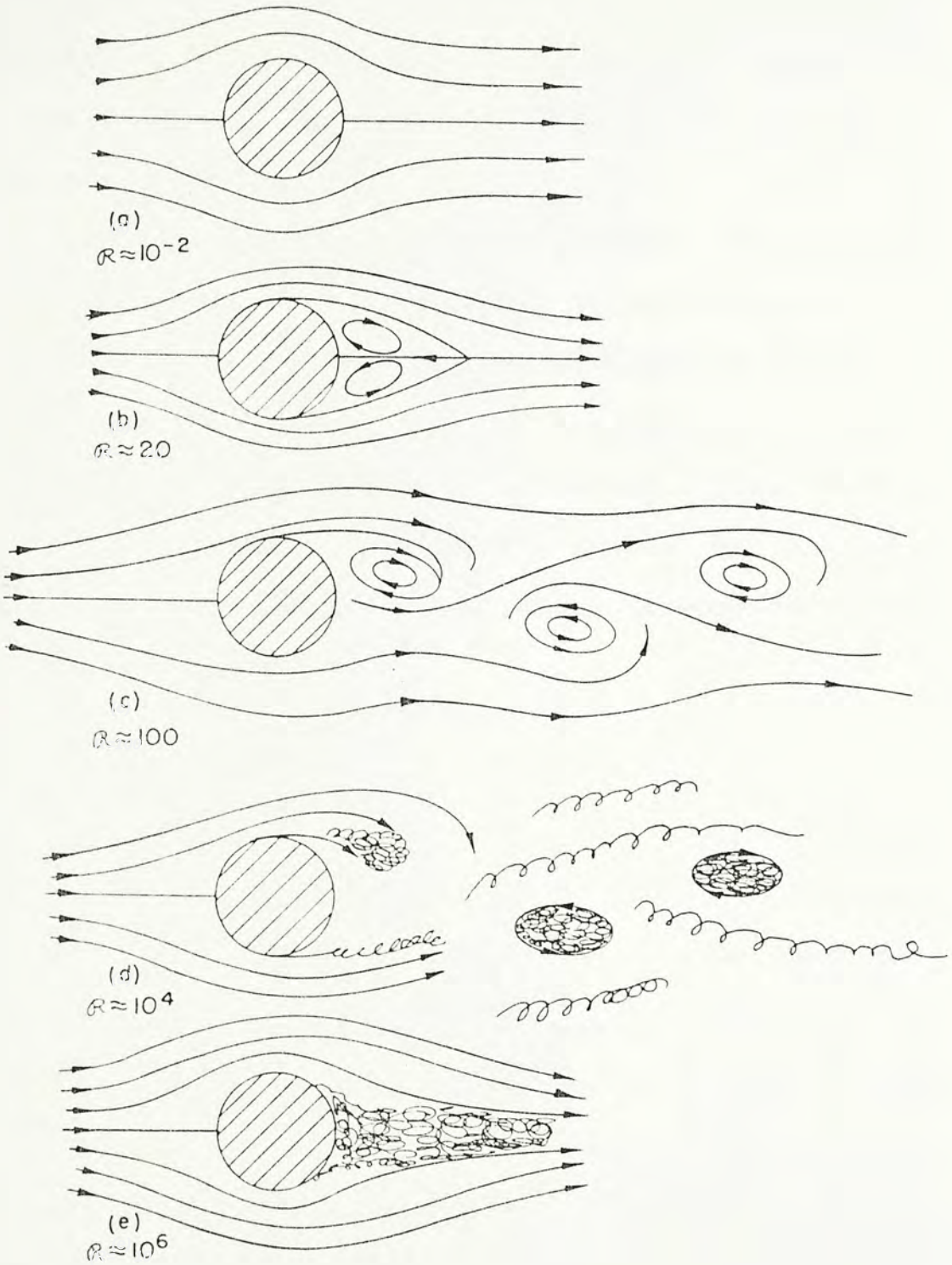

Fig. 1.1 Flow pattern at different Reynolds numbers. a) $R \doteq 10^{-2}$, b) $R \doteq 20$, c) $R \doteq 100$, d) $R \doteq 10^4$, e) $R \doteq 10^6$ (after Feynman, Leighton and Sands (1964), p.41-8)

microscopic equations by a series of truncations, or whether turbulence arises from some features missing from the Navier-Stokes equations.

The Navier-Stokes equations are partial differential equations, hence describe a system with infinite degrees of freedom. They can be transformed into an infinite system of ordinary differential equations by introducing Fourier coefficients for the hydrodynamical variables. This system can further be truncated into a finite system of ordinary differential equations (ODE). The famous Lorenz model is obtained in this fashion:

$$\begin{aligned} \dot{x} &= -\sigma(x-y) \\ \dot{y} &= -xz + rx - y \\ \dot{z} &= xy - bz \end{aligned} \tag{1.2}$$

where σ, r and b are three parameters in the model. It is a typical example of truncating the partial differential equations describing the thermal convection between two infinite plates into a system of ODE with 3 variables. It was found that in certain parameter ranges, the results were very erratic (Lorenz, 1963).

The reduction from systems with many degrees of freedom into systems with only a few degrees of freedom such as the Lorenz model makes numerical calculations on computers much easier. It is justified since dissipation causes the volume of phase space to contract during evolution, hence becoming

low-dimensional. Ordinary differential equations such as the Lorenz model can be further simplified to low-dimensional iterated maps called the Poincare map of the system. The construction of a Poincare map is shown in Fig. 1.2 . It shows a particular orbit of the ODE in the xyz phase space. Choose a section say $y = k$ = constant. Record the points A, B,.... when the orbit hits the plane from above. Since the orbit is deterministic, point A will uniquely determine point B . Thus the points on $y = K$ can be described by a two-dimensional map. It is called the Poincare map of the ODE.

Though some of these mathematical systems appear simple , they exhibit complex patterns of behavior that can serve as models for chaotic phenomena. They might even help us understand the old mystery of turbulence in fluids. This explains why there is a rapid increase of research interest in the study of chaos among physicists.

A more detailed definition of chaos was given by Ott (1981) in the context of a one-dimensioal map

$$x_{n+1} = F(x_n)$$

A bounded sequence generated by F is said to be chaotic if it satisfies the following properties:

(1) there is a sensitive dependence on initial conditions (successive iterates of two close initial points will separte exponentially)

(2) the average correlation function for a given sequence satisfies $c(m) \longrightarrow 0$ as $m \longrightarrow \infty$ where

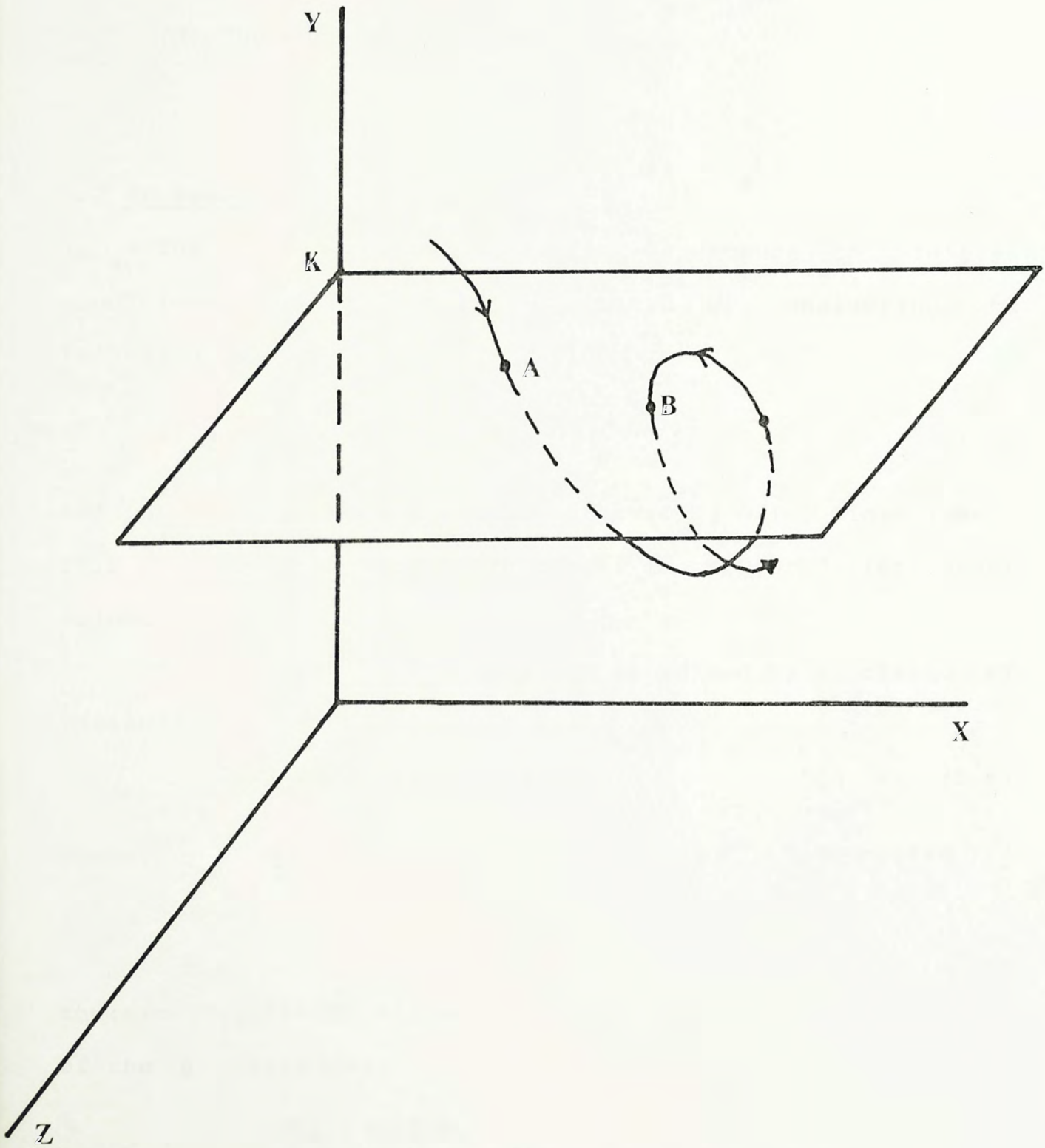

Fig. 1.2 Construction of the Poincare map.

$$c(m) = \lim_{N\to\infty} \frac{1}{N} \sum_{n=1}^{N} (x_n - \langle x \rangle)(x_{n+m} - \langle x \rangle)$$

$$\langle x \rangle = \lim_{N\to\infty} \frac{1}{N} \sum_{n=1}^{N} x_n$$

(3) The sequence is nonperiodic

1.2 An example

The concept of sensitive dependence on initial conditions can be easily illustrated by considering the following map

$$x_{n+1} = \mu x_n (1-x_n) \tag{1.3}$$

for μ =4. It maps the unit interval [0,1] into itself. This map will be studied in detail in chapter 2 for other values of μ .

For μ =4 , the map can be solved by a change of variable

$$x_n = \frac{1}{2}(1-\cos 2\pi\, \theta_n) \tag{1.4}$$

hence, $$\frac{1}{2}(1-\cos 2\pi \theta_{n+1}) = \frac{4}{2}(1-\cos 2\pi\, \theta_n)\frac{1}{2}(1+\cos 2\pi \theta_n)$$

$$= \frac{1}{2}(1-\cos 4\pi\, \theta_n)$$

therefore (1.3) is equivalent to the much simpler iteration of the θ variable:

$$\theta_{n+1} = 2\,\theta_n$$

or $$\theta_n = 2^n \theta_0 \tag{1.5}$$

Given any initial θ_0 , the sequence θ_n can be

calculated uniquely. However, if there is some initial uncertainty $\Delta\theta_0$, then the uncertainty will increase exponentially as $\Delta\theta_n = 2^n \Delta\theta_0$. This uncertainty will eventually fill the phase space (0 to 2π) for any non-zero $\Delta\theta_0$ Hence the 'orbit' of two closely related initial points, θ_0 and $\theta_0+\Delta\theta_0$, will separate exponentially, making prediction impossible in practice. In contrast to this example, consider a case from classical mechanics. Consider a ball moving between two walls separated by a distance ℓ . Suppose all collisions are completely elastic, so that the ball move to and fro between the walls, with constant speed. If the initial speed of the ball has some small uncertainty Δv_0 , then for sufficiently large number of collisions, the uncertainty of the displacement of the ball will increase

$$\Delta x_n = \Delta v_0 \, t_n = \Delta v_0 \, n \, T \qquad (1.6)$$

Here T is the time needed for the ball to move from one wall to the other. In this case the prediction of the position of the ball is difficult for sufficiently long time. But it is not considered to be chaotic since the growth of Δx_n is not exponential in n . There is no sensitive dependence on initial conditions.

1.3 Historical remarks

Although the onset of turbulence has been a long-standing problem in physics, the interest among physicists in

the study of chaos was only aroused during the past few years. The Lorenz model on thermal convection was studied in 1963 (Lorenz , 1963). The solution of the three coupled ordinary differential equations gives irregular fluctuations for some parameter values. This randomness arising from completely deterministic equations was surprising but at that time there was not much attention. In 1971, a new mechanism for the onset of turbulence was proposed by Ruelle and Takens (1971). The term 'strange attractor' was first used for dissipative dynamical systems. In an excellent review, May (1976) discussed period-doubling bifurcations in simple population models in biology. Then came the breakthrough. Scaling law and universal constants were found in one-dimensional mappings (Feigenbaum ,1978). The renormalization group analysis was used in the study of chaos. After this a lot of work was done in this field and many international meetings were organized to discuss this strange behavior---randomness in deterministic systems.

Before ending this introduction, it must be emphasized that chaos is not just complete disorder; there are many regularities and universal properties embedded in chaotic results.

CHAPTER 2

Results of One-dimensional Mapping

2.1 Introduction

The study of one-dimensional mappings contributes a lot to the understanding of transition from periodicity to chaos, especially for period-doubling bifurcations. The nonlinear one-dimensional maps can describe the evolution of a population of insects or the relation between price and quantity of goods in economical models. Moreover, the results of one-dimensional mapping can often be applied to higher dimensional systems because dissipation causes the volume of phase space to contract during evolution, making the phase volume nearly low-dimensional. As a result, universal properties of one-dimensional mapping also occur in higher dimensional systems

2.2 Pitchfork bifurcation and period-doubling route to chaos

2.2.1 Map with one maximum

Consider the logistic mapping

$$f(\mu,x)=\mu x(1-x) \qquad 0<\mu<4 \qquad (2.1)$$

The function maps the interval (0,1) into itself and is the simplest example of maps with one maximum. The function f and its derivative $\frac{df}{dx}$ are continuous and f is monotonic increasing and monotonic decreasing on the two sides of the maximum.

We use the notation f^n to represent the nth iterate of

f:

$$f^n = \underbrace{f \circ f \circ f \ldots\ldots\ldots \circ f}_{n \ f's}$$

The fixed points x^* of f will be important; x^* is a fixed point of f if $f(x^*)=x^*$. For some μ, there may be no fixed point but there exists a set of points which will be visited by all initial points. We call this set an attractor. An attractor may be periodic or chaotic depending on whether the iterates are periodic or not. The basin of attraction is the domain inside which all initial points are attracted to the attractor.

2.2.2 Criterion of stability

A stable fixed point is one which attracts all nearby points, whereas unstable fixed points do not attract all nearby points. The condition of stability can be derived easily. Consider what happens if a point x near the fixed point x^* is iterated. Let

$$x_n = x^* + \varepsilon_n$$

$$x_{n+1} = x^* + \varepsilon_{n+1}$$

where ε_n and ε_{n+1} are small numbers.

Since $$x_{n+1} = f(x_n)$$

$$= f(x^* + \varepsilon_n)$$

$$\doteq f(x^*) + f'(x^*)\varepsilon_n$$

$$\varepsilon_{n+1} \doteq f'(x^*)\,\varepsilon_n$$

or $$\frac{\varepsilon_{n+1}}{\varepsilon_n} \doteq f'(x^*)$$

we have the following criteria:

$$\left|f'(x^*)\right| < 1 \quad , x^* \text{ is stable} \tag{2.2}$$

$$\left|f'(x^*)\right| = 1 \quad , x^* \text{ is marginally stable}$$

$$\left|f'(x^*)\right| > 1 \quad , x^* \text{ is unstable}$$

Suppose there is a 2-cycle

$$x_1 = f(x_2)$$

$$x_2 = f(x_1) = f^2(x_2)$$

This 2-cycle is stable if

$$\left|f^{2\prime}(x_2)\right| < 1$$

or $$\left|f'(x_1)\, f'(x_2)\right| < 1$$

In general, a p-cycle $x_1 \to x_2$, $x_2 \to x_3$, ..., $x_p \to x_1$ is stable if

$$\left|\prod_{j=1}^{p} f'(\mu, x_j)\right| < 1 \tag{2.3}$$

2.2.3 Pitchfork bifurcation

Using these criteria, and a small pocket calculator or a microcomputer, one can discover what happens if the parameter

μ in the difference equation

$$x_{n+1} = f(\mu, x_n) \qquad (2.4)$$

$$= 4\mu x_n(1-x_n)$$

is continuously changed. Solving

$$x = 4\mu x(1-x)$$

gives 2 fixed points

$$x_1^* = 0$$

$$x_2^* = 1 - \frac{1}{4\mu}$$

The derivatives at the fixed points are

$$f'(x_1^*) = 4\mu$$

$$f'(x_2^*) = 2(1-2\mu)$$

Hence the trivial fixed point x_1^* is stable for $0 < \mu < \frac{1}{4}$ and unstable for $\mu > \frac{1}{4}$. However, for $\mu > \frac{1}{4}$, x_2^* is now stable. The fixed point x_2^* becomes marginally stable when $\mu = 3/4$ since $f'(x_2^*) = -1$ at $\mu = 3/4$. As a result, for $\mu > 3/4$, both fixed points x_1^* and x_2^* are unstable. What happens to a typical sequence of iterations for an initial x_o for $\mu > 3/4$? The answer is that there is a stable 2-cycle consisting of two fixed points of f^2. The transition of a p-cycle to a 2p-cycle when the p-cycle is no longer stable is called period-doubling. The condition for such a transition is

$$\prod_{j=1}^{p} f'(\mu, x_j) = -1 \qquad (2.5)$$

This is also called pitchfork bifurcation.

As μ is increased further, the 2-cycle will become unstable and a 4-cycle emerges, which will bifurcate to an 8-cycle for still larger μ . This $1 \longrightarrow 2 \longrightarrow 4 \longrightarrow 8 \longrightarrow \ldots\ldots 2^n \ldots$. bifurcation process will continue until a limit point μ_∞ is reached. Beyond μ_∞ is the chaotic region.

We summarize the periodic windows for the logistic mapping

p=1	$0 < \mu < \mu_1 = 0.75$
p=2	$\mu_1 < \mu < \mu_2 = 0.8623724$
p=4	$\mu_2 < \mu < \mu_3 = 0.8860226$
p=8	$\mu_3 < \mu < \mu_4 = 0.8911018$
.....	.....

$$\mu_\infty = 0.892486417968$$

The region $\mu > \mu_\infty$ is found to be chaotic. There are mainly aperiodic motions with infinite numbers of small periodic windows embedded inside. These periodic motions will undergo period doubling as μ is increased. For example the period 3 will bifurcate to period 6 and period 12 .....

$$3 \longrightarrow 6 \longrightarrow 12 \longrightarrow 24 \rightarrow \ldots\ldots 3.2^n \ldots\ldots \rightarrow \text{chaos}$$

Each of the three branches is similar to the whole bifurcation diagram. This is called self-similarity. For the aperiodic regime, although the iterates are chaotic, they jump between subintervals called islands (I). For μ increases

from μ_∞ to 2, they jump between 2^n I to II. This is called the reversed bifurcation sequence of chaotic bands.

2.3 Universality

2.3.1 Universal ratios

The period-doubling bifurcation process to chaotic region occurs not only in the mapping (2.4). For example, completely similar features occur also in nonlinear mapping

$$x_{n+1} = x_n e^{\mu(1-x_n)} \tag{2.6}$$

or

$$x_{n+1} = \mu \sin(\pi x_n) \qquad x \in (0,1) \tag{2.7}$$

Certain universal properties were found in these mappings. The most important one is that there exist universal ratios , which were first discoversd by Feigenbaum (1978).

Define μ_n to be the parameter value at which the slope of $f^{2^{n-1}}$ is equal to -1, and a 2^{n-1}-cycle bifurcates to a 2^n-cycle. It was found that asymptotically the spacing $\mu_n - \mu_{n-1}$ decreases geometrically, i.e. $\mu_n - \mu_{n-1} \propto \delta^{-n}$, or more practically, the limit

$$\delta = \lim_{n\to\infty} \frac{\mu_n - \mu_{n-1}}{\mu_{n+1} - \mu_n} \tag{2.8}$$

exists and moreover, the limiting value is universal

$$\delta = 4.66920161091....$$

Besides, the separation of adjacent elements of period-doubling attractors in the x direction is asymptotically, reduced by a universal constant $-\alpha$ from one doubling to the

next (Fig. 2.1), i.e.

$$x_{n+1} - x_n \propto (-\alpha)^{-n}$$

Here α = 2.5029078751.... is again universal.

2.3.2 Dependence of δ and α on z

So far the iterations of the mapping

$$x_{n+1} = f(\mu, x_n)$$

$$= 4 \mu x_n (1-x_n)$$

are discussed. This mapping has three properties:

(1) This mapping maps the unit interval [0,1] into itself.

(2) The function f is monotonic increasing when $x < 1/2$ and monotonic decreasing when $x > 1/2$. The maximum is located at $x = 1/2$. This type of mapping is called unimodal.

(3) Near $x = 1/2$, $f(\mu, x) = f_{max} - a(x-x_c)^z + ...$ where $f_{max} = f(\mu, x_c)$, $x_c = 1/2$ and $z=2$.

Examining the mappings

$$x_{n+1} = 1 - \mu x_n^2$$

$$x_{n+1} = x_n e^{\mu(1-x_n)}$$

or $$x_{n+1} = \mu \sin(\pi x_n)$$

when expanding about their maximum points, they all have z=2. Therefore they are all unimodal mappings with quadratic maximum. The values of δ and α obtained by Feigenbaum are

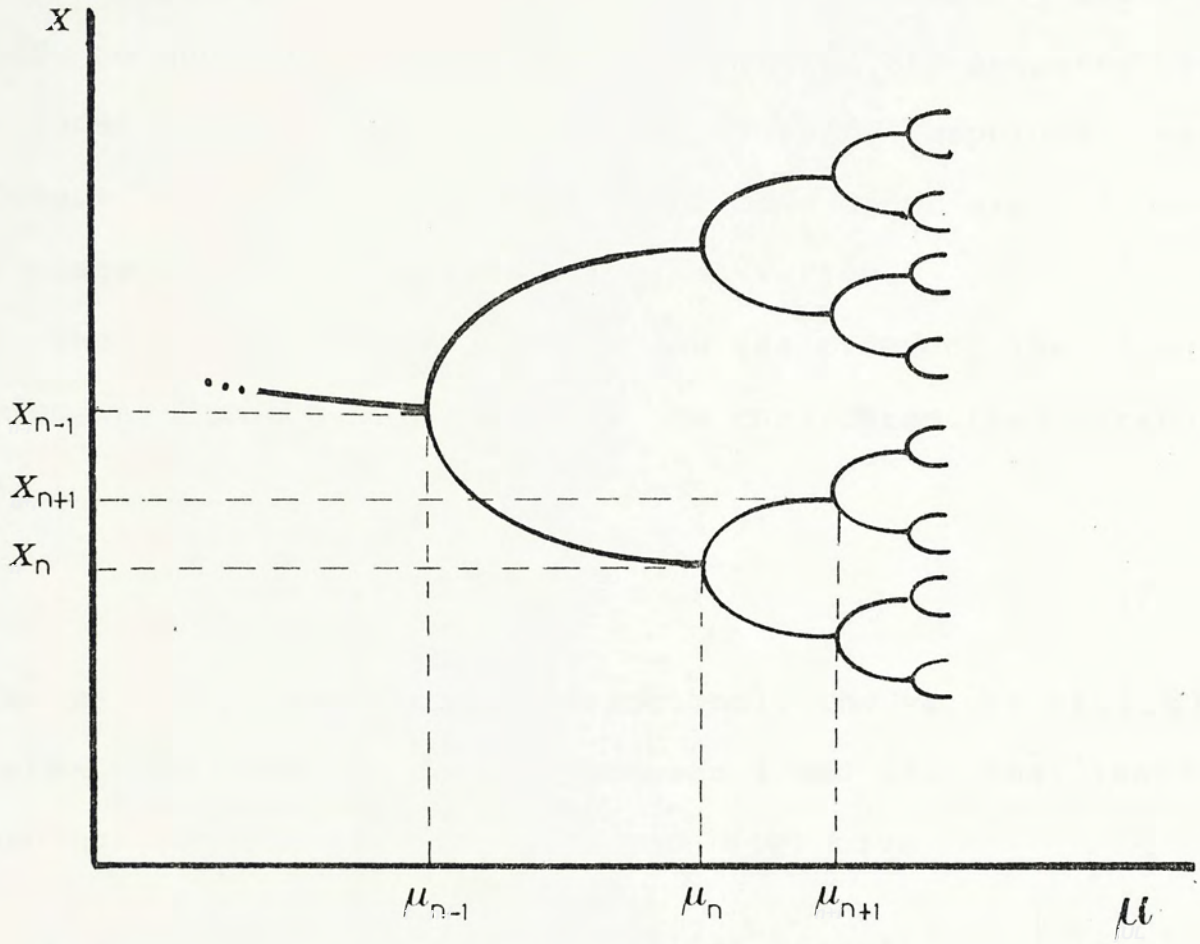

Fig. 2.1 Bifurcation diagram for the map of (2.1)

based on maps with a quadratic maximum. In general, δ and α depend on the order of the local maximum. This property of the local maximum can be used to classify mappings into different classes. Those having the same order are of the same class and have the same universal ratios.

The dependence of δ and α on the order of the local maximum was studied by Hu (1983). He considered the iterated maps

$$f(x)=1-a|x|^{z} \tag{2.9}$$

where z can be even, odd or fractional. The values of $\delta(z)$ and $\alpha(z)$ were computed for z between 1 and 11. The least-squares polynomial fits for $\delta(z)$ and $\alpha(z)$ give

$$\delta = 2.00+4.818(z-1)-3.563(z-1)^{2}+1.95(z-1)^{3}$$
$$-0.621(z-1)^{4}+0.116(z-1)^{5}-0.0127(z-1)^{6}$$

$$\alpha = 1.00+2.309(z-1)^{-1}-1.418(z-1)^{-2}+0.638(z-1)^{-3}$$
$$-0.0761(z-1)^{-4}+.....$$

2.4 MSS sequence

2.4.1 Universal sequence

In the above discussion, the ratios δ and α are universal within certain classes such as those mappings with quadratic maximum. For unimodal mappings with different maximum classes, the values of δ and α are different. However, there are some properties that are universal in the

sense that they are universal for all unimodal mappings, no matter what the orders of the maximum are.

Consider a unimodal mapping $f(\mu, x)$, $x \in I$ where $I = (-1,1)$. It was found that the ordering of stables periods as μ was changed was universal (Metropolis et al., 1973). Take the central point C corresponds to the value of x at which f is maximum. Any value of x can be defined to be right (R) or left (L) depending on whether they are to the right or left of the central point C. Define words K of stable periods by considering the iterations of f and counting the successive iterations by labelling them by R or L. For a super-stable cycle $x_1^* \longrightarrow x_2^* \longrightarrow \ldots \longrightarrow x_p^* \longrightarrow x_1^*$, it corresponds to a word with combination of R and L. For example, there are 3 stable period 5 , taking the following order when μ is increased.

$C \longrightarrow R \longrightarrow L \longrightarrow R \longrightarrow R \longrightarrow C$ denoted as RLR^2

$C \longrightarrow R \longrightarrow L \longrightarrow L \longrightarrow R \longrightarrow C$ denoted as RL^2R

$C \longrightarrow R \longrightarrow L \longrightarrow L \longrightarrow L \longrightarrow C$ denoted as RL^3

It was found that the order of appearence of the words for increasing parameter is universal for a wide class of unimodal maps. Table 2.1 gives all words K for periods less than or equal to 7.

2.4.2 Self-similarity

Word	Period
R	2
RLR	4
RLR^3	6
RLR^4	7
RLR^2	5
RLR^2LR	7
RL	3
RL^2RL	6
RL^2RLR	7
RL^2R	5
RL^2R^3	7
RL^2R^2	6
RL^2R^2L	7
RL^2	4
RL^3RL	7
RL^3R	6
RL^3R^2	7
RL^3	5
RL^4R	7
RL^4	6
RL^5	7

Table 2.1 MSS sequence with period ≤ 7

Although the bifurcation diagram for $\mu > \mu_\infty$ is very complicated, there are certain regular patterns such as the MSS sequence discussed above. More surprisingly, a property of self-similarity was discovered by Derrida et al. (1979). Self-similarity means that the whole bifurcation diagram is similar to some of its parts. This can be easily illustrated by considering the bifurcation diagram of the quadratic map

$$F(x) = 1-ax^2$$

For a between -1/4 and 2, some periodic windows of the MSS sequence are shown in Fig. 2.2a . For a smaller region inside, there is a sequence of same ordering of periodic cycles as the original bifurcation diagram with only here the periodic cycles are doubled (Fig. 2.2b). For another domain of a (Fig. 2.2c) there is a similar sequence of cycles that are three times the original sequence. This important property of scale invariance enables the use of renormalization and scaling in the study of chaos.

2.4.3 Sarkovskii Theorem

This theorem was proved by Sarkovskii(1964). It concerns with the orderings of periodic orbits in unimodal mapping. Consider the following ordering

$$3 \longrightarrow 5 \longrightarrow 7 \longrightarrow 9 \longrightarrow .....3.2 \longrightarrow 5.2 \longrightarrow 7.2 \longrightarrow 9.2 \rightarrow$$

$$..... \longrightarrow 3.2^2 \longrightarrow 5.2^2 \longrightarrow 7.2^2 \longrightarrow 9.2^2 \longrightarrow ..... \longrightarrow 3.2^n \longrightarrow 5.2^n \rightarrow$$

$$7.2^n \longrightarrow 9.2^n \longrightarrow .....2^m \longrightarrow ..... \longrightarrow 32 \longrightarrow 16 \longrightarrow 8 \longrightarrow 4$$

$2 \longrightarrow 1$ (2.10)

For unimodal mapping $F(a,x)$ with a p-cycle, it must have a point leading to a q-cycle for every $q \leftarrow p$ in the definition of the above ordering. This theorem concerns different x at the same parameter a . It does not say anything about the stability of the cycles or the measure in obtaining these cycles. For example, for a just larger than 1.75 in the mapping $F(x) = 1-ax^2$, there is a stable period 3. However, the vertical line at a (Fig. 2.3) also cuts the unstable cycles extending from the left. These include all the ordering in 2.10 . This picture helps to explain the statement ' period 3 implies chaos ' proposed by Li and Yorke (1975).

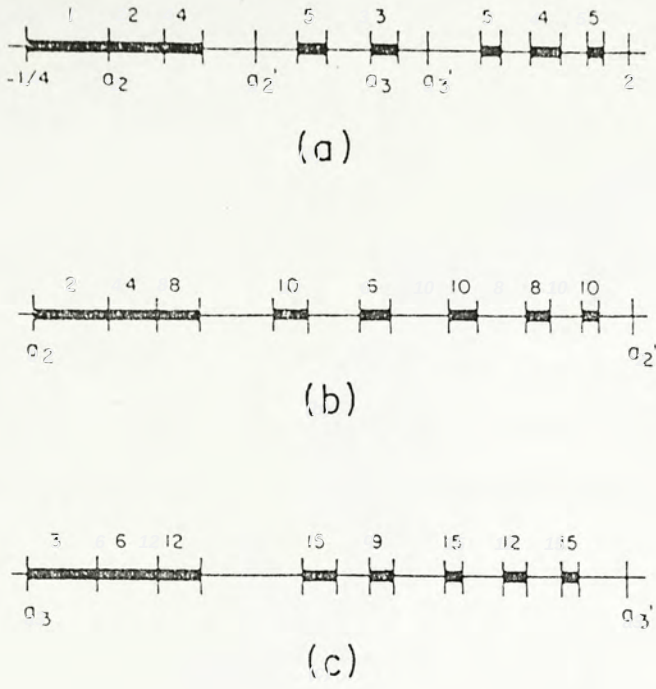

Fig. 2.2 Self-similarity in the bifurcation diagram. The numbers denote the periods. a) $-1/4 < a < 2$, b) $a_2 < a < a_2'$ c) $a_3 < a < a_3'$. (after Hu (1982), p.280)

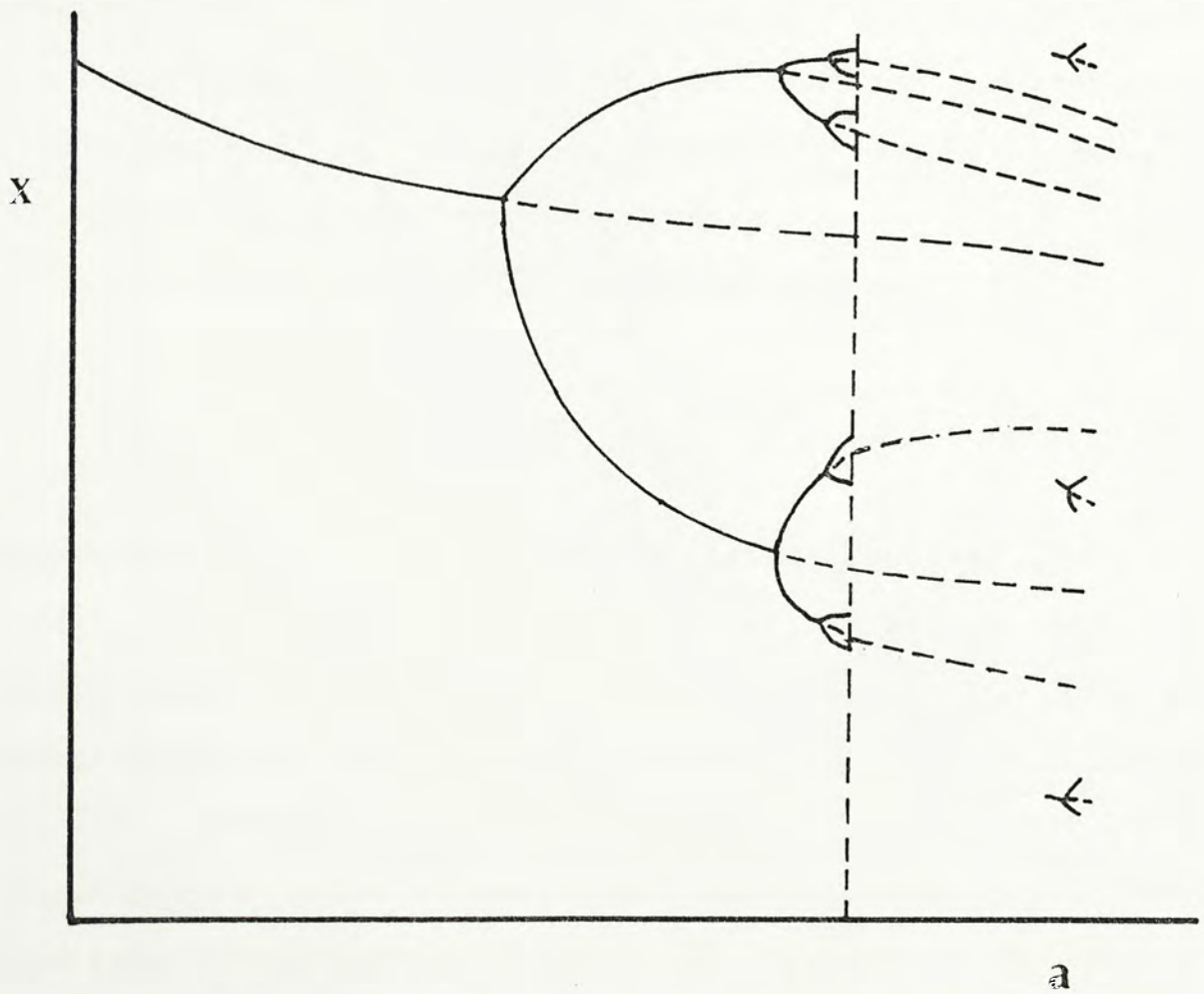

Fig. 2.3 Bifurcation diagram of the map $1-ax^2$ (Schematic). ———— represents stable periods, – – – – – – represents unstable periods.

2.5 One-dimensional maps with multiple basins

2.5.1 Introduction

In the previous sections we have discussed period doubling and chaotic behavior using one-dimensional maps with a single parameter as models. The map such as

$$f(a,x) = 1-ax^2$$

is unimodal. It is a map with one critical point (M1). It was proved by Guckenheimer, Oster and Ipaktchi (1976) that for a first order difference equation with one parameter, the maximum number of periodic attractors is equal to the number of critical points. The sufficient condition for the cycles to be stable, as noted by Singer (1978), is that the Schwarzian derivative must be negative.

The Schwarzian derivative is defined as

$$S\ f(x) = \frac{f'''(x)}{f'(x)} - \frac{3}{2}\left(\frac{f''(x)}{f'(x)}\right)^2 \qquad (2.11)$$

For example, for $f(x) = 1-ax^2$, $f'''(x)$ is equal to zero. Thus $S\ f(x)$ is negative. Therefore, this map has at most one stable periodic attractors. However, $S\ f(x) < 0$ does not imply there must be one stable periodic attractor. There may be no periodic attractor, especially when $a > a_\infty$ (accumulation point of period doubling). As a result, for this type of map with at most one stable periodic attractor, the initial condition is irrelevant. All initial values will be attracted to the attractor. It is well-known that this

type of map undergoes two types of bifurcations, pitchfork and tangent bifurcation(which will be discussed in detail in next chapter). However, for maps with two critical points, there is another bifurcation called split bifurcation. In the following sections, we will discusse some results of one-dimensional maps with multiple basins.

2.5.2 Split bifurcation

Consider the cubic difference equation studied by Testa and Held (1983):

$$x_{n+1} = f(a,x_n) \qquad (2.12)$$

$$= ax_n^3+(1-a)x_n$$

This is a map with two critical points (Fig. 2.4).

Solving $x = ax^3+(1-a)x$

$$ax^3-ax = 0$$

$$x = 0 \quad \text{or} \quad x = \pm 1$$

Hence $x=0$ and $x=\pm 1$ are always fixed points of f. The stability of these fixed points can be obtained by studying

$$\left.\frac{df}{dx}\right|_{x=0} = [3ax^2+(1-a)]_{x=0}$$

$$= 1-a$$

$$\left.\frac{df}{dx}\right|_{x=\pm 1} = 2a+1$$

The condition $\left|\frac{df}{dx}\right| < 1$ implies the fixed points at x=+1 are always unstable. The fixed point at x=0 is stable for $1<a<2$.

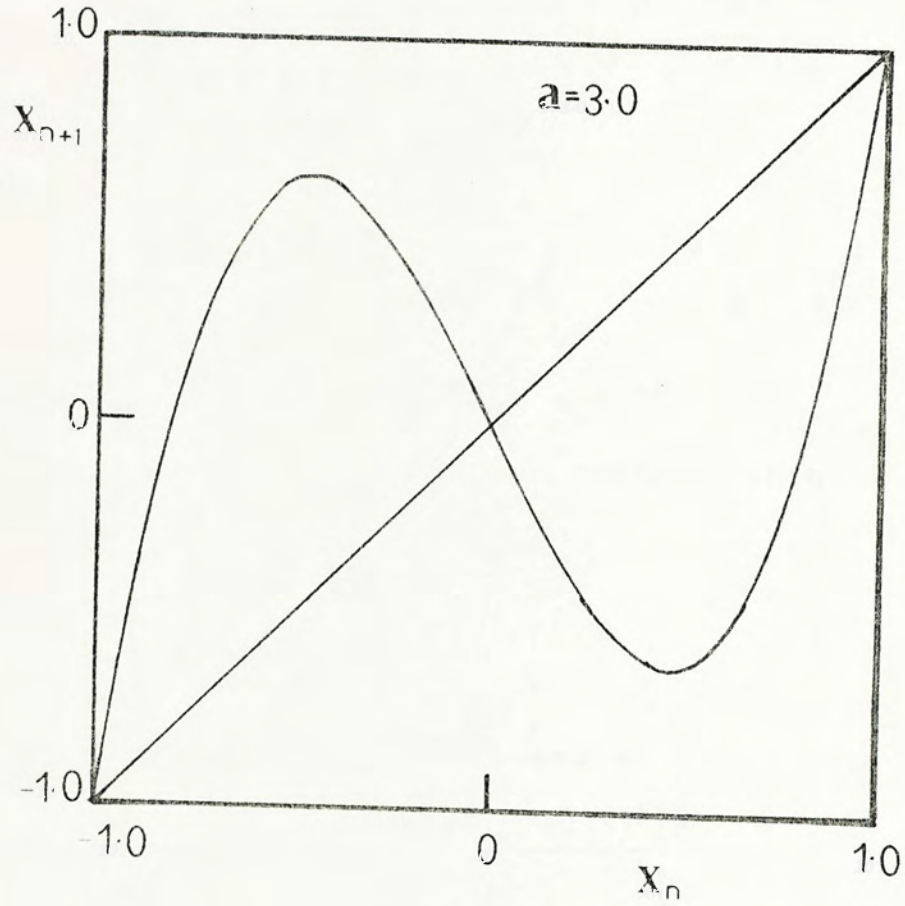

Fig. 2.4 Cubic map of (2.12) with 2 critical points (a = 3.0). (after Testa and Held (1983), p.3085)

At a = 2, a 2-cycle emerges. Due to the antisymmetry of f, the 2-cycle must be $\pm \delta$, satisfying the relation

$$\pm \delta = f(\mp \delta)$$

which gives $\pm \delta = \pm \sqrt{(a-2)/a}$

and $$\left.\frac{d f^2(x)}{dx}\right|_{x=\pm\delta} = (2a-5)^2$$

So this 2-cycle is stable for $2 < a < 3$.

At a=3, a split bifurcation occurs (Fig. 2.5). Four fixed points of f^2 emerge. Solving

$$x = f(f(x))$$

gives the four fixed points $\pm \alpha$ and $\pm \beta$:

$$\pm\alpha = \left[\frac{(a-1) + [(a-1)(a-3)]^{\frac{1}{2}}}{2a}\right]^{\frac{1}{2}}$$

$$\pm\beta = \left[\frac{(a-1) - [(a-1)(a-3)]^{\frac{1}{2}}}{2a}\right]^{\frac{1}{2}}$$

There are two period-2 attractors $(\alpha, -\beta)$ and $(-\alpha, \beta)$. Different initial conditions will be attracted to different 2-cycles. Here 2 fixed points of $f^2(\pm\delta)$ become unstable and 4 stable fixed points of f^2 ($\pm\alpha$, $\pm\beta$) emerge. In general for a split bifurcation, n fixed points of f^n become unstable while 2n stable fixed points of f^n emerge. For pitchfork bifurcation , 2n stable fixed points of f^{2n} emerge. In the bifurcation diagram, a split bifurcation is similar to a pitchfork bifurcation with half of the pitchfork missing (Fig. 2.6)

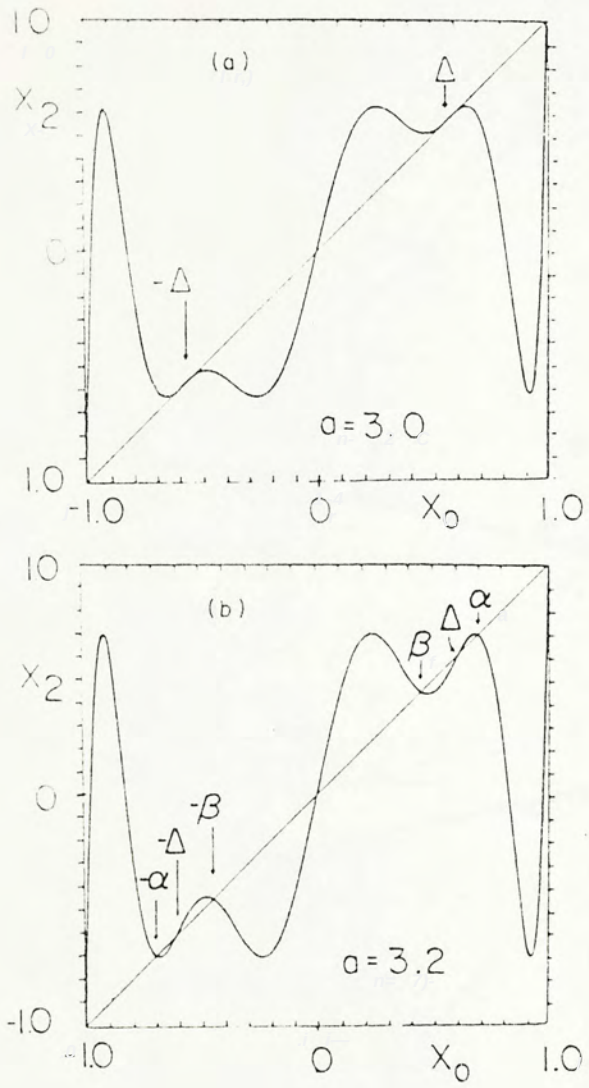

Fig. 2.5 Second iterate of (2.12) showing split bifurcation. a) a = 3.0, b) a = 3.2. (after Testa and Held (1983), p.3086)

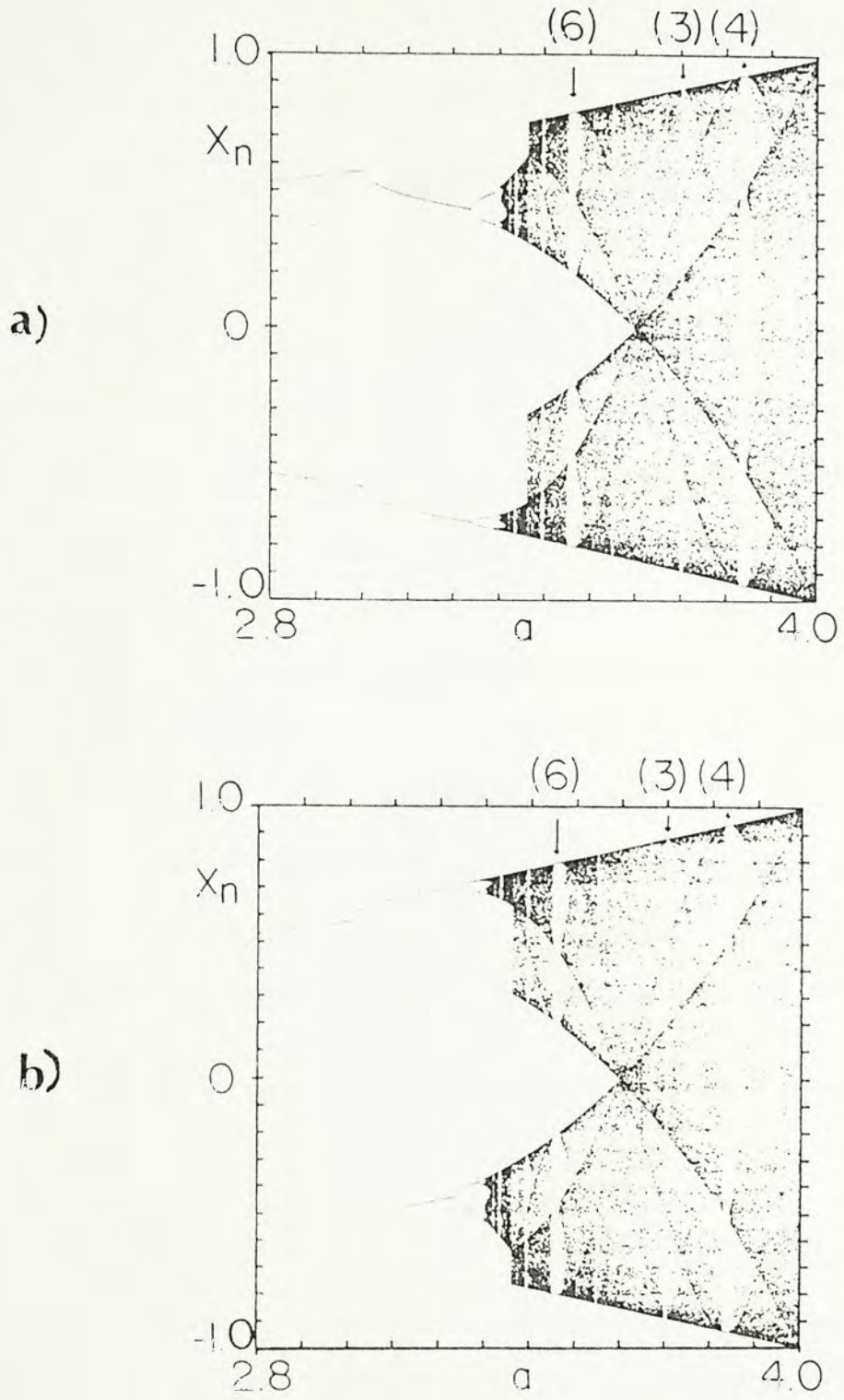

Fig. 2.6 Bifurcation diagram of the map (2.12) for $2.8 < a < 4.0$. a) initial value $x_0=0.5$, b) initial value $x_0=-0.5$ (after Testa and Held (1983), p.3086)

CHAPTER 3

Renormalization group approach

3.1 Introduction

Besides using numerical analysis by computers to solve various nonlinear models, the renormalization group (RG) approach is another important and powerful method in gaining information about the onset of chaos. The RG method was developed in quantum field theory. It found great success in the study of critical phenomena and other physical problems. Basically, the renormalization group is a method to reduce step by step the degrees of freedom in a physical system, without compromising the underlying physics. There are many analogies between critical and chaotic phenomena, and the similarity between them leads one to use RG in the study of chaos.

3.2 Functional RG equation

The important property of self-similarity in the bifurcation diagram makes the RG a useful method in the study of chaos. The two constants in period-doubling, δ and α, which measure the rate of bifurcation and amount of rescaling, are universal and depend only on the order of the local maximum of unimodal maps. To understand these numbers, a functional RG equation was developed by Feigenbaum (1978,1979).

Consider one-dimensional mappings $x \longrightarrow f(\lambda, x)$. Let λ_∞ be the accumulation point for the period doublings and

X_∞ maximizes $f(\lambda_\infty, x)$. Then it was shown that

(a) $\lim_{p\to\infty} (-\alpha)^p \left[f^{2^p}\left(\lambda_\infty, X_\infty + \frac{y}{(-\alpha)^p} \right) - X_\infty \right] = g(y)$

(b) $g(y)$ is universal up to scaling, and

(c) $g(y)$ satisfies the renormalization group equation

$$g(g(-y/\alpha)) = -\frac{1}{\alpha} g(y) \tag{3.1}$$

This functional equation can be obtained by a simple derivation. Assuming that at λ_∞, iteration is accompanied by a reduction by a factor $-\alpha$ in the x-direction. Near the accumalation point i.e. for large n, assume $g(x)$ is given by

$$f^{2^n}(x) = (-\alpha)^{-n}\, g((-\alpha)^n x)$$

$$f^{2^n} \circ f^{2^n} = (-\alpha)^{-n}\, g[(-\alpha)^n (-\alpha)^{-n}\, g((-\alpha)^n x)]$$

$$f^{2^{n+1}}(x) = (-\alpha)^{-(n+1)}\, g((-\alpha)^{n+1} x)$$

Equating the terms, $g(g(x)) = -\frac{1}{\alpha} g(-\alpha x)$

or $$g(x) = -\alpha\, g(g(-x/\alpha))$$

Define an operator T such that for a given function $G(x)$

$$T\,G(x) = -\alpha\, G(G(-x/\alpha)) \tag{3.2}$$

It is obvious that $g(x)$ is a fixed point function of the operator T, that is,

$$T\,g(x) = g(x)$$

and applying T to $f(x)$ gives

$$T\,f(x) = -\alpha\, f(f(-x/\alpha)) = -\alpha\, f^2(-x/\alpha)$$

$$T^2 f(x) = (-\alpha)^2 f^{2^2}(x/(-\alpha)^2)$$

$$T^n f(x) = (-\alpha)^n f^{2^n}(x/(-\alpha)^n)$$

so that at $\lambda = \lambda_\infty$, $\lim_{n\to\infty} T^n f(x) \longrightarrow g(x)$

If we linearize around the fixed point function, let

$$g_\epsilon(x) = g(x) + \epsilon\, h(x) \tag{3.3}$$

then
$$g_\epsilon(g_\epsilon(x)) = g_\epsilon(g(x)+\epsilon\, h(x))$$

$$= g(g(x)+\epsilon\, h(x)) + \epsilon h(g(x)+\epsilon\, h(x))$$

$$= g(g(x)) + \epsilon\,[g'(g(x))h(x)+h(g(x))]$$

Hence, the eigenfunction $h(x)$ satisfy

$$g'(g(x))h(x) + h(g(x)) = -(\lambda_\epsilon/\alpha)\, h(\alpha x) \tag{3.4}$$

Functional RG equations (3.1) and (3.4) are the basis for universality theory of period doubling.

3.3 Simple calculation of α and g

In solving $g(g(x)) = -\frac{1}{\alpha} g(-\alpha x)$, one can obtain both α and g. However, no exact solution for this functional equation is found. Nevertheless, it is well-known that polynomial approximation is a common method to find $g(x)$ and α. We here show the first two lowest order approximation calculation.

Let $g(x) = 1-ax^2$

where a is a constant. Put this form into the functional equation and keep only quadratic terms.

$$g(g(x)) = 1-a(1-ax^2)^2$$

$$\doteq 1-a(1-2ax^2)$$

$$= (1-a) + 2a^2x^2$$

Also, $$-\frac{1}{\alpha}\, g(-\alpha x) = -\frac{1}{\alpha}(1-a(-\alpha x)^2)$$

$$= -\frac{1}{\alpha} + a\alpha x^2$$

Therefore we have,

$$1-a = -\frac{1}{\alpha}$$

$$2a^2 = a\alpha \qquad (3.5)$$

Solving the two equations gives the two unknowns

$$a = (1+\sqrt{3})/2 = 1.366$$

$$\alpha = 1+\sqrt{3} = 2.733$$

Comparing with exact value of α (=2.503), the result is not bad for low-order approximation. The result will be improved for higher order approximation.

For $g(x) = 1-ax^2+bx^4$ with a and b constants. Keeping x^4 terms only, we have

$$g(g(x)) = (1-a+b) + (2a^2-4ab)x^2 + (4b^2+6a^2b-2ab-a^3)x^4$$

$$-\frac{1}{\alpha}\, g(-\alpha x) = -\frac{1}{\alpha} + a\alpha x^2 - b\alpha^3 x^4$$

Comparing the terms, we have

$$1-a+b = -\frac{1}{\alpha}$$

$$2a-4b = \alpha \tag{3.6}$$

$$4b^2+6a^2b-2ab-a^3 = -b\alpha^3$$

So we have a system of three nonlinear algebrac equations with three unknowns α , a and b . It is difficult to obtain exact solution to this system of equation. Instead, we use the method of iteration. Rewrite the equations in the form

$$\alpha = 2(1+\frac{1}{\alpha} -b)$$

$$a = \frac{\alpha}{2} + 2b$$

$$b = \frac{a^3 - 4b^2}{6a^2 - 2a + \alpha^3}$$

Using the results of previous order as initial values

$$\alpha_o = 2.732$$

$$a_o = 1.366$$

$$b_o = 0$$

The computer quickly gives the convergent results for this order

$$\alpha = 2.53403$$

$$a = 1.522242$$

$$b = 0.127613$$

The value of α obtained is nearer to the exact value. It is believed that higher order will give better results.

3.4 Simple renormalization calculation of δ

The value of α can be obtained by polynomial approximation as described above. For δ, we can calculate its value by a simple renormalization group calculation. The basic idea of this RG calculation is due to Derrida et al.(1979). Their idea is that the 2nth iterated map at a value a' is similar in shape to the nth iterated map at another parameter a. In particular, equate the slope of the n periods $s_n(a)$ to that of 2n periods $s_{2n}(a')$

$$s_n(a) = s_{2n}(a') \tag{3.7}$$

The fixed point of this recursive relation gives the accumulation point of bifurcation.

$$s_n(a_\infty) = s_{2n}(a_\infty) \tag{3.8}$$

and $$\delta = \left.\frac{\partial a}{\partial a'}\right|_{a_\infty}$$

Consider $f(a,x) = 1-ax^2$

Solving $x = 1-ax^2$ gives the 1-cycle

$$x^* = \frac{-1+\sqrt{1+4a}}{2a} \tag{3.9}$$

$$s_1(a) = -2ax^* = 1-\sqrt{1+4a} \tag{3.10}$$

The 2-cycle is given by

$$x_1^* = \frac{1+\sqrt{4a-3}}{2a}$$

$$x_2^* = \frac{1-\sqrt{4a-3}}{2a} \qquad (3.11)$$

and $$s_2(a) = (-2ax_1^*)(-2ax_2^*)$$

$$= (1+\sqrt{4a-3})(1-\sqrt{4a-3})$$

$$= 4(1-a)$$

For lowest order approximation, set

$$s_1(a_\infty) = s_2(a_\infty)$$

$$1-\sqrt{1+4a_\infty} = 4(1-a_\infty)$$

$$a_\infty = (7+\sqrt{17})/8 = 1.3903882$$

$$\delta = \left.\frac{2a}{2a'}\right|_{a_\infty}$$

Since $$s_n(a) = -1$$

$$s_n(a') = -1$$

$$1+\sqrt{1+4a} = 4(1-a') = -1$$

$$\left.\frac{2a}{2a'}\right|_{a_\infty} = 2\sqrt{1+4a_\infty}$$

Therefore, $$\delta = 2\sqrt{1+4(1.3903882)}$$

$$= 5.1224575$$

The accumulation point of period doublings and bifurcation ratio are determined simultaneously. The result is not bad as a first order approximation. Using this RG method, the

universal bifurcation ratio was calculated to third-order by Hu and Mao (1982). Their results agree very well with exact values (Table 3.1)

3.5 Dependence of g on the order of local maximum

3.5.1 Introduction

Suppose a family of maps $f(\lambda, x)$, where λ is a control parameter, undergoes a sequence of pitchfork bifurcation accumulating at $\lambda = \lambda_\infty$. It is well-known that the iterates $f^{2^p}(\lambda_\infty, x)$, suitably scaled in the x-direction by a factor $-\alpha$, defines a universal function ψ satisfying

$$\psi \circ \psi\left(\frac{x}{\alpha}\right) = -\frac{1}{\alpha}\psi(x) \qquad (3.12)$$

It is believed that both α and ψ are determined uniquely, up to scaling in ψ, by the order of maximun of f. However, we have found that this is not always the case and there exist some exceptions. This point can be elaborated as follows.

First let us restrict attention to the class of functions of power series in x with maximun at x=o.

$$P = \{ f : f \text{ is a power series in } x \}$$

A subset T of P is said to be invariant if $f \in T \Rightarrow f \circ f \in T$. The following subset is of special interest.

$$T_n = \{ f : f = \text{power series in } x^n \}$$

We give some examples to T_2 and T_6

Order	a_∞	δ
1	1.3903882	5.1224575
2	1.4014203	4.6141828
3	1.4011487	4.6753244
exact	1.4011552	4.6692011

Table 3.1 RG calculation of δ by Hu and Mao

$$T_2 : \quad 1-\lambda x^2, \quad (1-\lambda x^2)^3$$

$$T_6 : \quad 1-\lambda x^6, \quad 1-\lambda(x^6+x^{12}+x^{18})$$

Since these subsets are invariant it is obvious that if we start with a function in some T, then the limiting function is again in T.

Let $f(x) \in T_6$, define $\tilde{f}(x) \in T_2$ by

$$\tilde{f}(x) = f(x^{\frac{1}{3}})^3 \tag{3.13}$$

here the principal root is to be taken. The tranformation M

$$f \xrightarrow{M} \tilde{f} \tag{3.14}$$

is preserved under composition. If

$$f \circ g = k$$

then
$$\begin{aligned}\tilde{k}(x) &= k(x^{\frac{1}{3}})^3 \\ &= [\, f(g(x^{\frac{1}{3}}))\,]^3 \\ &= [\, f(\tilde{g}(x)^{\frac{1}{3}})\,]^3 \\ &= \tilde{f}(\tilde{g}(x))\end{aligned}$$

In particular $\tilde{f}^{3^p} = \tilde{f}^{3^p}$, and the following commuting diagram is obtained.

$$\begin{array}{lcc} T_6 & f = 1-\lambda x^6 & \xrightarrow{\text{limiting function}} \quad g_6 \\ & \Big\downarrow M & \qquad\qquad\qquad\qquad \Big\downarrow M \\ T_2 & \tilde{f} = (1-\lambda x^2)^3 & \xrightarrow{\text{limiting function}} \quad h \end{array}$$

Let $$g_6(x) \xrightarrow{M} h(x) \tag{3.15}$$

Since g_6 satisfies

$$g_6(g_6(x/\alpha_6) = -\frac{1}{\alpha_6} g_6(x) \tag{3.16}$$

where $\alpha_6 = 1.468$, it follows that

$$h(h(x/\alpha_6^3)) = -\frac{1}{\alpha_6^3} h(x) \tag{3.17}$$

Thus we have found a function h which has the following properties:

(1) It satisfies the RG relation ($\alpha' = \alpha_6^3 = 3.163 \neq 2.503$)

(2) It has a quadratic maximum because

$$\begin{aligned} h(x) &= g_6(x^{\frac{1}{3}})^3 \\ &= [\text{ power series in } (x^{\frac{1}{3}})^6]^3 \\ &= [\text{ power series in } x^2]^3 \\ &= \text{power series in } x^2 \end{aligned}$$

This would seem to contradict the claim that for all functions h which satisfy (1) and (2)

(a) α' should be equal to 2.503

(b) h should be related to g_2 by a scale tranformation.

However, it is found that neither is the case. Since the limiting function of $\tilde{f} = (1-\lambda x^2)^3$ is equal to h. Let us

examine $\tilde{f}$ more carefully.

3.5.2 Properties of a special map

It is found numerically that for $\tilde{f} = (1-\lambda x^2)^3$ that

(1) The maximum at x=o of this function is quadratic, but there are 2 other points of zero slope at the two sides of the maximum (Fig. 3.1). In other words, the function does not satisfy condition on the Schwarzian derivative

$$S\ f(x) = \frac{f'''(x)}{f'(x)} - \frac{3}{2}\left[\frac{f''(x)}{f'(x)}\right]^2 < 0$$

(2) The accumulation point of period doubling =1.68326019820 46

(3) The rate of bifurcation δ = 9.296543

(4) α for the 'central down' sequence (Fig 3.2a) = -3.162 = $(-1.468)^3$

(5) α for the 'central up' sequence (Fig. 3.2b) =-1.468

The value of λ_∞ and δ are the same as that of $1-\lambda x^6$. There are 2 different values of α, one for the 'central up' sequence and one for the 'central down' sequence. In calculating the limiting function

$$h(x) = \lim_{p\to\infty} (-\beta)^p \left[\tilde{f}^{2^p}(\lambda_\infty, x/(-\beta)^p)\right] \qquad (3.18)$$

β is taken the value of α for the 'central down' sequence, that is, α_c^3. If we take β equal to α for the 'central up' sequence, the limit does not exist. Fig. 3.3 shows the graph of limiting function h(x) and $g_2(x)$. Both are scaled to 1 at x=0.

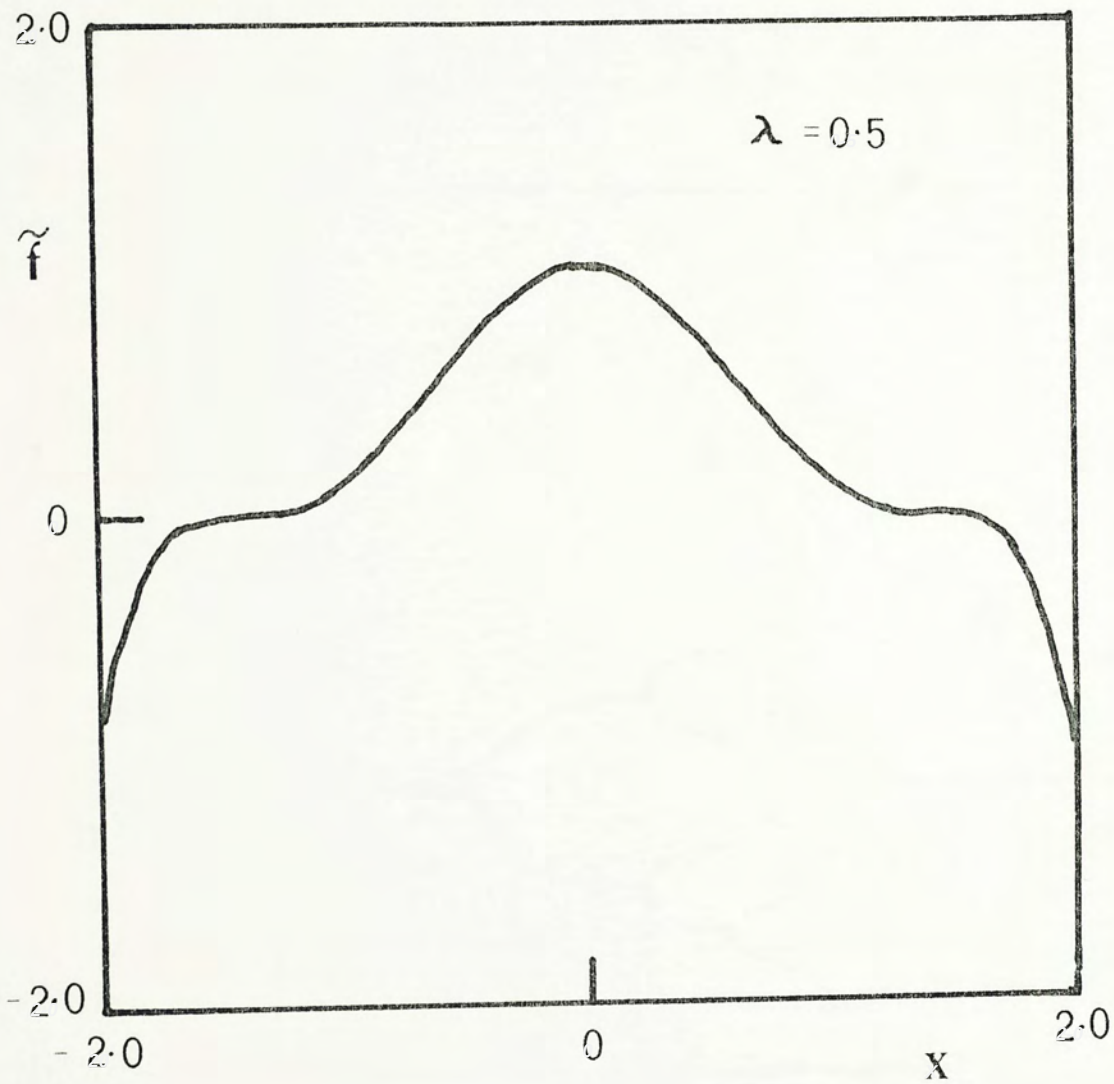

Fig. 3.1 Graph of the function $\tilde{f} = (1-\lambda x^2)^3$ for $\lambda = 0{\cdot}5$.

a)

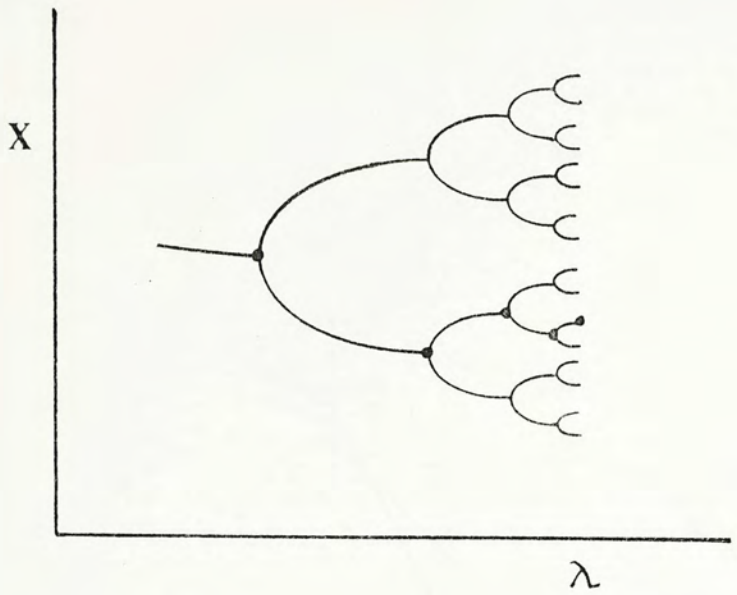

b)

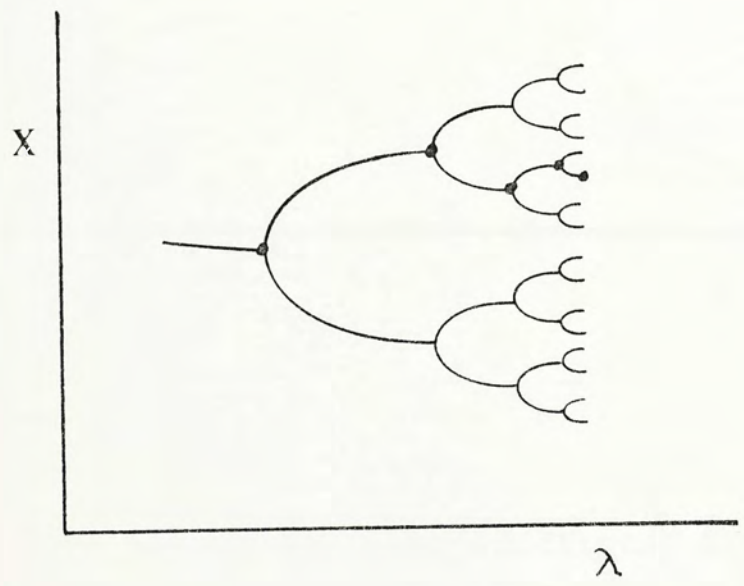

Fig. 3.2.3 Schematic bifurcation diagram for the map $\tilde{f} = (1-\lambda x^2)^3$. The heavy dots show a) the central down sequence, b) the central up sequence.

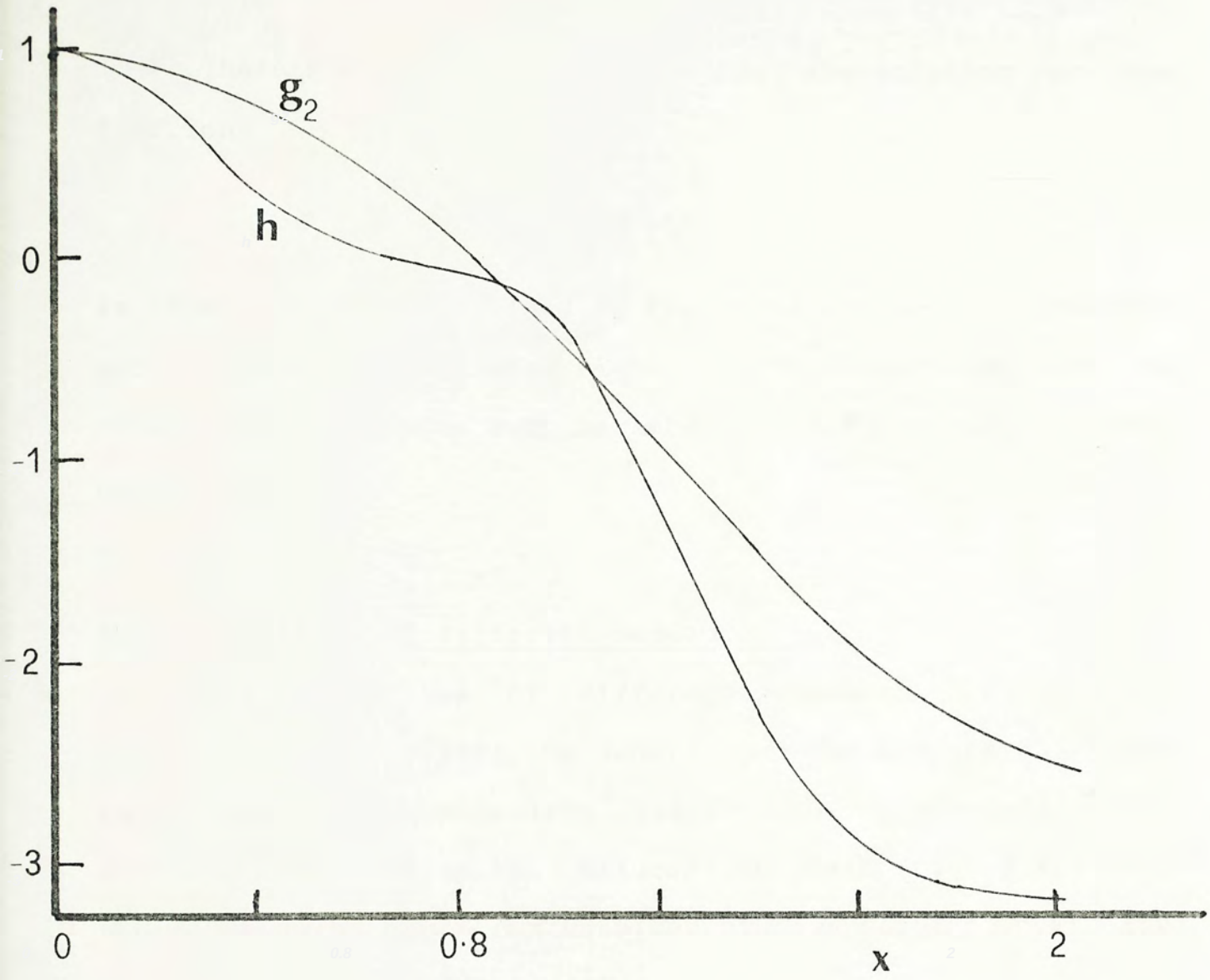

Fig. 3.3 Graph of the limiting functions $h(x)$ and $g_2(x)$. Both are scaled to 1 at x=0.

Therefore our conclusion is that the solution for the functional equation

$$\Psi \circ \Psi \left(\frac{x}{\alpha}\right) = -\frac{1}{\alpha}\Psi(x)$$

is not uniquely determined by the order of the local maximum and suitable boundary conditions. It is conjectured that the Schwarzian derivative must be less than zero in order to have unique solution.

3.6 Properties of different sequences

The properties of different sequences of a map was studied by Young (1984). He generalized the properties of the usual central sequence (Fig. 3.4a) to the up sequence X'_p, obtained by going up the bifurcation chain (Fig. 3.4b) and the down sequence X''_p, obtained by always going down the bifurcation chain (Fig. 3.4c).

Young found that for the up sequence

$$X'_{p+1} - X'_p = b'_1 \delta^{-p} + b'_2 (\alpha^2)^{-p} + \ldots \qquad (3.19)$$

and for the down sequence

$$X''_{p+1} - X''_p = b''_1 \delta^{-p} + b''_2 (\alpha^2)^{-p} + \ldots \qquad (3.20)$$

in which b'_1 and b''_1 are zero if $\frac{\partial f}{\partial \lambda}(\lambda_\infty, X_\infty) = 0$. For example for the map $1-\lambda x^2$, $b'_1 = 0$ but for the map $4\lambda x(1-x)$, $b'_1 \neq 0$. Furthermore, the limiting function for the up sequence

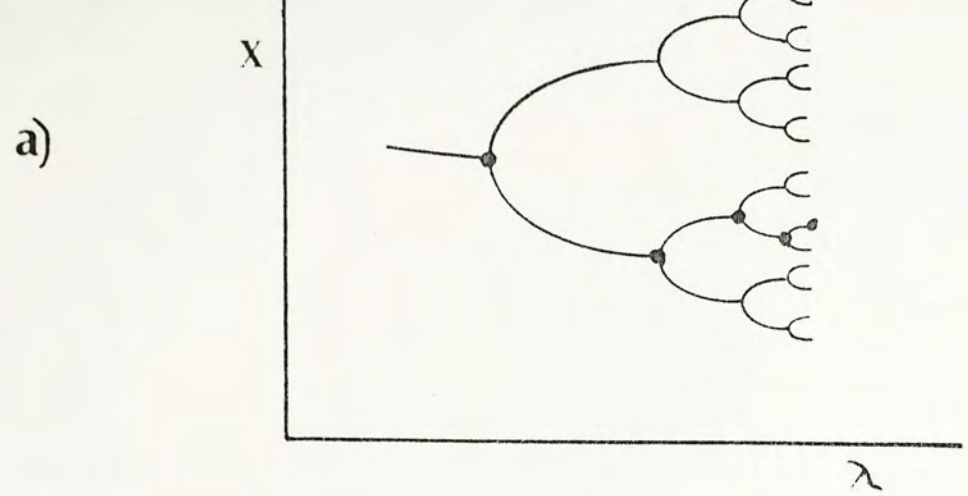

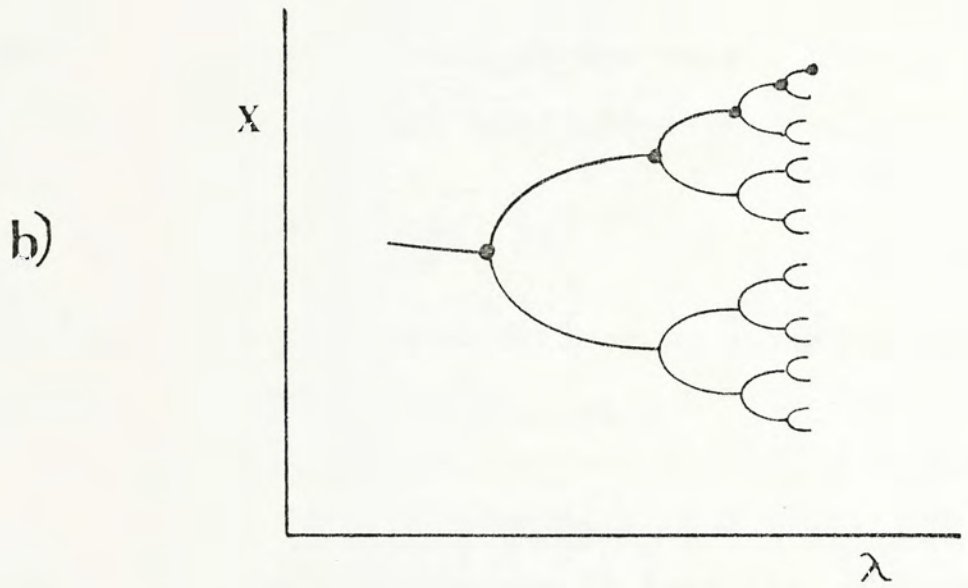

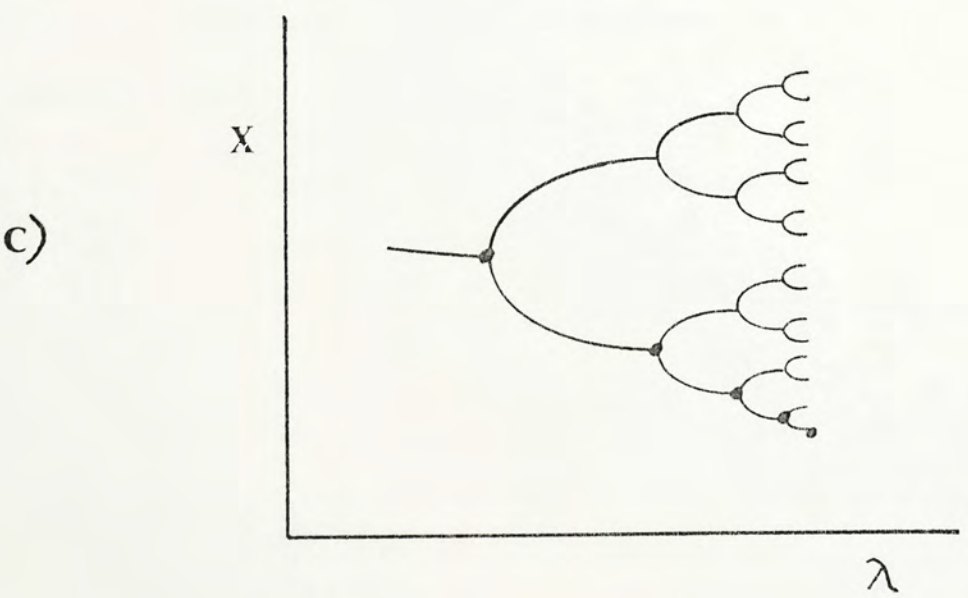

Fig. 3.4 Bifurcation diagram of a map $f(\lambda, x)$ showing a) the central sequence, b) the up sequence, c) the down sequence.

$$\alpha^{2p}\{\, f^{2^p}(\lambda_\infty , X'_\infty + x/\alpha^{2p}) - X'_\infty \,\}$$
$$\to \tilde{g}(x) \qquad (3.21)$$

(where $X'_\infty = \lim_{p\to\infty} X'_p$) exists and satisfies

$$\tilde{g}(\tilde{g}(x)) = \frac{1}{\alpha^2} g(\alpha^2 x) \qquad (3.22)$$

This $\tilde{g}(x)$ is related to the Feigenbaum scaling function g (i.e. for the central sequencee) by

$$\tilde{g}(x) = g(\sqrt{x})^2 \qquad (3.23)$$

The above results were derived by a simple topological fact. At the p-th bifurcation point

$$f(\lambda_p , X_p) = X'_p , \qquad f(\lambda_p , X'_p) = X''_p$$

That is, the up sequence is just the image under f of the central sequence. The down sequence is the image under f of the up sequence. (3.19) was shown by a simple Taylor series expansion:

$$X'_p = f(\lambda_p , X_p)$$
$$= f + \frac{\partial f}{\partial \lambda} (\lambda_p - \lambda_\infty) + \frac{\partial f}{\partial x} (X_p - X_\infty) +$$
$$\frac{\partial^2 f}{\partial \lambda \partial x} (\lambda_p - \lambda_\infty)(X_p - X_\infty) + \frac{1}{2} \frac{\partial^2 f}{\partial x^2} (X_p - X_\infty)^2$$

Since

$$\lambda_p - \lambda_\infty \propto \delta^{-p}$$
$$X_p - X_\infty \propto (-\alpha)^{-p}$$
$$f(\lambda_\infty , X_\infty) = X'_\infty$$

it follows that

$$X'_p = X'_\infty + c_1 \delta^{-p} + c_2 (-\alpha\delta)^{-p} + c_3 (\alpha^2)^{-p} + \ldots.$$

The first two eigenvalues in ascending order (i.e. δ and α^2) were observed numerically. Similar argument can be applied to the down sequence.

3.7 Generalized RG approach to pitchfork bifurcation

3.7.1 Introduction

There are many renormalization group calculations of pitchfork bifurcation in one-dimensional map $x \longrightarrow f(\lambda, x)$ which make use of the idea that $f^{2^{p+1}}$ looks like a scaled replica of f^{2^p}. We have discussed the RG of Feigenbaum at preferred values of λ (the super-stable values). The functional RG equation

$$g(g(x)) = -\frac{1}{\alpha} g(\alpha x)$$

was developed. $g(x)$ is the limiting function of the iterate $f^{2^{p-1}}(\lambda_p, x)$ at the super-stable values λ_p when x is scaled by $(-\alpha)^p$. The ratio of bifurcation δ emerges when we linearize around $g(x)$.

With the same principle in mind, the RG of Derrida et al. (discussed in section 3.4) paid emphasis on the λ scaling instead. Derrida et al. was able to calculate δ by using the relation

$$\frac{\partial f^{2^p}}{\partial x}(\lambda, x) = \frac{\partial f^{2^{p+1}}}{\partial x}(\lambda', x')$$

where $x = f^{2^p}(\lambda, x)$ and $x' = f^{2^{p+1}}(\lambda', x')$ are the fixed

points of f^{2^p} and $f^{2^{p+1}}$ at λ and λ' respectively. So we can calculate α from the functional equation and obtain δ from the RG of Derrida et al. Recently, Young and Liu (1984) were able to calculate δ and α simultaneously by a generalized RG analysis which scales the λ and x variables at the same time. Their work is a synthesis and generalization of the RG of Feigenbaum and Derrida et al.

3.7.2 Generalized RG analysis

The basic idea is also $f^{2^{p+1}}$ is a scaled version of f^{2^p}. The RG is realized as a nonlinear transformation of the coefficients of a double Taylor series expansion of $f(\lambda, x)$. Suppose the function $f(\lambda, x)$ and $f^2(\lambda, x)$ are expanded at their bifurcation points (Λ, X) and (Λ', X') respectively.

$$f(\lambda, x) = \sum_{ij} b_{ij} (\lambda - \Lambda)^i (x-X)^j$$

$$f^2(\lambda, x) = \sum_{ij} b'_{ij} (\lambda - \Lambda')^i (x-X)^j$$

or

$$f(\lambda, x) = X + \sum_{ij} b_{ij} \mu^i y^j \qquad (3.24)$$

$$f^2(\lambda, x) = X' + \sum_{ij} b'_{ij} \mu'^i y^j \qquad (3.25)$$

where $\mu = \lambda - \Lambda$, $y = x - X$

$\mu' = \lambda - \Lambda'$, $y' = x - X'$

The transformation T is defined as $\vec{b}' = T\vec{b}$, that is the transformation between the coefficients b_{ij} of f and b'_{ij} of f^2. The function f^2 looks like f only when f^2 is scaled in x and λ direction, therefore a scaling operator

S is defined:

$$S(\delta, \alpha) : b'_{ij} \longrightarrow b''_{ij} = b'_{ij}\, \delta^{-i}(-\alpha)^{-(j-1)}$$

The RG transformation $\mathcal{R}$ of Young and Liu is given by

$$\mathcal{R}(\delta, \alpha) = S(\delta, \alpha)\, T \qquad (3.26)$$

The fixed point of this transformation was studied, Numerically, the universal ratio δ and α were determined by truncating the double Taylor series of f and f^2 into finite terms:

$$f(\lambda, x) = X + \sum_{ij}^{M} b_{ij}\, \mu^i\, y^j \qquad (3.27)$$

$$f^2(\lambda, x) = X + \sum_{ij}^{N} c_{ij}\, \mu^i\, y^j \qquad (3.28)$$

where truncation means $2i+j \leqslant M$ in (3.27) and $2i+j \leqslant N$ in (3.28) and is denoted by (M,N). For $N = M^2 \to \infty$, the truncation is expected to give the exact results. The (3,3) order was solved analytically and gave $\delta = 4$, $\alpha = 4$. Higher order calculations gave better results as compared with accepted values of δ and α. Their results are summarized in Table 3.2

3.7.3 Generalized RG equation

From the renormalization group analysis discussed above, Young and Liu showed that as $p \to \infty$, the limit $\Psi_p(\mu, y)$ defined to be

Order	δ	α
3,3	4	4
3,9	3.9895	2.5594
4,16	4.6018	2.4888
5,25	4.6686	2.5067
exact	4.6692	2.5023

Table 3.2

Values of δ and α from generalized RG of Young and Liu

$$(-\alpha)^p [f^{2^p}(\lambda_\infty - \mu/\delta^p,\ x_\infty + y/(-\alpha)^p) - x_\infty]$$

exists and satisfies the generalized RG equation:

$$\Psi(\mu/\delta, \Psi(\mu/\delta, -y/\alpha)) = -\frac{1}{\alpha}\Psi(\mu,y) \qquad (3.29)$$

where λ_∞ is the bifurcation accumulation point and x_∞ maximizes $f(\lambda_\infty, x)$.

Let $\Psi(\mu,y) = \lim_{p\to\infty} \psi_p(\mu,y)$, it is obvious that $\Psi(0,x)$ is just the $g(x)$ of Feigenbaum. Writing

$$\Psi(\mu,y) = g(y) + \mu\, h(y) + O(\mu^2)$$

By (3.29) , it can be shown easily that

$$g(g(-y/\alpha)) = -\frac{1}{\alpha} g(y) \qquad (3.30)$$

and h satisfies

$$g'(g(y))h(y) + h(g(y)) = -(\delta/\alpha)\, h(\alpha y) \qquad (3.31)$$

Therefore (3.31) can be obtained easily and the meaning of eigenfunction h becomes clear.

We have verified 'experimentally' that the limit

$$\lim_{p\to\infty} \psi_p(\mu,y) = \psi(\mu,y)$$

exists (Liu, Lo and Young, 1984). The value of $\psi_p(\mu,y)$ for 3 different values of μ and y calculated from the function $f(\lambda, x) = 1 - \lambda x^2$ are shown in Table 3.3 . These values were calculated with 16 digit arithmetic. Since round-off errors and errors in the constants λ_∞, δ and α become more

p	μ=0.5, y=1	μ=1, y=1	μ=-0.5, y=0.5
1	-0.487393440	-0.609935989	0.896750964
2	-0.610524725	-0.775248596	1.019022342
3	-0.632751027	-0.804565486	1.047360834
4	-0.637735161	-0.811021188	1.053528845
5	-0.638751437	-0.812348159	1.054864259
6	-0.638972810	-0.812636616	1.055150758
7	-0.639019411	-0.812297588	1.055212332
8	-0.639029437	-0.812710707	1.055225532
9	-0.639031571	-0.812713504	1.055228364
10	-0.639032028	-0.812714095	1.055228964
11	-0.639032130	-0.812714269	1.055229084
12	-0.639032292	-0.812714448	1.055229102
13	-0.639030194	-0.812712460	1.055233806

Table 3.3

Convergence of $\Psi_p(\mu, y)$ as $p \to \infty$ for selected μ and y

and more important when p becomes larger, the apparent divergence of Ψ_p as p gets larger 13 can be easily understood. The parameters involved in calculating the limit $\Psi_p(\mu, y)$ should be as accurate as possible.

Besides, we have verified that for other different functions within the quadratic maximun class such as $1-\lambda x^2$, $4\lambda x(1-x)$, $x \exp[\lambda(1-x)]$, $\lambda \sin\pi x$ and $\lambda(1-1/2x^2+1/24x^4)$, the limits Ψ_p exist and are universal up to scaling

$$\Psi(0,0) = 1, \qquad \Psi(-1,0) = 2 \tag{3.32}$$

which is arbitrarily chosen. The corresponding λ_∞ and X_∞ for the functions are given in Table 3.4 . Fig. 3.5 shows the dependence of $\Psi(\mu, y)$ on y for different μ .

3.8 Remarks

Although in this chapter we have concentrated on the use of RG to study the period doubling route to chaos, it must be emphasized that RG can be used to study other routes to chaos. In fact, Hirsh et al. (1982) have developed RG to study intermittency (which will be discussed in Chapter 4) and Feigenbaum et al. (1982) and Rand et al. (1982) have developed RG theory for transition from quasi-periodicity to chaos. Thus RG is a unified and powerful tool in understanding the regularities in the transitions to chaos, and provides an analytic method to understand the results from numerical study by computers.

f	λ_∞	X_∞
$1-\lambda x^2$	1.4011551890920506	0
$4\lambda x(1-x)$	0.8924864179677362	0.5
$x \exp[\lambda(1-x)]$	2.692368854390526	0.3714201816196288
$\lambda \sin \pi x$	0.8655792688186374	0.5
$\lambda(1-1/2x^2+1/24x^4)$	2.10778725230321	0

Table 3.4 Values of λ_∞ and X_∞ for different functions

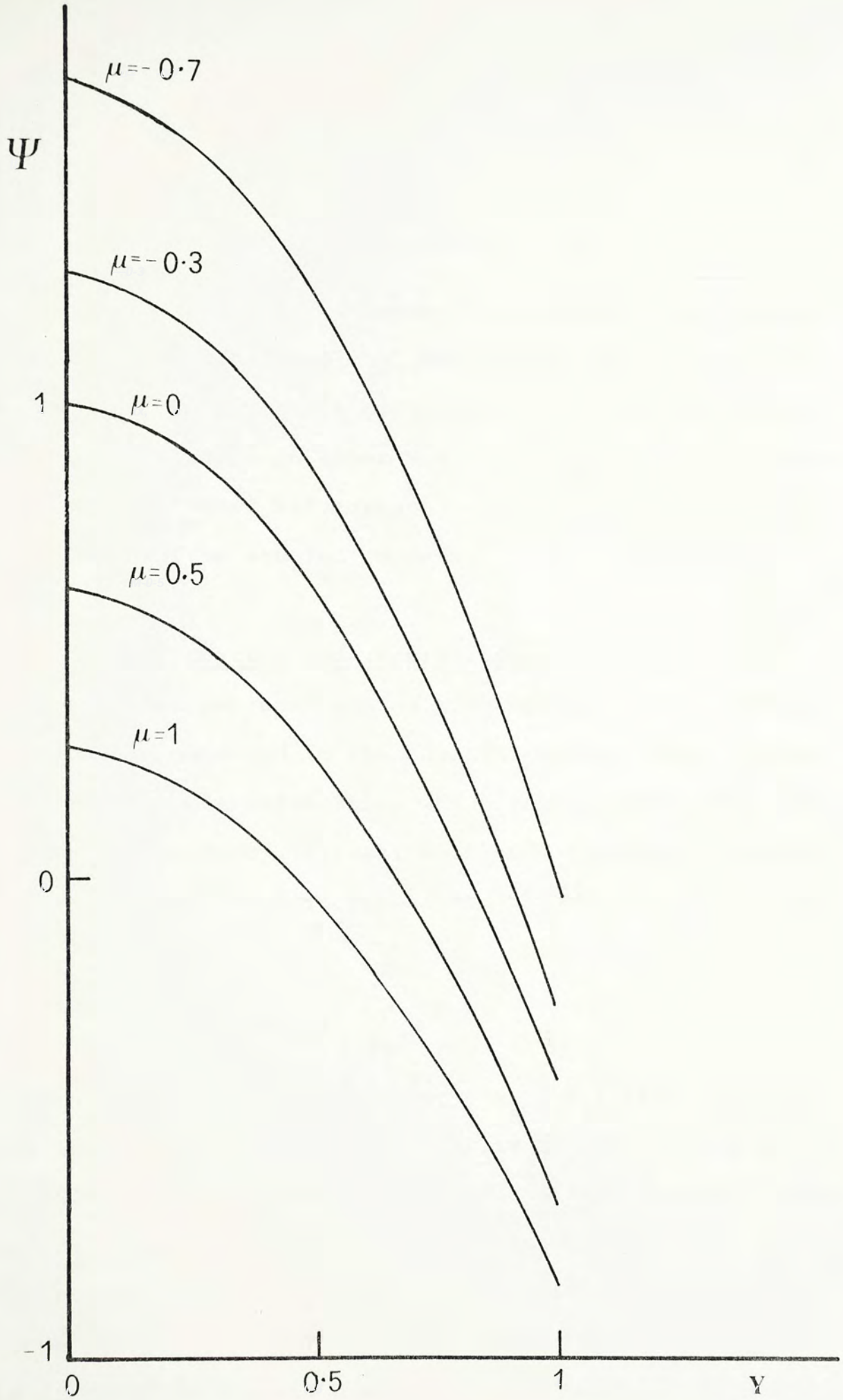

Fig. 3.5 Dependence of the generalized limiting function of pitchfork bifurcation $\Psi(\mu, y)$ on y for selected μ.

CHAPTER 4

Other roads to chaos

In chapter 2 we have concentrated on period-doubling in one-dimensional map. The period-doubling route to chaos is due to pitchfork bifurcations. There are other routes to chaos based on other bifurcation such as tangent bifurcation and Hopf bifurcation. In this chapter, these bifurcations will be studied in detail.

4.1 Tangent bifurcation and intermittency

Beyond the period-doubling accumulation point various odd cycles are embedded in the chaotic region. They appear through the tangent bifurcation which takes place when the eigenvalue (i.e. the derivative in one dimension) passes through +1 instead of -1 in pitchfork bifurcation. Consider a map

$$x_{n+1} = f(a, x_n) \tag{4.1}$$

at three different values of a ($a_1 < a_2 < a_3$) (Fig. 4.1). At $a=a_2$ a 1-cycle is created when f(x) is tangent to the 45° -line. There is no stable cycles for $a=a_1$ but when a gets closer to a_2, successive iterates of a point pass very slowly through the channel region of closest approach to the 45° -line (Fig. 4.2). The iterates seem to converge to a stable fixed point but since there is no stable fixed point, they pass away gradually. After some iterations they come back to this channel region and repeat the same motion. Every

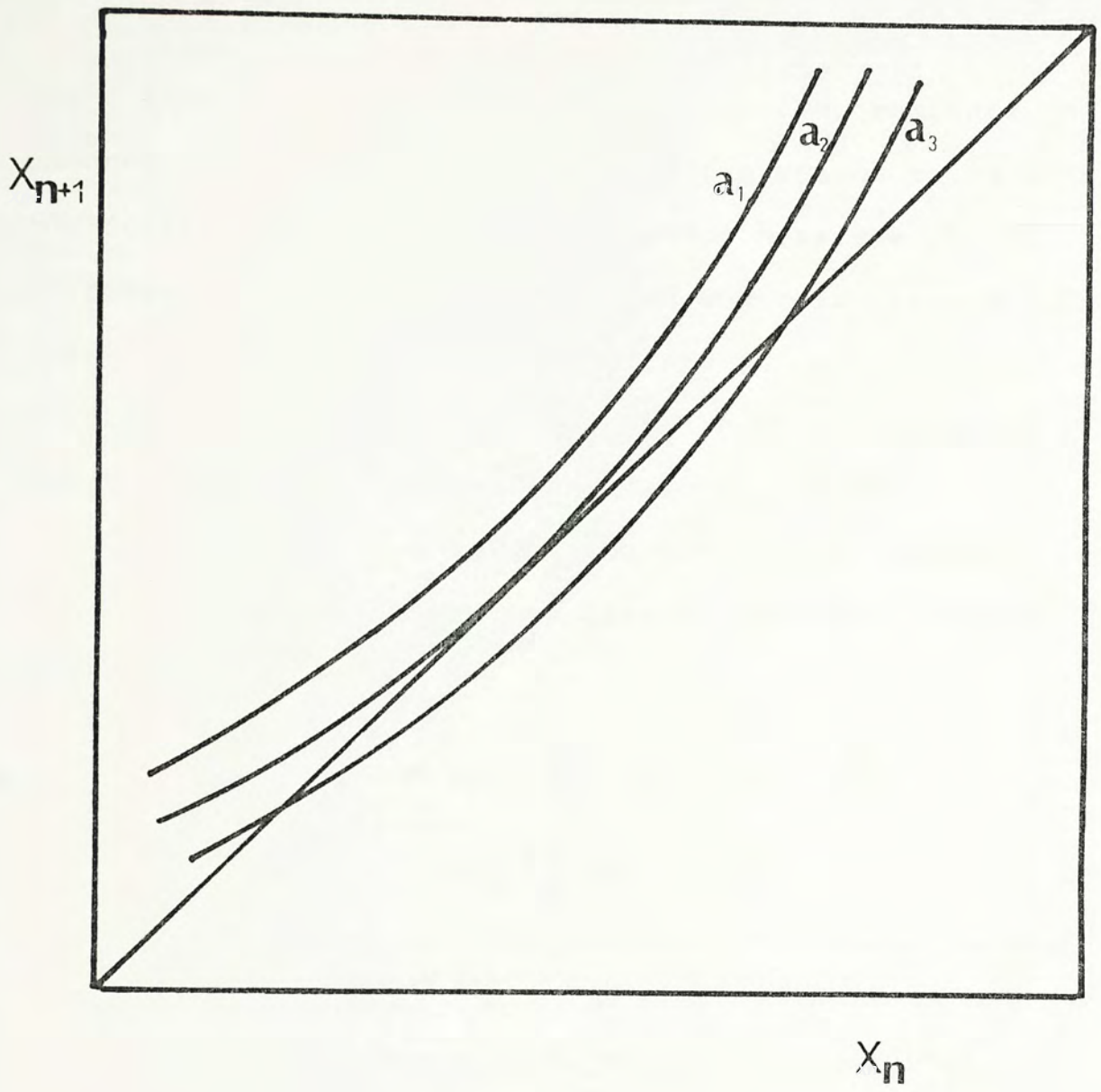

Fig. 4.1 A one-dimensional map at three different parameter values showing the tangent bifurcation.

time when one iteration falls near the entrance of the channel region, it will take many iterations to pass through the 'corridor' (Fig. 4.2). The motion near the channel region corresponds to the laminar region and this regular laminar flow iterrupted by irregular bursts is called intermittency. Intermittency is another possible route to chaos and it was first proposed by Manneville and Pomeau (1979).

The nearer a to a_2 the longer the average laminar time. We can estimate this time as follows. Expand f(a,x) near a_2 and x_*.

$$f(a,x) = x_* + \frac{\partial f}{\partial x}(x - x_*) + \frac{\partial f}{\partial a}(a - a_2) + \frac{1}{2}\frac{\partial^2 f}{\partial x^2}(x - x_*)^2 + \ldots \qquad (4.2)$$

since $\frac{\partial f}{\partial x} = 1$

$$f(a,x) = x_* + (x-x_*) + h(a-a_2) + k(x-x_*)^2 + \ldots \qquad (4.3)$$

If $\frac{1}{2}\frac{\partial^2 f}{\partial x^2}$ is zero, take the next term and denote it by $k(x-x_*)^z$. Therefore

$$x_{n+1} - x_* = x_n - x_* + h(a-a_2) + k(x_n - x_*)^z \qquad (4.4)$$

Near the channel region $x_{n+1} - x_n$ is very small. Let $\xi = x - x_*$ and treat n as $\Delta t = 1$ unit. Then

$$\frac{d\xi}{dt} = h(a_2 - a) + k\xi^z$$

The passage time

$$t \propto (a_2 - a)^{-(1-1/z)}$$

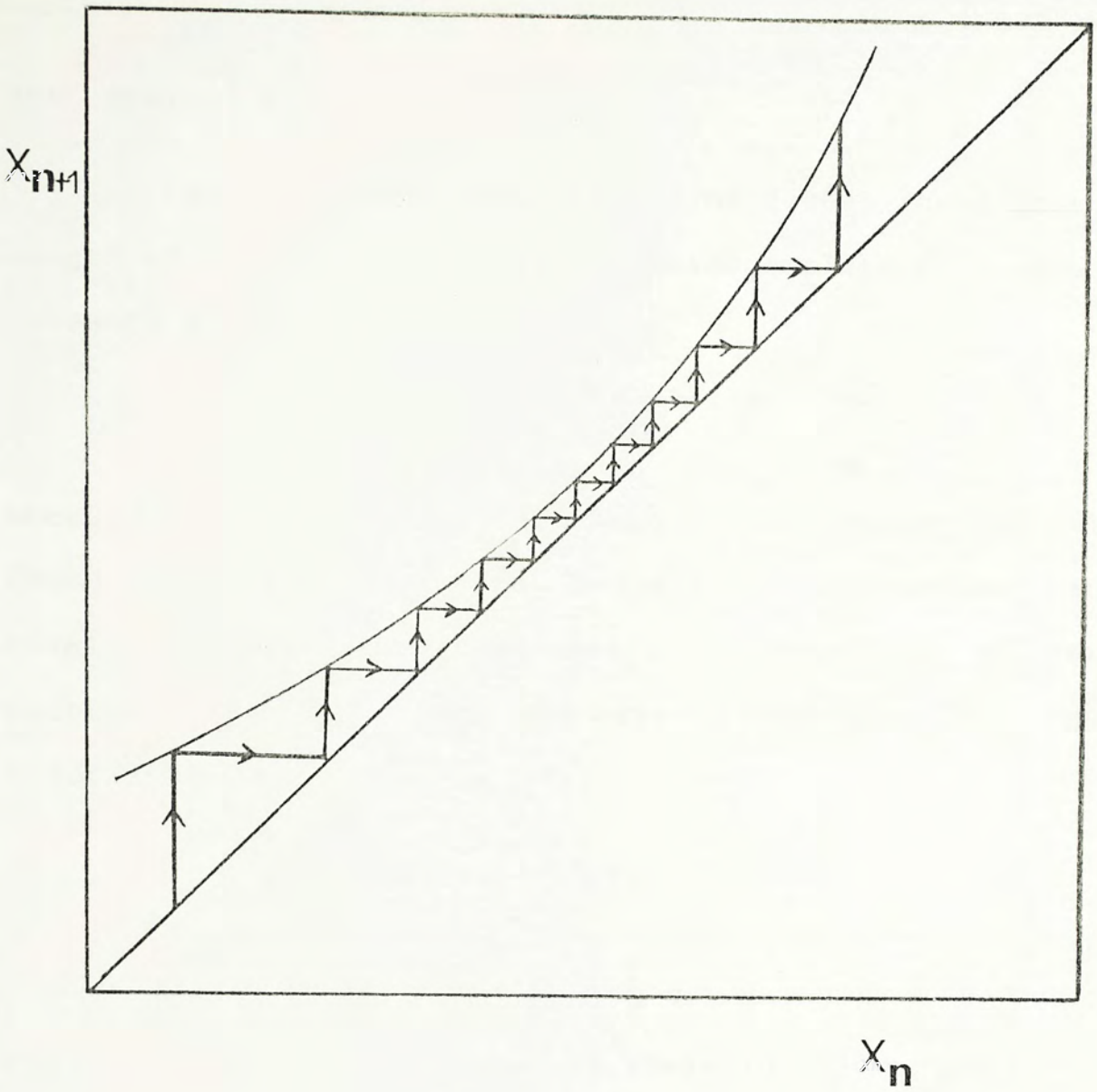

Fig. 4.2 Near tangent bifurcation it takes many iterations to pass through the channel region.

For $z=2$, $\quad t \propto (a_2-a)^{-1/2}$ (4.5)

Hirsh, Huberman and Scalapino (1982) found that the length of laminarity ℓ, with noise amplitude σ present, takes on a universal scaling form

$$\ell(\epsilon,\sigma) = \epsilon^{-(1-\frac{1}{z})} f\left(\sigma / \epsilon^{\frac{(z+1)}{2z}}\right) \qquad (4.6)$$

where $\epsilon = a_2-a$. Hirsh, Nauenberg and Scalapino (1982) later found that the exponents and scaling properties can be obtained by the same functional group equations of period-doubling with a change of boundary condition for tangent bifurcation

$$g(x) = -\alpha g(g(-x/\alpha))$$
$$g(0) = 0, \quad g'(0) = 1 \qquad (4.7)$$

They obtained exact solution to these functional equations.

The fact that both period-doubling and intermittency can be described by the same functional RG equations make RG a powerful and unified method to study the transition to chaos. According to this Hao (1984) called period-doubling and intermittency twin phenomena. For dynamical systems with period-doubling there should be intermittency as well.

4.2 Hopf bifurcation and the Ruelle-Takens-Newhouse route

The bifurcation from a fixed point to a closed orbit as the parameter passes a critical value is called Hopf bifurcation. Consider the two dimensional map

$$x_{n+1} = \mu (\cos\theta\ x_n + \sin\theta\ y_n)$$
$$y_{n+1} = \mu (-\sin\theta\ x_n + \cos\theta\ y_n) \qquad (4.8)$$

Each iteration corresponds to a rotation of angle θ while the radius increases by a factor μ. For $\mu < 1$ the iterates will converge to a stable fixed point but for $\mu > 1$ they will move out during rotation. For $\mu = 1$ the iterates will rotate in a unit circle so the fixed point is a limit cycle. Therefore this map has a Hopf bifurcation when $\mu > 1$.

Next consider another example of Hopf bifurcation which occurs in differential equations in polar coordinates.

$$\frac{dr}{dt} = r\ (\mu - r^2)$$
$$\frac{d\theta}{dt} = 1 \qquad (4.9)$$

In this case the critical value $\mu_c = 0$. For $\mu < \mu_c$, $\dot{r} < 0$ and hence r approaches zero for large t. However, for $\mu > \mu_c$ the fixed point at r=0 is unstable and the locus spirals into the invariant circle if $r^2 > \mu$ and spirals to the invariant circle for $r^2 < \mu$ (Fig. 4.3).

Solving the differential equations gives

$$r^2 = \frac{\mu r_0^2 e^{2\mu t}}{r_0^2 (e^{2\mu t} - 1) + \mu}$$
$$\theta = t$$

Hence the locus is

$$r^2 = \frac{\mu r_0^2 e^{2\mu\theta}}{r_0^2 (e^{2\mu\theta} - 1) + \mu} \qquad (4.10)$$

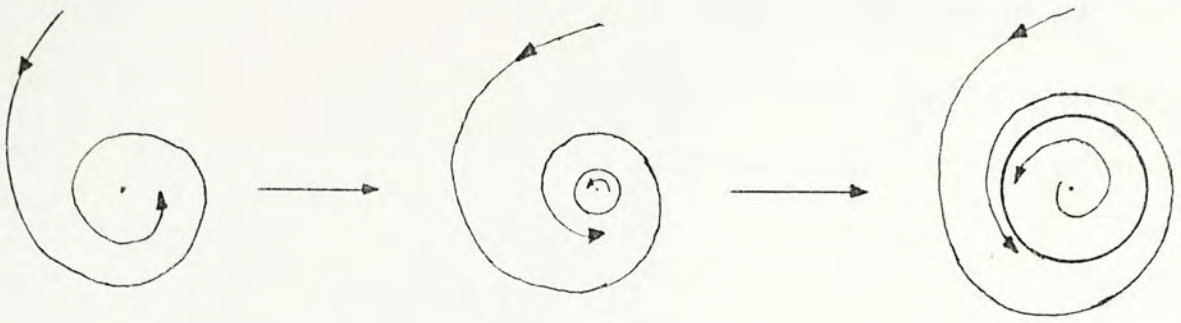

Fig. 4.3 Change of loci when μ is increased showing the Hopf bifurcation. (after Hu (1982), p.290)

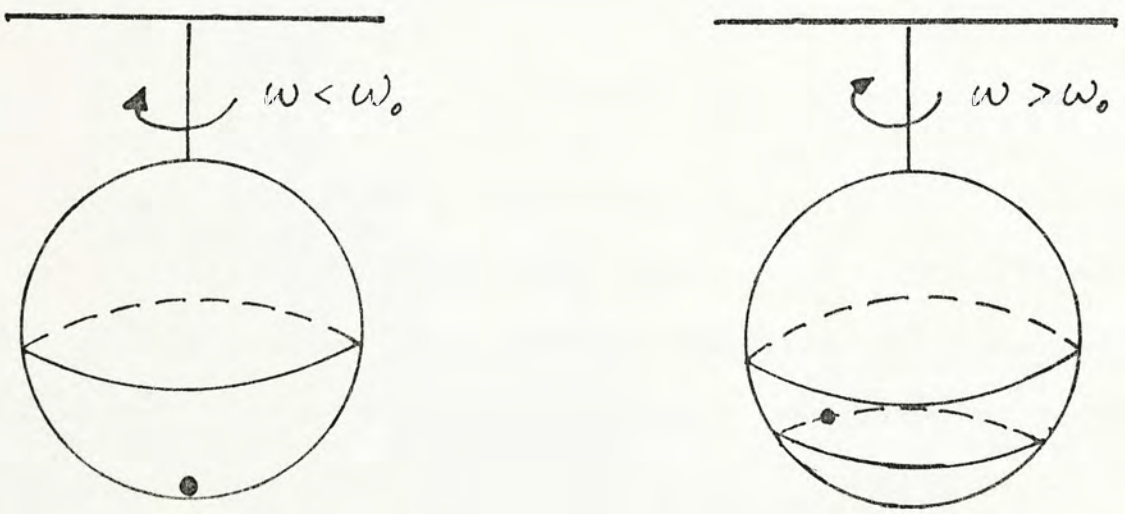

Fig. 4.4 Hopf bifurcation in classical physics. a) rotation frequency $\omega < \omega_0$, b) $\omega > \omega_0$. The locus changes from a fixed point to a limit cycle when ω passes ω_0 .

The condition for a Hopf bifurcation can be obtained by a linear analysis around the unstable fixed point (origin). First transform the differential equations to rectangular coordinates:

$$\frac{dx}{dt} = [\mu - (x^2 + y^2)]\, x - y$$

$$\frac{dy}{dt} = [\mu - (x^2 + y^2)]\, y + x \qquad (4.11)$$

Linearize about the origin gives

$$\frac{d\begin{pmatrix}\Delta x\\ \Delta y\end{pmatrix}}{dt} = \begin{pmatrix}\mu & -1\\ 1 & \mu\end{pmatrix}\begin{pmatrix}\Delta x\\ \Delta y\end{pmatrix}$$

The eigenvalues of the matrix are

$$\lambda_{\pm} = \mu \pm i \qquad (4.13)$$

For Hopf bifurcation to take place, $\mu_c = 0$

Therefore $|\lambda| = 1$ (Hopf bifurcation) (4.13)

Consider an example from classical mechanics so that we can have a more intuitive idea about Hopf bifurcation. A rigid, hollow sphere with a small ball inside it hangs from the ceiling. It rotates with frequency ω about a vertical axis through the centre (Fig. 4.4)

For small ω , the small ball remains at the bottom of the sphere so the bottom is a fixed point. For $\omega > \omega_0$ the bottom is no longer stable and the fixed point is a stable invariant circle. Different ω correspond to different stable circles. There is a Hopf bifurcation as ω passes ω_0.

Landau (1944) and Hopf (1948) suggested a possible

route to chaos by attributing the appearence of increasing number of quasiperiodic motions produced by sucessive Hopf bifurcations. They argued that a fixed point became unstable and bifurcated to a limit cycle which corresponded to a periodic motion of the system. In the next bifurcation the limit cycle became unstable and a 2-torus appeared. If the two frequencies of the 2-torus were incommensurable the motion was quasiperiodic. Finally, there were infinite numbers of incommensurable frequencies produced and the system was in a state of full turbulence. This was called the Landau-Hopf route to turbulence.

Denote quasiperiodic motion with n incommensurable frequencies by Q_n. The Landau-Hopf route can be represented by

$$Q_n \xrightarrow{n \to \infty} \text{chaos} \tag{4.14}$$

4.3 Transition from quasiperiodicity to chaos

4.3.1 Difficulties in the Landau-Hopf route

The Landau-Hopf route to chaos is a route based on transition from quasiperiodicity to chaos. However it is not a possible route. Experimentally turbulent spectra turn into broad noisy bands after developing a few independent frequencies. According to this route, the power spectrum should remain discrete as successive new incommensurable frequencies appear. Theoretically there are a few difficulties in this mechanism for turbulence:

(1) There is no reasonable mathematical model which

follows this route.

(2) The feature of sensitive dependence on initial condition does not appear in this model.

(3) This route ignores frequency locking. In nonlinear systems new incommensurable frequencies cannot be produced infinitely without interacting with each other. Nearby frequencies tend to be locked.

4.3.2 Alternatives to the Landau-Hopf route

Since there are a lot of difficulties in the Landau-Hopf route to chaos, scientists proposed other mechanisms for onset of chaos. Ruelle and Takens (1971) showed that quasipreiodic motion with 4 incommensurable frequencies is in general unstable. They proposed a new concept--strange attractor which corresponds to turbulent motion. The unstable motion with 4 incommensurable frequencies can be perturbed into a strange attractor. Later, Newhouse, Ruelle and Takens (1978) reduced the above mechanism to a system with 3 incommensurable frequencies, that is,

$$Q_3 \longrightarrow \text{chaos} \qquad (4.15)$$

Roughly speaking, after 3 successive Hopf bifurcations with essentially independent modes, a strange attractor may appear. Recently Feigenbaum et al. (1982) and Rand et al. (1982) developed RG theory of $Q_2 \longrightarrow$ chaos transitions and discovered universal characteristic for this transition.

4.4 Summary

Now we have three establised roads (Scenarios) to turbulence in dissipative systems:

(1) The Ruelle-Takens-Newhouse scenario is based on Hopf bifurcation.

(2) The Feigenbaum scenario is based on pitchfork bifurcation.

(3) The Pomeau-Manneville scenario is based on tangent bifurcation (saddle-node bifurcation).

New routes based on new bifurcations are possible in this rapid-developing field.

CHAPTER 5

Strange attractor

5.1 Example of strange attractor

The concept of strange attractor is very important in the study of chaotic motions. In chapter 4 we have discussed 3 routes to chaos associated with pitchfork, tangent and Hopf bifurcations. Two of them are also possible routes to a strange attractors:

(1) {stationary point} ⟶ {bifurcation to a periodic orbit} ⟶ {period doubling bifurcation} ⟶

{accumulation point of an infinite number of period doubling bifurcations} ⟶ {strange attractor}

(2) {stationary point} ⟶ {bifurcation to a periodic orbit} ⟶ {bifurcation to a doubly periodic orbit}

⟶ {strange attractor}

Therefore, the presence of strange attractor can lead to chaotic motion. In dissipative systems, the volume of phase space contracts during evolution so that for long time the dimension of the attractor D is lower than the dimension of the original phase space. If the attractor consists of a finite numbers of fixed points then D = 0. For limit cycle and 2-torus D = 1 and 2 respectively. All these dimensions are integers but for strange attractor the dimension is non-integer.

We first give an example of a strange attractor. Consider the Henon map:

$$x_{n+1} = y_n - ax_n^2 + 1$$
$$y_{n+1} = bx_n \qquad (5.1)$$

For $a = 1.4$, $b = 0.3$ with initial point $x_o = 0.63135448$ and $y_o = 0.18940634$, 10000 successive points obtained by the map are plotted in Fig. 5.1a. Plots starting with other initial points are nearly the same, except for an initial transient. The set of all the points form an attractor which is not a curve or an area surrounded by a curve (as can be seen from the figure). The dimension of this 'strange' attractor is not equal to 1 (for a curve) or 2 (for an area). The value is between 1 and 2, with non-integer value. The concept of non-integer dimension will be discussed in the next section.

Another interesting feature of this strange attractor is that there is scale invariance. Fig. 5.1b shows a blow-up of the square region in Fig. 5.1a and Figs. 5.1c and 5.1d are successive blow-ups of the preceding square regions. After suitable enlargement, the detail parts of the attractor is similar to the whole structure. Furthermore, if we change a to 1.3 (b = 0.3 unchanged), the entire attractor suddenly disappears and a 7-cycle is formed (Fig. 5.2).

5.2 Characteristic of a strange attractor

From the above example, we can summarize certain characteristic of a general strange attractor:

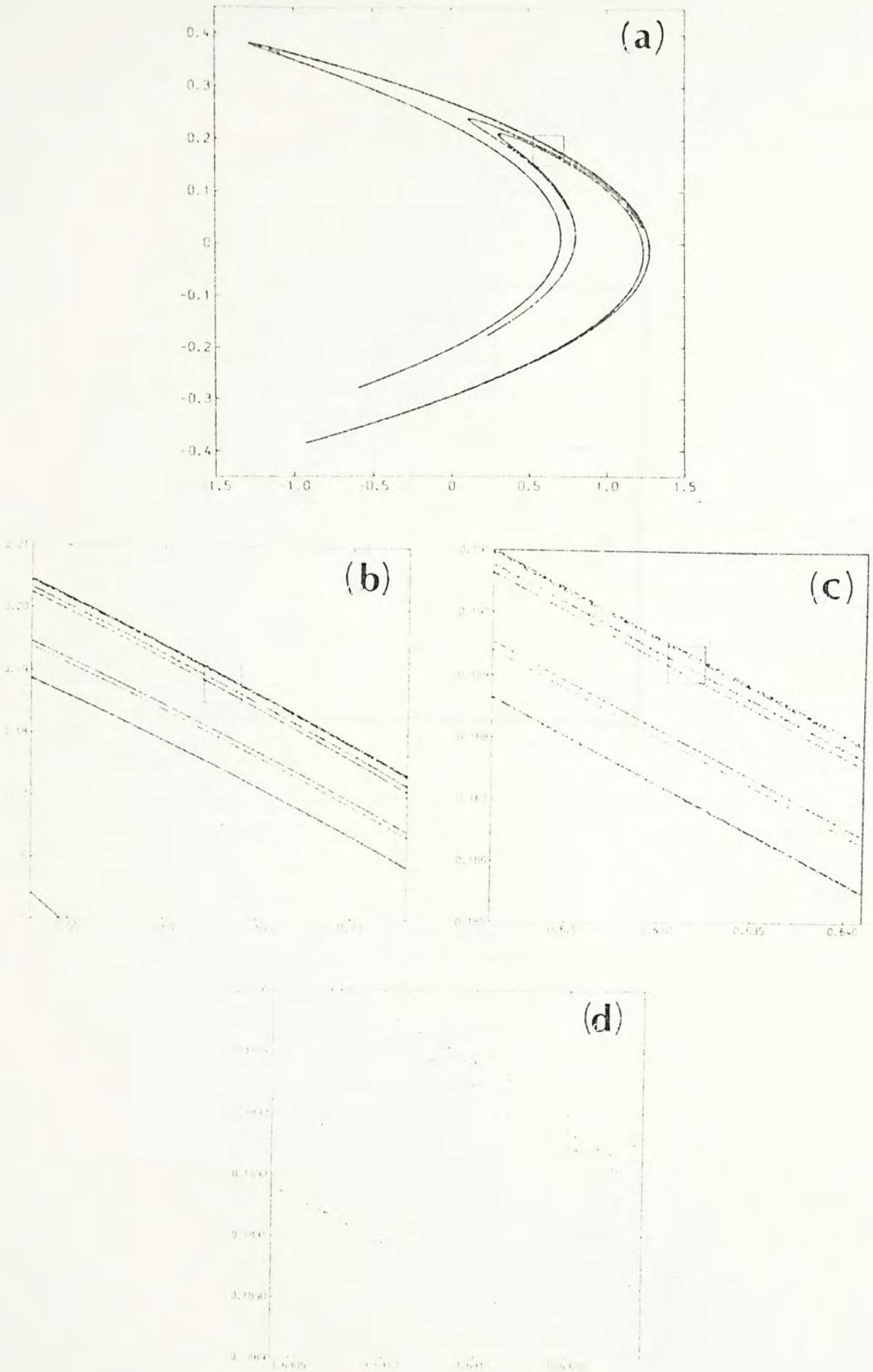

Fig. 5.1 a) Attractor of the Henon map; b), c) and d) show blow-up of the preceeding squared regions. (after Ott (1981), p.660-661)

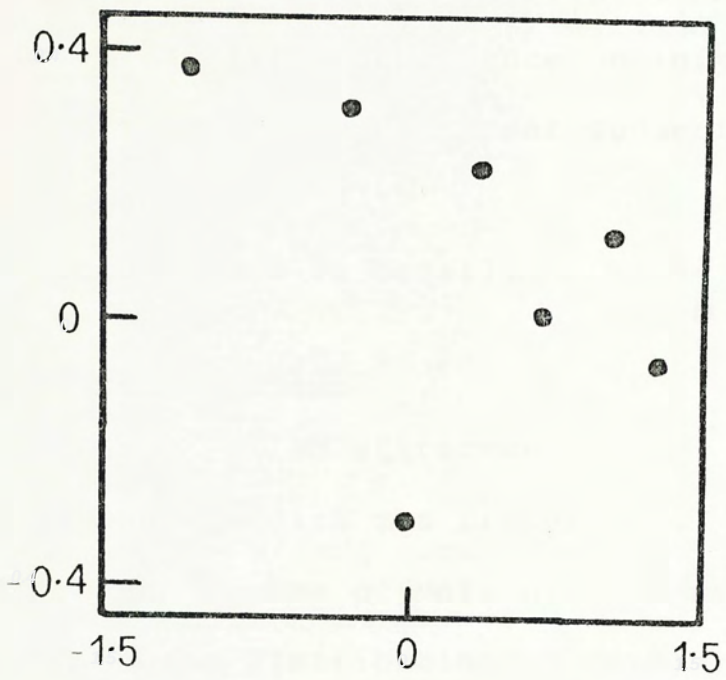

Fig. 5.2 Attractor of the Henon map suddenly changes to a 7-cycle when a is changed to 1.3 . (after Hu (1982), p.292)

(1) The dimension is non-integer

(2) There exists scale invariance.

(3) Nearby trajectories separate at an exponential rate. So there is sensitive dependence on initial conditions.

(4) The attractor may disappear suddenly as the system parameters are changed.

We now discuss them in detail.

5.2.1 Non-integer dimension

The dimension of an attractor is the most important information to characterize its properties. It gives the lower bound on the number of variables needed to model the dynamics. For discrete distribution of points in m-dimension, Hausdorf (1919) gave a general definition of dimension

$$d = \lim_{\epsilon \to 0} \frac{\ln N(\epsilon)}{\ln (\epsilon)} \qquad (5.2)$$

where $N(\epsilon)$ is the total numbers of m-dimensional cubes of sides ϵ necessary to cover the attractor, which is a subset of the m-dimensional ordinary space. The limit $\epsilon \longrightarrow 0$ is taken in order to make the cubes as small as possible.

This definition is consistent with our general concept about dimension. For example, for ordinary point, line and surface, $N(\epsilon)$ is equal to 1, ϵ^{-1} and ϵ^{-2} respectively, giving d = 0, 1 and 2.

The Cantor set is the simplest example of non-integer dimension. It is formed by deleting the central one-third of a unit interval and repeating the same operation to the remaining parts (Fig. 5.3). What is the dimension of this

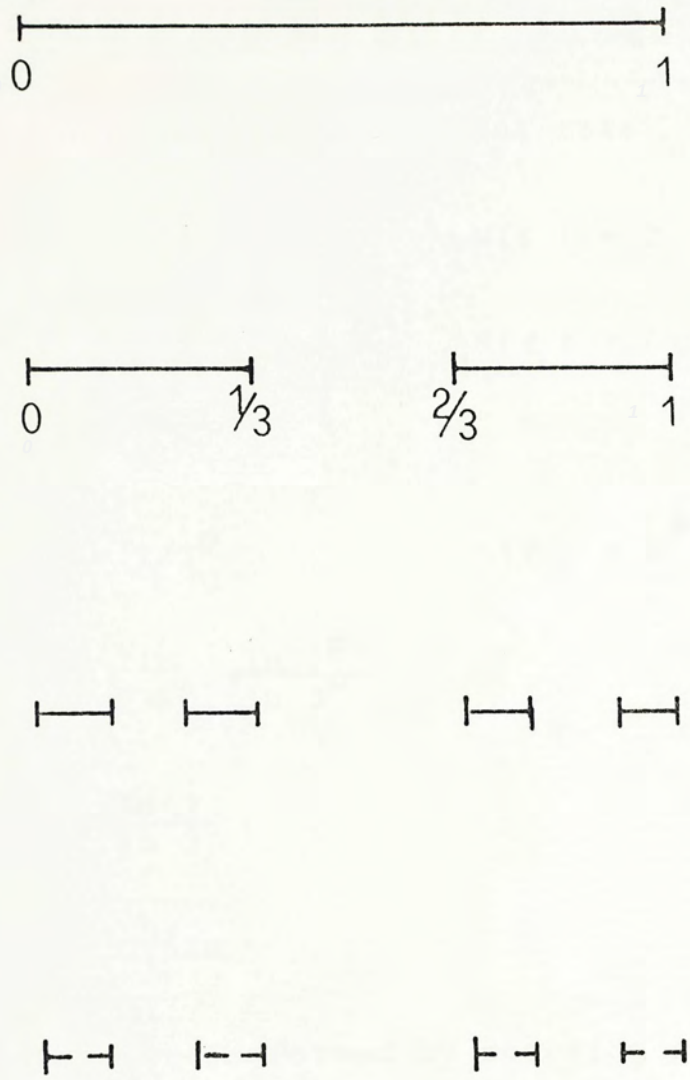

Fig. 5.3 Construction of the Cantor set. Every time the central one-third part is deleted.

limiting set ?

Obviously, after one operation, take

$$\epsilon = 1/3 \qquad N(\epsilon) = 2$$

similarly

$$\epsilon = 1/9 \qquad N(\epsilon) = 4$$

$$\vdots \qquad\qquad \vdots$$

$$\epsilon = 1/3^p \qquad N(\epsilon) = 2^p$$

Hence

$$d = \lim_{\epsilon \to 0} \frac{\ln 2^p}{\ln 3^p}$$

$$= \frac{\ln 2}{\ln 3}$$

$$= 0.630$$

The Cantor set is formed by deleting some parts out of a line and it has a dimension less than one. If some parts are added to a curve, the object should have a dimension greater than one. Consider another example of geometrical object. Take a equilateral triangle and build 3 equilateral triangles of sides one-third of the previous one on the three sides of the larger triangle. Repeat the same procedure infinitely (Fig. 5.4).

It is easy to show that after every step, the length of the object formed is 4/3 times the previous one. Therefore the dimension of the ultimate object formed is

$$d = \ln 4/\ln 3 = 1.26$$

The length of this object is infinitely long, but it is

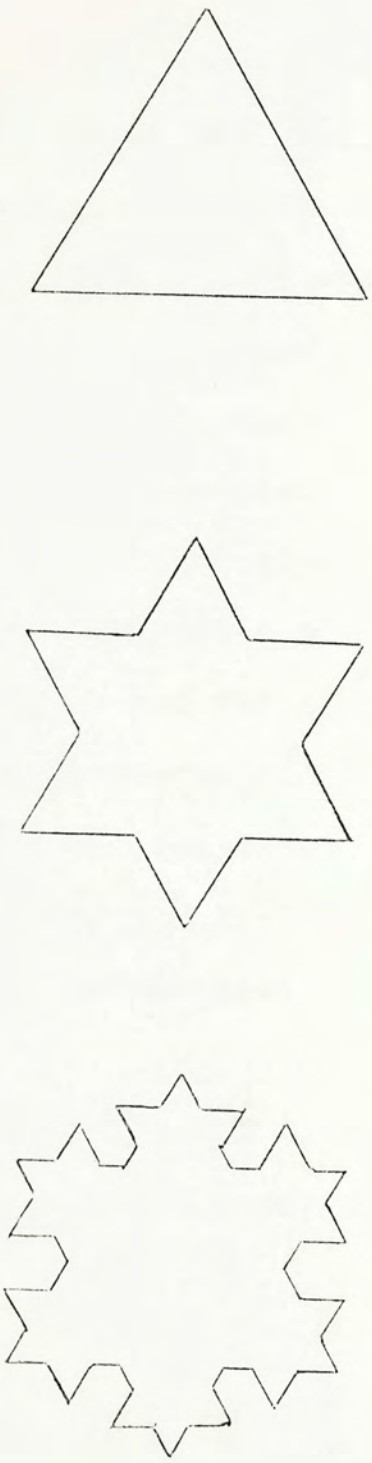

Fig. 5.4 Construction of another geometrical object with non-integer dimension. Three small eqilateral triangles are built on the preceding larger triangle.

confined in a bounded region in such a way that it is stretched and folded again and again. Thus we may think intuitively a strange attractor with non-integer dimension as an object which is infinitely long stretched and folded many many times and confined in a bounded region.

For dissipative system with internal friction or heat conduction, the motion is irreversible. The volume of phase space will contract during evolution. We can classify three cases for this contraction (Fig. 5.5). For the first case all lengths are contracting. For the second one there are both length contraction and expansion, but in different direction. For the third case, besides length contraction and expansion, the volume of phase space is stretched and folded over and over. Finally it will become a strange attractor with non-integer dimension.

There are other definitions of dimension. Before giving the definitions we first examine the following two-dimensional map

$$\begin{aligned} x_{n+1} &= x_n + y_n + \delta \cos 2\pi y_n \quad \text{mod } 1 \\ y_{n+1} &= x_n + 2y_n \quad \text{mod } 1 \end{aligned} \tag{5.3}$$

For small values of δ, Sinai (1972) showed that the attractor has dimension equal to 2. For $\delta = 0.1$, 80000 successive iterates of an initial point $x_o = 0.5$, $y_o = 0.5$ are shown in Fig. 5.6. As initial conditions are changed, the locations of the individual points change but the locations of the dark bands do not. Certain regions are visited far

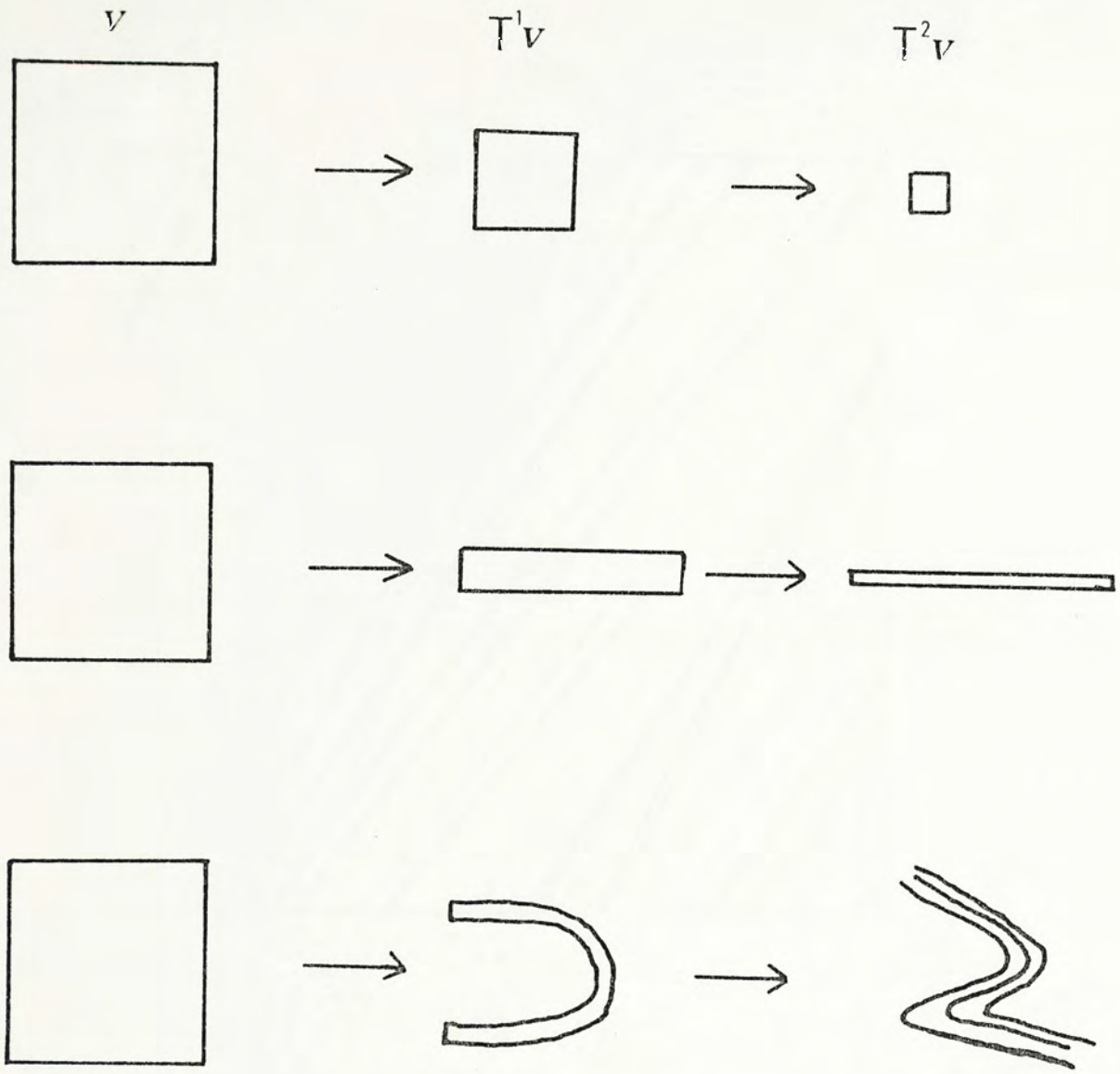

Fig. 5.5 Three cases of contraction of phase space during evolution in dissipative systems. (after Eckmann (1981), p.645)

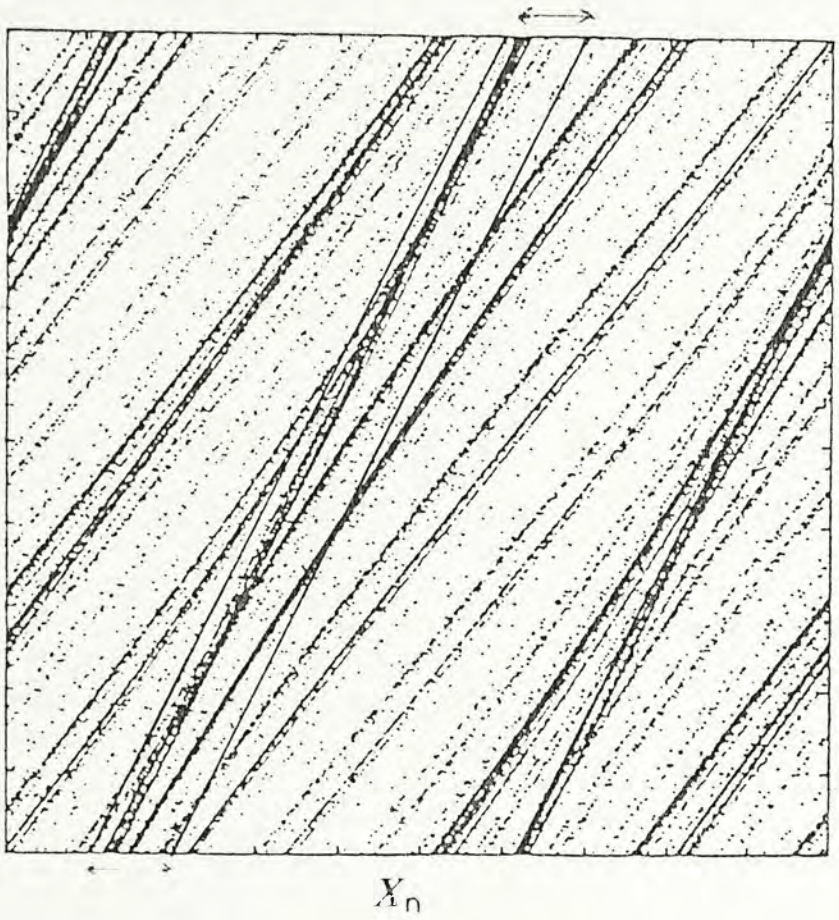

Fig. 5.6 Attractor of the map (5.3) with δ = 0.1. 80000 successive iterates of an initial (x_0, y_0) = (0.5,0.5) are shown. (after Farmer, Ott and Yorke (1983), p.155)

more often than others. For example, the outlined parallelogram contains 27% of the points of a typical trajectory. The Hausdorf dimension does not take into account the possible inhomogeneity of the attractor, that is, no matter how many times the trajectory passes through a given cube, the cube is counted only once. To correct this one may take the frequencies a given cube is visited into account. Let P_i be the probability that i-th cube is visited. Then the imformation dimension is defined to be

$$d_I = \lim_{\epsilon \to 0} \frac{I(\epsilon)}{\ln\left(\frac{1}{\epsilon}\right)} \tag{5.4}$$

where $$I(\epsilon) = -\sum_{i=1}^{N(\epsilon)} P_i \ln P_i$$

$N(\epsilon)$ is the total number of cubes visited. If there is no inhomogeneity, $P_i = 1/N(\epsilon)$ and $I(\epsilon) = \ln N(\epsilon)$ so $d_I = d$.

Although there are many different definitions of dimension, there are mainly two types of dimension. One type depends on the metric properties only like the Hausdorf dimension. The other type depends on metric and probabilistic properties such as the information dimension. Numerical calculations support the conjecture that all the metric dimensions take on the same value while all the frequency dependent dimensions take on another smaller common value.

5.2.2 Lyapunov exponents

Consider a p-dimensional map

$$x_{n+1} = F(x_n)$$

where x_n is a p-dimensional vector (similar consideration can be applied to differential equations). Let

$$J_n = (J(x_n)J(x_{n-1}).....J(x_1))$$

where $J(x) = \frac{\partial F}{\partial X}$ is the Jacobian matrix of the map. Let

$$j_1(n) > j_2(n) > ..... > j_p(n)$$

be the magnitudes of the eigenvalues of the matrix J_n. Define the Lyapunov numbers to be

$$\lambda_i = \lim_{n\to\infty} [j_i(n)]^{1/n} \qquad i=1,2,...,p \qquad (5.5)$$

with the positive real n-th root taken. They usually depend on the initial condition. They describe the average stability properties of an orbit on an attractor.

For two-dimensional map with Lyapunov numbers λ_1 and λ_2, n iterations transform a small circle of radius δ to an ellipse with major and minor axis $(\lambda_1)^n \delta$ and $(\lambda_2)^n \delta$ respectively. For strange attractor, at least one of the Lyapunov numbers should be greater than one since average neighbour points diverge at an exponential rate. The Lyapunov exponents are just the logarithmns of the Lyapunov numbers. There is only one Lyapunov exponent for one dimensional map $f(\mu, x)$

$$\overline{\lambda}(\mu) = \lim_{n\to\infty} \frac{1}{n} \sum_{i=0}^{n-1} \ln \left| f'(\mu, x_i) \right| \qquad (5.6)$$

This Lyapunov exponent provides a measure of the sensitive dependence on initial conditions.

Suppose two nearby points x_0 and x_0' are separated by ϵ_0. They will separate by ϵ_1 after one iteration where

$$\epsilon_1 = \epsilon_0 \left| f'(x_0) \right|$$

After the second iteration, the separation becomes

$$\epsilon_2 = \epsilon_0 \left| f'(x_0) \right| \left| f'(x_1) \right|$$
$$= \epsilon_1 \left| f^{2'}(x_0) \right|$$

where $x_1 = f(x_0)$

Similarly, after n iterations the separation

$$\epsilon_n = \epsilon_0 \prod_{i=0}^{n-1} \left| f'(x_i) \right| = \epsilon_0 \exp \sum_{i=0}^{n-1} \ln \left| f'(x_i) \right|$$

i.e. $$\epsilon_n = \epsilon_0 \, e^{n \bar{\lambda}(\mu)} \qquad (5.7)$$

If $\bar{\lambda} > 0$, nearby points separate exponentially as $n \to \infty$ and correspond to chaotic orbits. For $\bar{\lambda} < 0$, they approach exponentially and correspond to periodic orbits.

Fig. 5.7 shows the plot of $\bar{\lambda}$ as a function of μ in the map $x_{n+1} = \mu x_n(1-x_n)$. For $\mu < \mu_\infty$ there are only stable cycles and $\bar{\lambda}$ is negative. For $\mu > \mu_\infty$, $\bar{\lambda}$ is mainly positive except at some sharp negative dips which correspond to periodic windows in the chaotic band. Huberman and Rudnick (1980) found that the envelope of $\bar{\lambda}$ for $\mu > \mu_\infty$ exhibits a power-law with

$$\tau = \ln 2 / \ln \delta \qquad (5.8)$$

a universal constant.

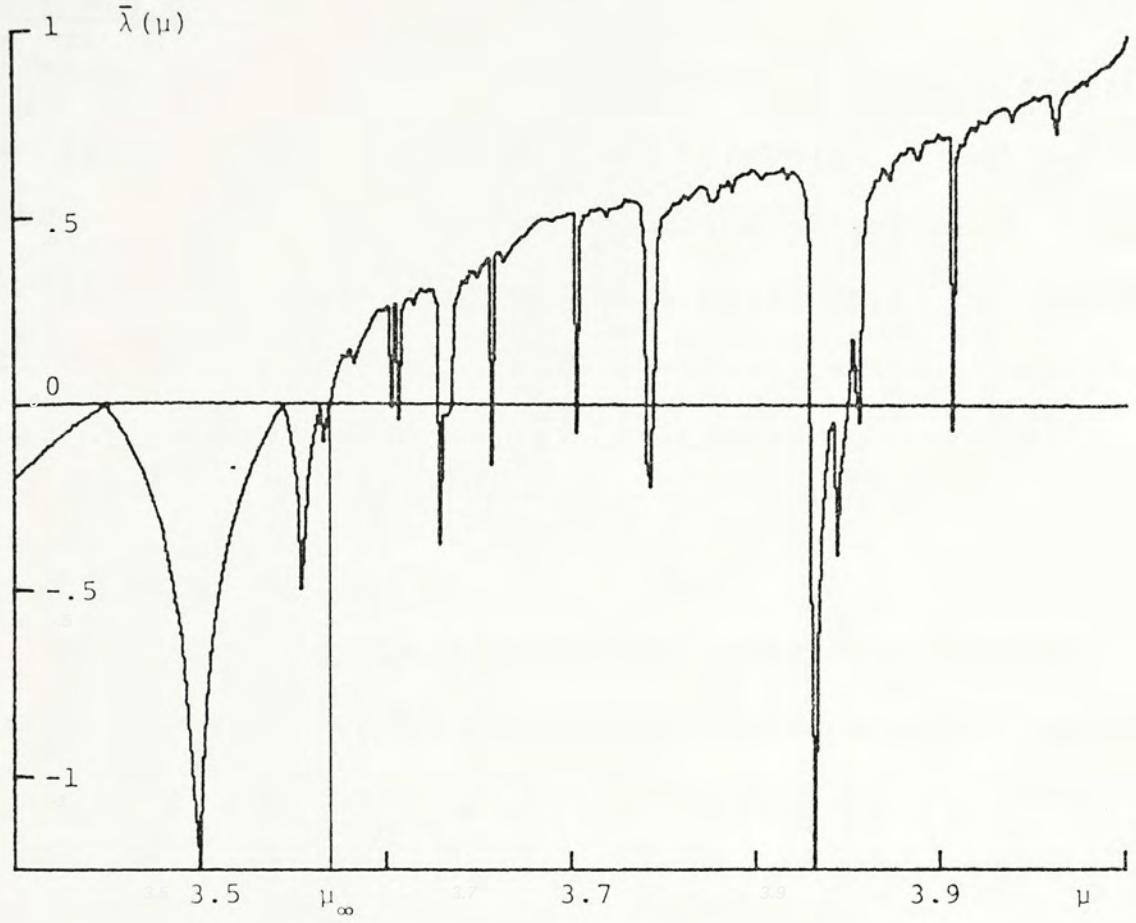

Fig. 5.7 Graph of the Lyapunov exponent as a function of μ in the map $x_{n+1} = \mu x_n(1-x_n)$. (after Collet and Eckmann (1980), p.33)

5.3 Crises of chaotic attractor

Sometimes there are sudden changes in chaotic attractor as a system parameter is changed. Grebogi et al. (1982) defined a crisis to be a collision between a chaotic attractor and a coexisting unstable fixed point or periodic orbit. After a crisis, there are qualitative changes of chaotic attractor.

5.3.1 Boundary crisis

The concept of crisis can be best illustrated by one-dimensional map (Grebogi et al.,1982). For example consider

$$x_{n+1} = C - x_n^2 \qquad (5.9)$$

At $C = -1/4$ a tangent bifurcation occurs and creates a pair of stable and unstable fixed points. It is easy to show that

$x = -1/2 + (1/4 + C)^{1/2}$ is a stable fixed point and

$x = -1/2 - (1/4 + C)^{1/2}$ is an unstable fixed point.

The stable fixed point undergoes a series of period-doubling followed by chaos. The basin of attraction for the stable branch for $-1/4 \leqslant C \leqslant 2$ is $x < x^*$ where $x^* = 1/2 + (1/4 + C)^{1/2}$. The unstable fixed point $x = -x^*$ is on the boundary of the basin of attraction. Outside the basin of attraction, all points are attracted to $x = -\infty$. At $C = 2$ the chaotic attracting orbit is destroyed and all initial points are attracted to $x = -\infty$ (Fig. 5.8). A crisis occurs at $C = 2$.

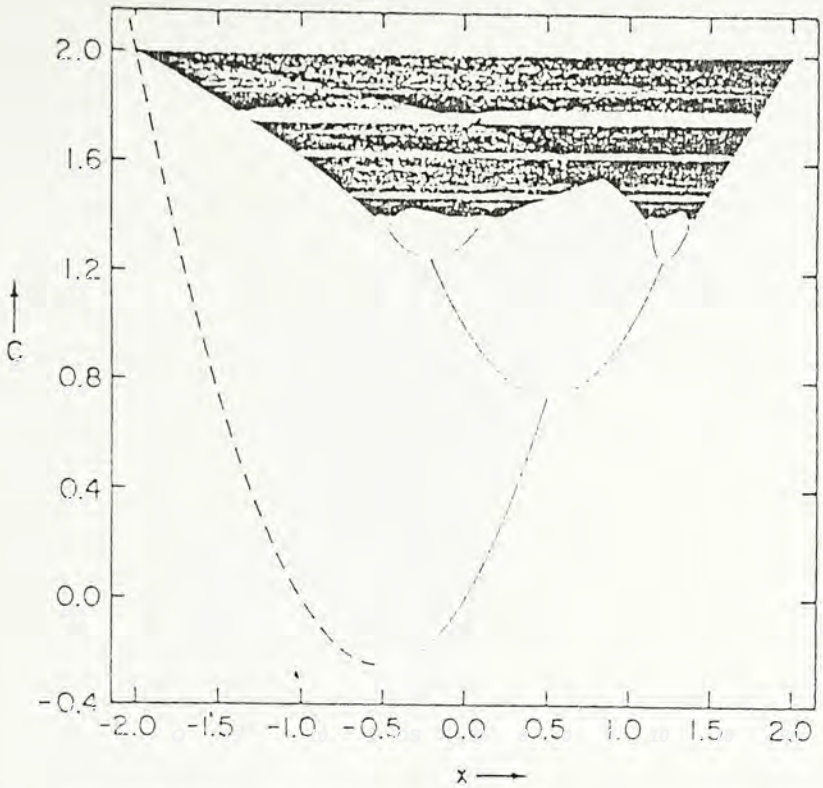

Fig. 5.8 Boundary crisis of the map (5.9). The unstable fixed points lie on the boundary of the basin of attraction. (after Grebogi, Ott and Yorke (1983), p.183)

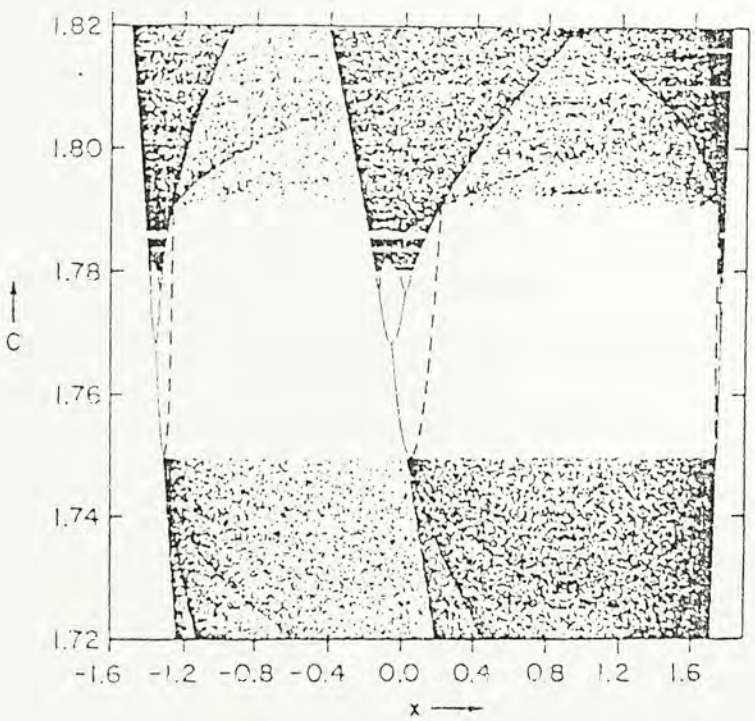

Fig. 5.9 Interior crisis of the map (5.9). The unstable fixed points lie within the basin of attraction. (after Grebogi, Ott and Yorke (1983), p.184)

The chaotic attractor and its basin of attraction disappear at $C = 2$ because an orbit started at $|x| < x^*$ will look chaotic at first but once it is below $-x^*$, it will be repelled by the unstable fixed points and attracted to $-\infty$. Grebogi et al. (1983) suggested that the inverse boundary crises, that is, the sudden appearence of a strange attractor and its basin of attraction may be another possible route to chaos. At $C = 2$ the collision of the chaotic band with the unstable fixed point is called boundary crisis since the unstable fixed point is on the boundary of the basin of attraction. Other types of crises are possible.

5.3.2 Interior crises

If the collision with an unstable orbit happens within the basin of attraction, the crisis is called an interior crisis (Fig. 5.9). Consider the map discussed above. A period-3 orbit is formed by tangent bifurcation. The stable period-3 undergoes a series of period-doubling and followed by chaos. The unstable period-3 lies within the basin of attraction of the stable orbit. At $C = C^* = 1.79$ the unstable orbit collides with the chaotic attractor and the three chaotic bands suddenly widen to form a single chaotic band. An interior crisis has occured.

CHAPTER 6

Limit cycle oscillation with external forcing

6.1 Motivation

In chapter 4 we have discussed various routes to chaos in deterministic systems. One of them is through the development of incommensurate frequencies, with at least two independent frequencies. A nonlinear oscillator coupled to external driving force is an example. Usually the oscillator itself has limit cycle oscillations with different natural frequencies as the parameters are changed.

The forced Brusselator:

$$\begin{aligned} \dot{x} &= A-(B+1)x+x^2y+\alpha\cos\omega t \\ \dot{y} &= Bx-x^2y \end{aligned} \tag{6.1}$$

is a system of ODE describing a nonlinear oscillator driven by an external periodic force. It has been extensively examined. One particular feature in this system is the beating-entrainment transition for weak driving force and full entrainment for larger driving force. The natural period T_o (which depends on the parameters A, B as well as the amplitude of oscillation) beats against the driving period T for weak driving force. Usually T_o and T are incommensurate. As the driving force increases, T_o will lock onto a rational multiple of T. This is called the beating-entrainment transition and the entrainment is partial in the sense that T_o is still present as a rational multiple of

T. With increasing force, the system goes through a period-doubling route to chaos, followed by an inverse cascade back to periodic motion at the driving period T. The system is completely entrained to the external driving period T and now the natural period T_o is completely forgotten.

In this chapter, we shall investigate the corresponding situation in iterated maps, which can be studied more efficiently by computer. The logistic maps e.g.

$$x_{n+1} = 1 - \lambda x_n^2 \tag{6.2}$$

provide limit cycle oscillations with periods T_o = $1,2,4,\ldots. 2^n$ as λ is increased. For $\lambda > \lambda_\infty = 1.401$, there are many narrow periodic windows corresponding to $T_o = 3.2^n$, 5.2^n,.....arranged according to the MSS sequence. Suppose an external driving force is added to (6.2):

$$x_{n+1} = 1 - \lambda x_n^2 + \sigma s_n \tag{6.3}$$

where s_n is a fixed sequence with integer period T, i.e. $s_{n+T} = s_n$. The $\sigma = 0$ limit is well-known. The presence of two different periods T_o and T makes this a convenient model to study the onset of chaos.

More generally one can envisage a force with arbitrary period, i.e. $s_n = s(\gamma n)$, where s(t) is a function of period 1, so that s_n formally has period $1/\gamma$. Considered in terms of the three parameters (λ , σ , γ), it is clear that there will be periodic windows or 'tongues' due to frequency locking near rational values of γ, in a Farey sequence. The model (6.3) corresponds to a cross section through the (λ ,

σ, γ) space at rational value of γ and may be thought of as a method of selecting and studying only one 'tongue' at a time.

6.2 Period 3 driving force

6.2.1 Small driving force

We first study the case T=3 with $s_1 = 0.5$, $s_2 = 0$ and $s_3 = -0.5$.

The results are presented as x- σ bifurcation diagrams for different fixed λ. They are obtained by plotting 100 iterations by (6.3) after neglecting some transients. Choosing different λ represents choosing different natural periods. To compare with the stroboscopic sampling of differential equations, only the set $Y_n = x_{3n}$ is shown. The other sets x_{3n+1} and x_{3n+2} can be obtained by iteration by (6.3) and hence are topologically similar. As usual we use the notation nP and nI to represent period n in the direct and the inverse sequence of chaotic bands in Y_n respectively. In x_n, these represent period 3n in the direct and inverse sequence respectively. Therefore full entrainment corresponds to 1P. Here we pay particular attention to the small σ region ($\sigma \lesssim 0.7$) which corresponds to the transition from partial entrainment to full entrainment.

For small λ, e.g. $\lambda = 0.5$, $T_o=1$ we have period 1 in Y_n (or period 3 in x_n) for a wide range of σ (Fig 6.1a). For $\lambda = 0.77$ the natural $T_o=2$, and there is a transition from partial entrainment (2P) for small σ to complete entrainment (1P) as σ is increased (Fig 6.1b). The case of

λ =0.9 (T_o = 2) is similar except complete entrainment occurs at larger σ (Fig 6.1c). For still larger λ , e.g. λ = 1.0, there is a sequence of 2P $\longrightarrow$ 4P $\longrightarrow$ 2P $\longrightarrow$ 1P as σ is increased (Fig.6.1d) . In the diagram, the 2P $\longrightarrow$ 4P $\longrightarrow$ 2P transition looks like a small bubble. As λ is increased further, the number of bifurcations in the cascade-anticascade 2P $\longrightarrow$ 4P $\longrightarrow$ .....2^nP ..... $\longrightarrow$ 4P $\longrightarrow$ 2P $\longrightarrow$ 1P increases. This means the system goes through a series of period doubling and period halving back to full entrainment. We observe that there are smaller bubbles inside bubbles. Finally, for larger λ , e.g. λ = 1.1 or 1.2, the cascade and anticasade are separated by an aperiodic band (Figs. 6.1e and 6.1f).

The results for small σ are summarized in the $\lambda - \sigma$ plane on Fig. 6.2. The boundary of major periodic windows are drawn. For fixed λ , each boundary is crossed twice as σ is increased, showing the mirror image symmetry.

6.2.2 Aperiodic band

The aperiodic band for λ = 1.1 is studied in detail. Aperiodic bands for other values of λ are similar. Some larger periodic windows can be observed in Fig. 6.1e. If we enlarge the parts corresponding to the period doubling cascade and anticascade (Fig. 6.3 and Fig. 6.4) , more windows and the merging of chaotic bands can be easily seen . Fig. 6.5 shows the blow-up of the rectangular part of Fig.

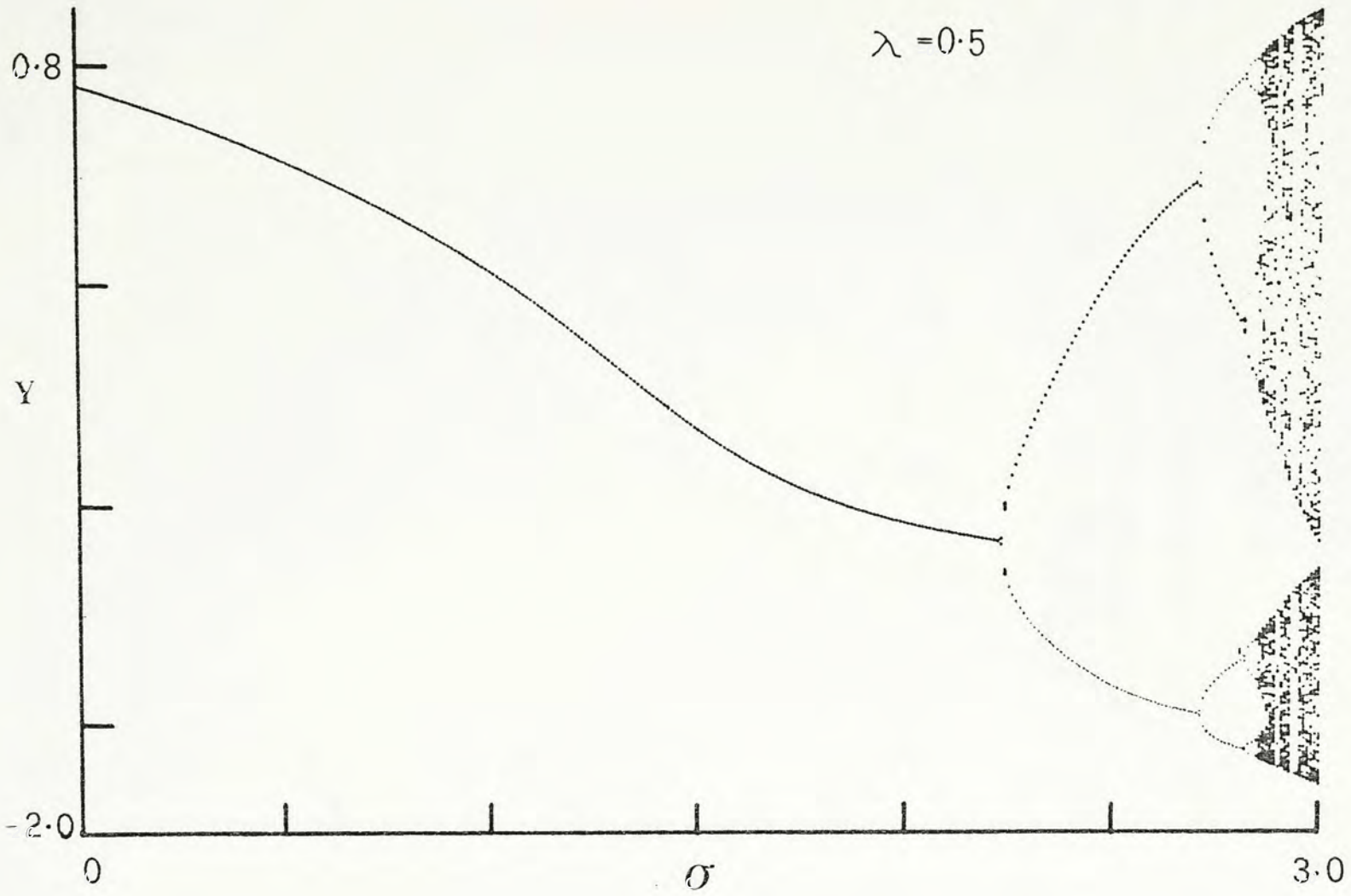

Fig. 6.1a

Fig. 6.1 y- σ bifurcation diagram for different λ. The attractors are obtained by plotting 100 iterations by (6.3) after neglecting some transients. a) λ = 0.5, b) λ = 0.77, c) λ = 0.9, d) λ = 1.0, e) λ = 1.1, f) λ = 1.2

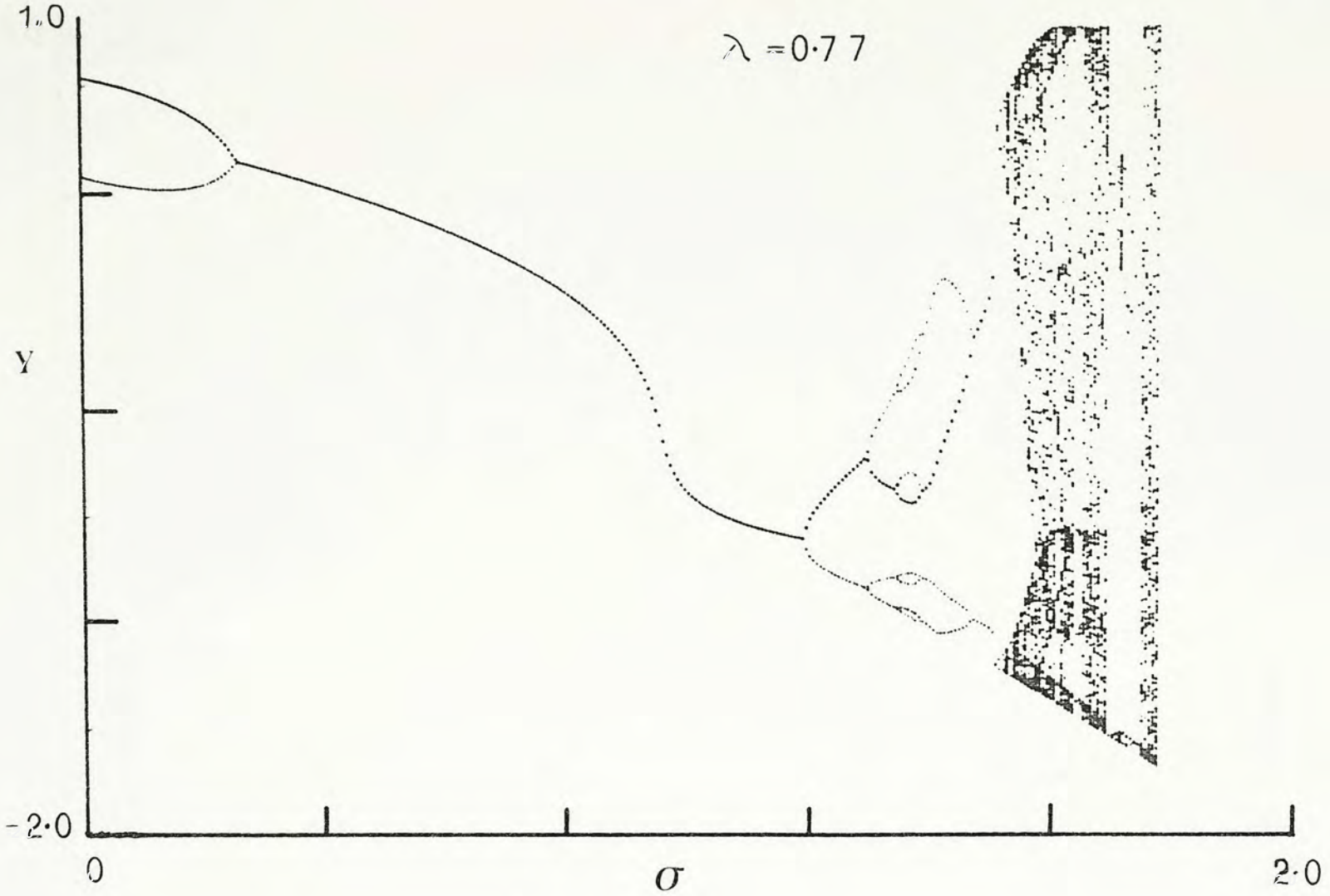

Fig. 6.1b

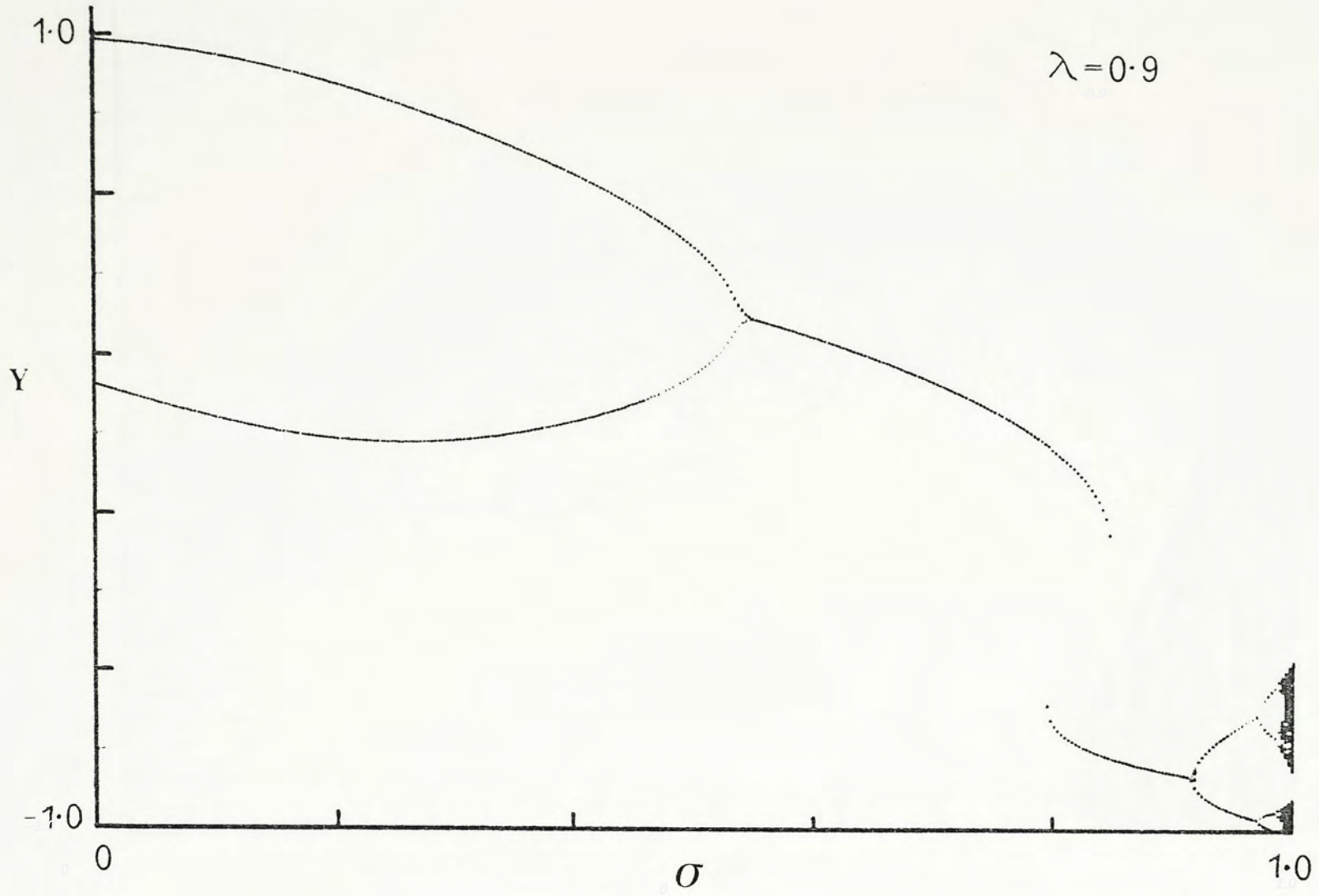

Fig. 6.1c

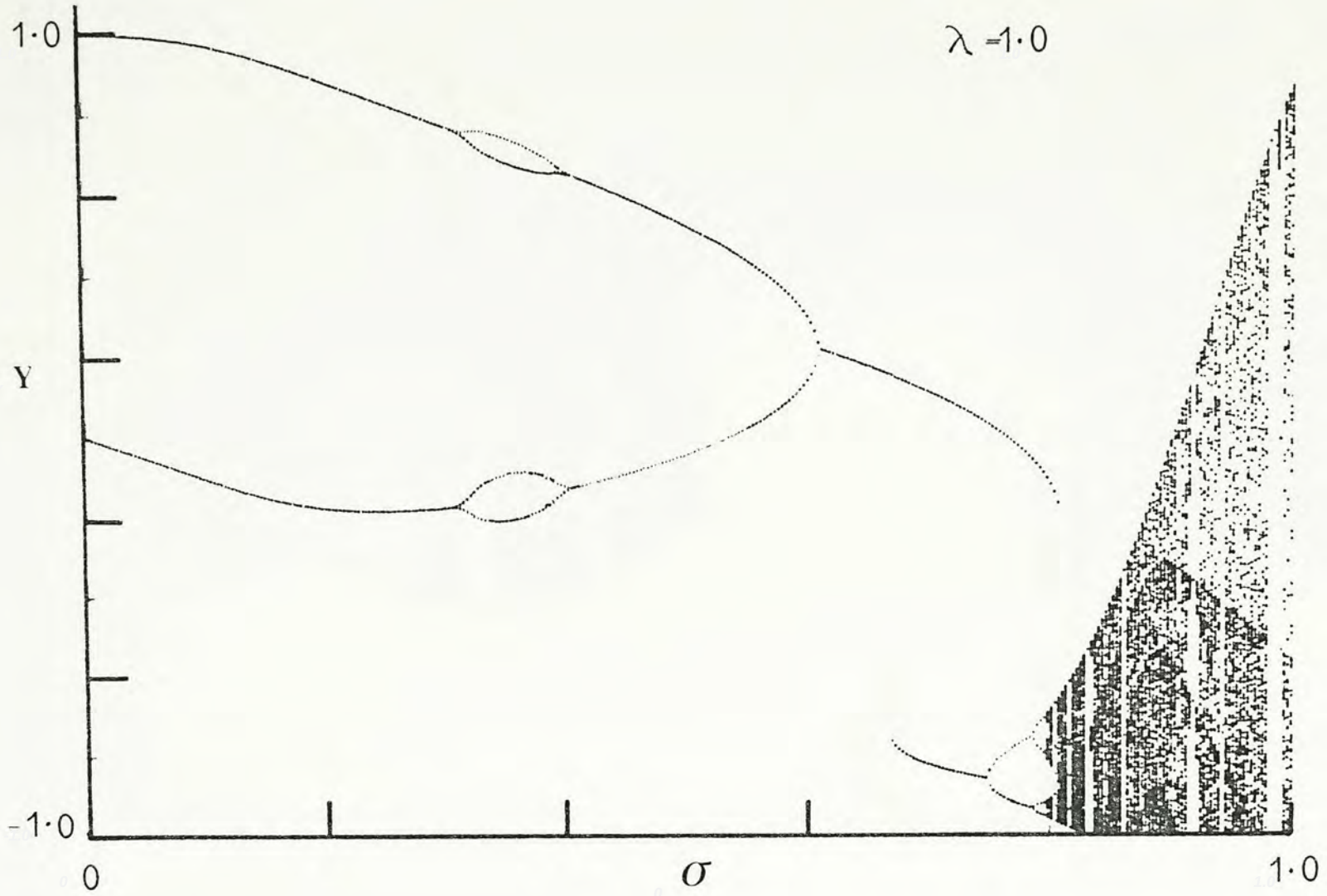

Fig. 6.1d

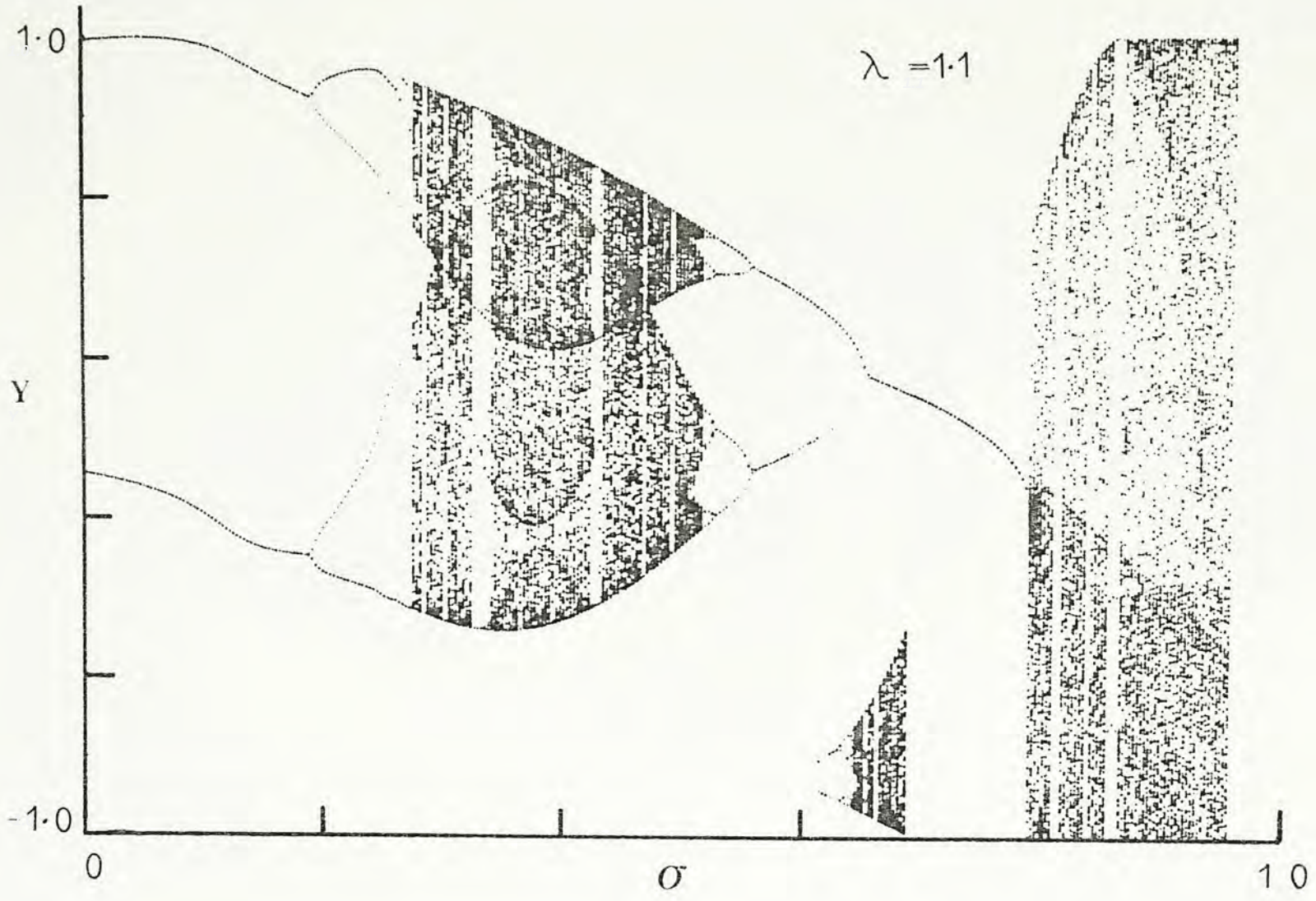

Fig. 6.1e

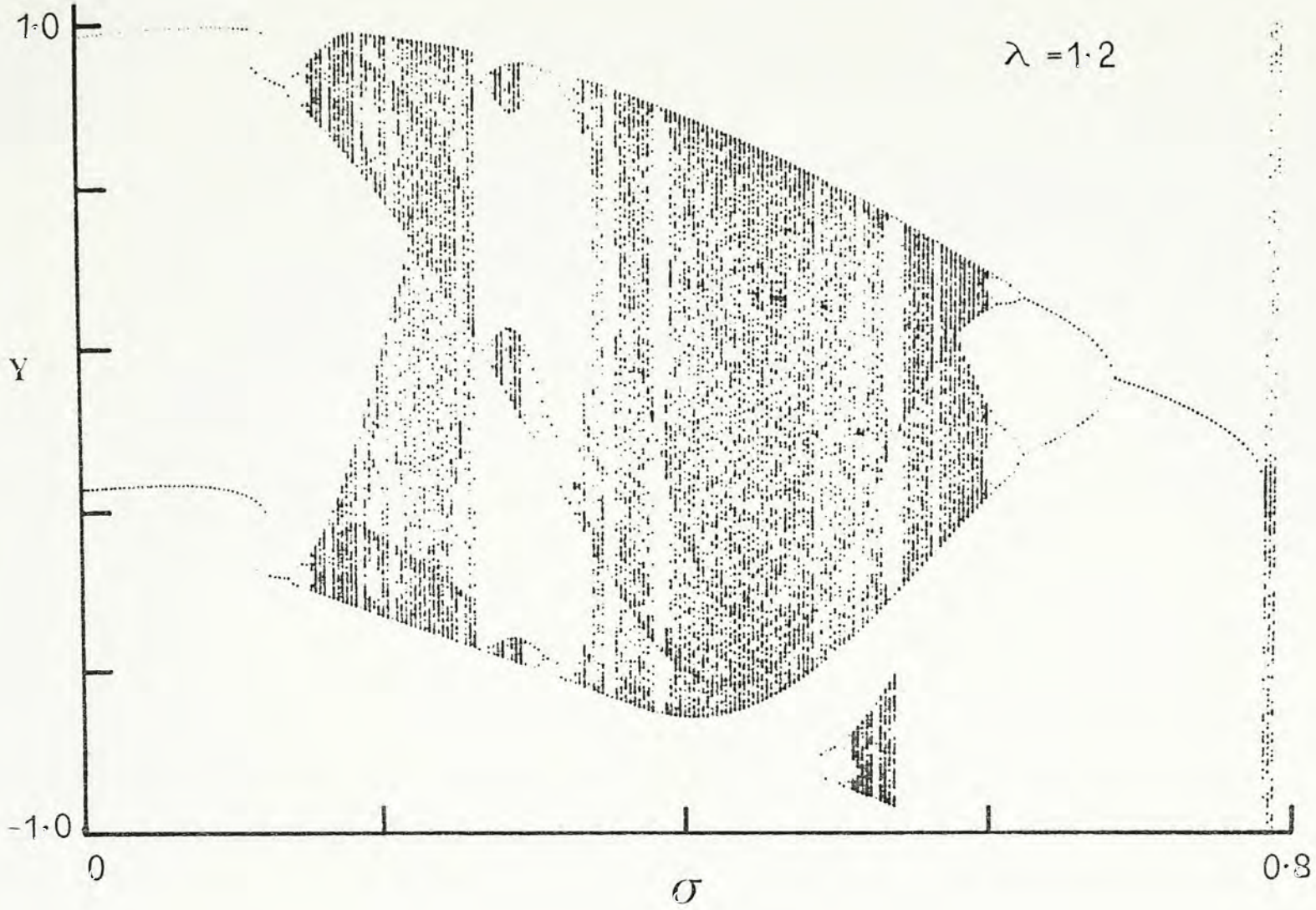

Fig. 6.1f

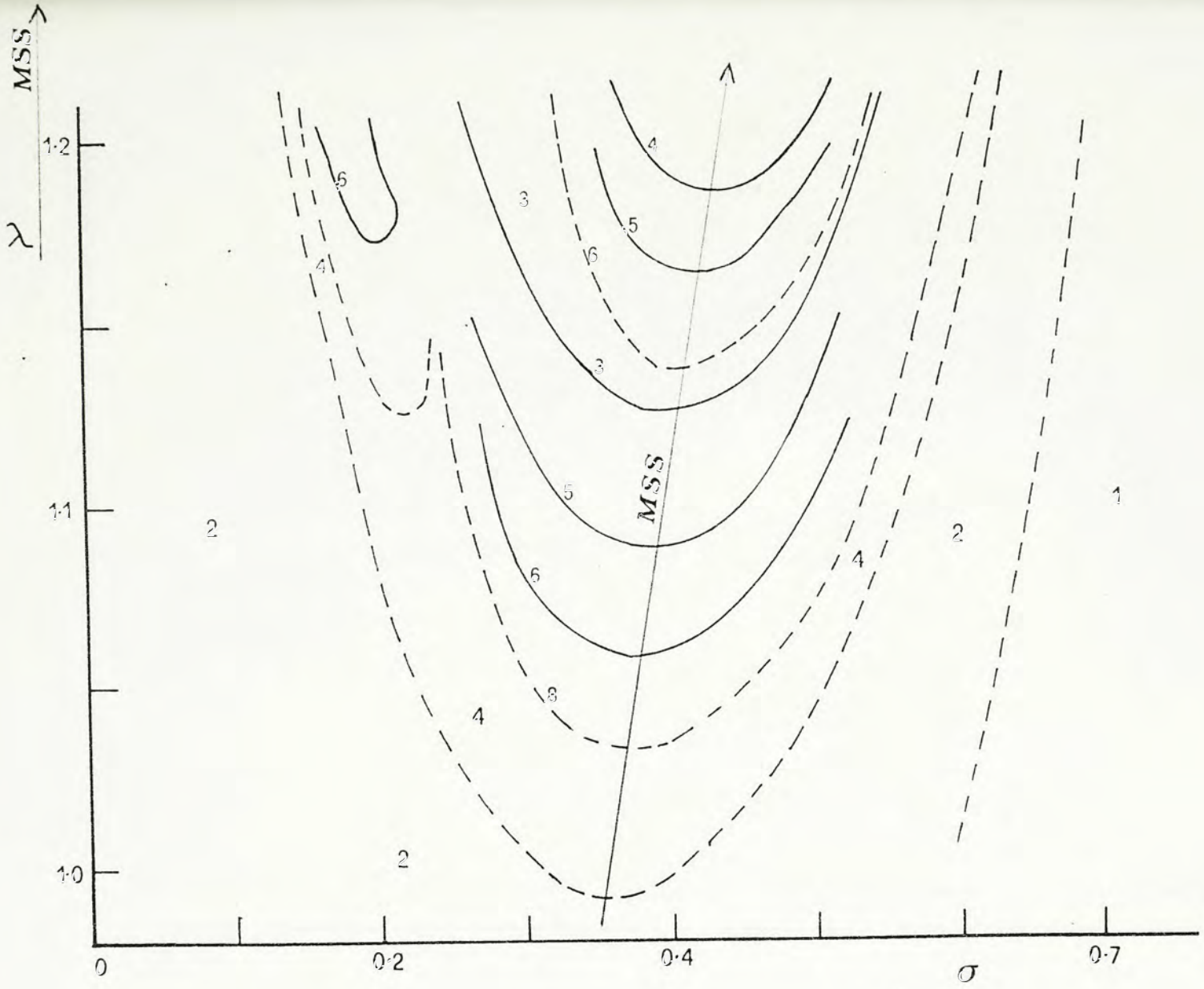

Fig. 6.2 λ - σ plane for small σ .

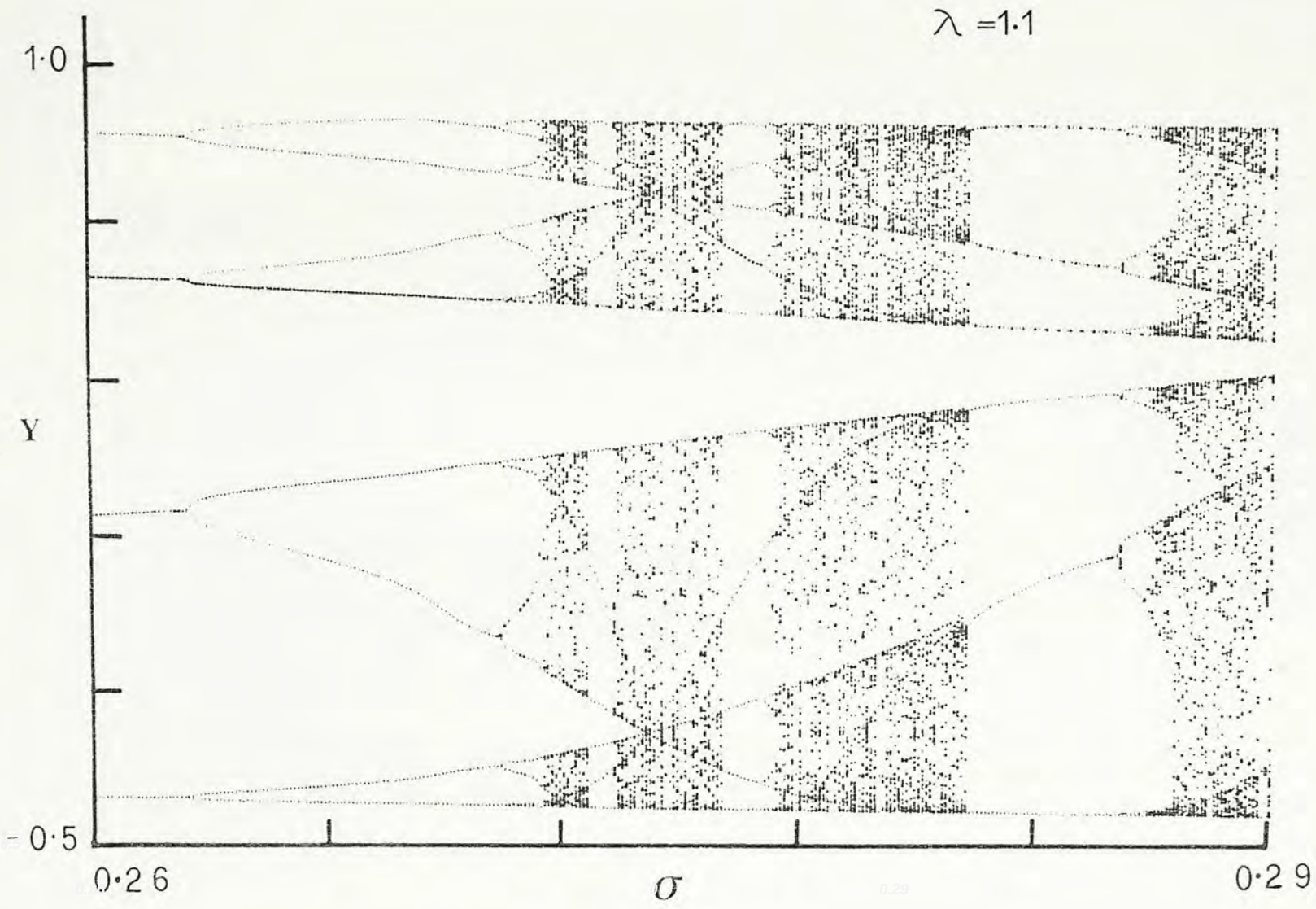

Fig. 6.3 $y - \sigma$ bifurcation diagram for λ =1.1 with σ from 0.26 to 0.29

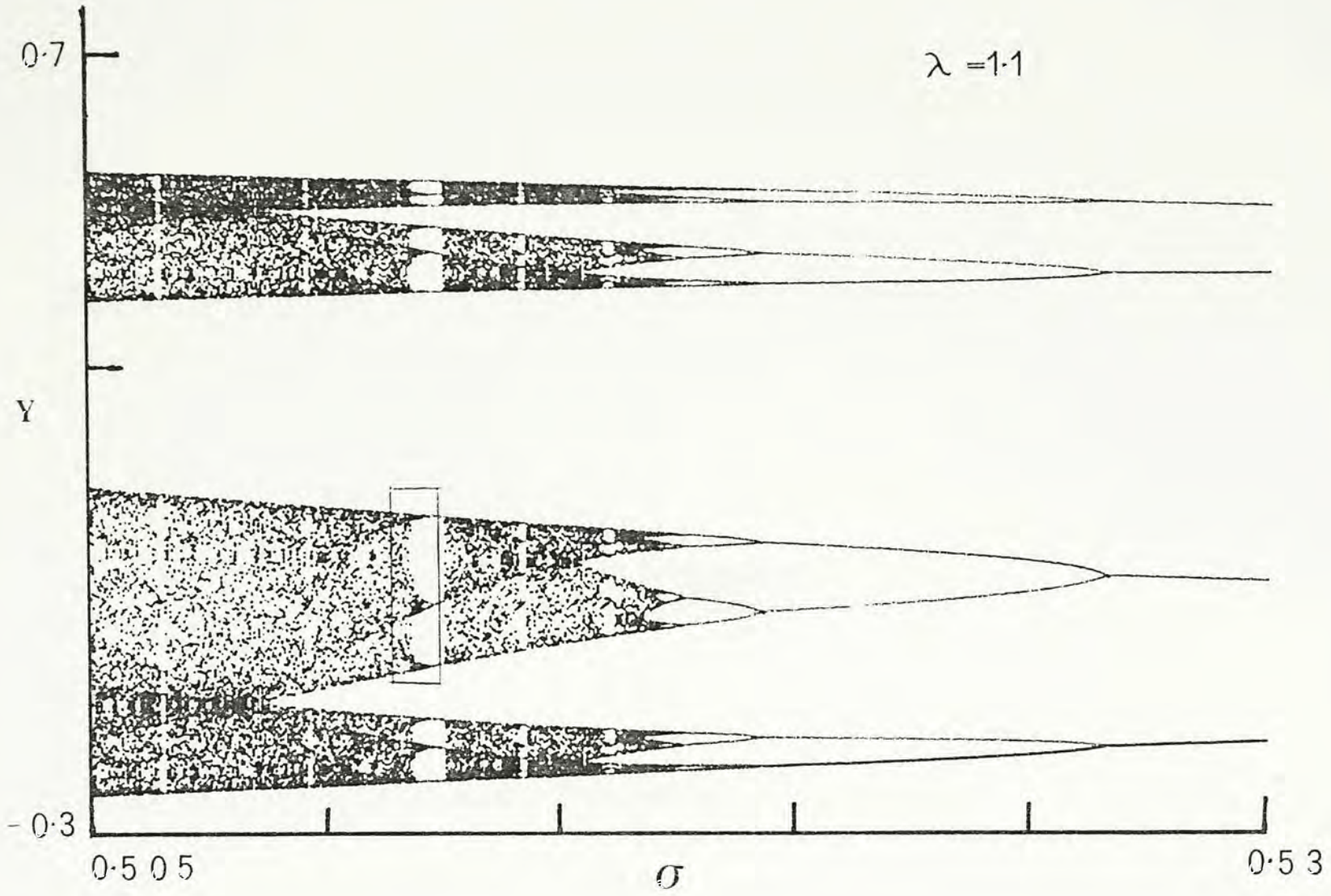

Fig. 6.4 η - σ bifurcation diagram for λ =1.1 with σ from 0.505 to 0.53

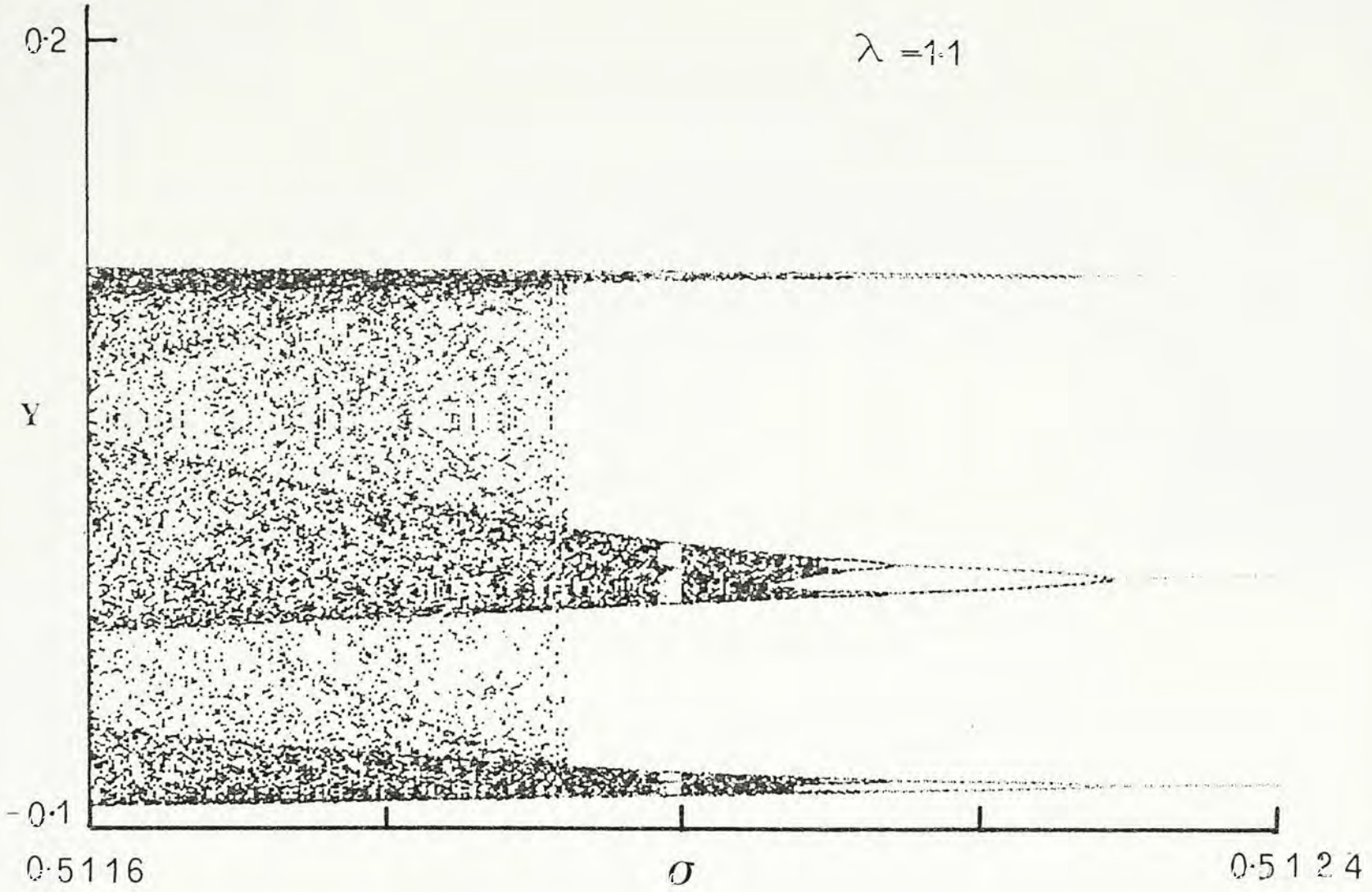

Fig. 6.5 Enlarged diagram for the rectangle in Fig. 6.4

6.4 . The feature of self-similarity is clearly observed. Other major windows embedded are found by searching in steps of 5×1.0^{-5} in σ and summarized in Table 6.1. For the primary windows, we can see there exists a mirror image symmetry. For $\sigma < \sigma_m = 0.38$, the periodic attractors are bounded on the left (small σ side) by a tangent bifurcation and on the right by period doubling. The situation is reversed for $\sigma > \sigma_m$.

Besides periodic windows, prominent dark bands embedded in the aperiodic region can be observed in Figs. 6.1e and 6.1f. These bands correspond to the inverse sequence. The distinction between periodic motion, the inverse sequence and chaos is best exhibited by the power spectrum associated with the sequence y_n. They are calculated by Fourier transforming 256 points in the sequence with 400 initial points discarded and are shown on a logarithic scale in Fig. 6.6.

In these power spectra, periodic motions are characterized by sharp peaks (delta function) and motions in the inverse sequence by peaks standing above noisy background, whereas chaos is represented by completely noisy power spectrum. The corresponding nP and nI power spectra are put together for comparision:

2P (σ=0.150), Fig. 6.6a ; 2I (σ=0.500), Fig. 6.6b;

4P (σ=0.230), Fig. 6.6c ; 4I (σ=0.514), Fig. 6.6d;

8P (σ=0.265), Fig. 6.6e ; 8I (σ=0.526), Fig. 6.6f;

5P (σ=0.330), Fig. 6.6g ; 5I (σ=0.338), Fig. 6.6h;

σ	Period
0.27275- 0.27325	12 <
0.27465- 0.27480	14 <
0.27620- 0.27705	10 <
0.27875- 0.27885	14 <
0.28010- 0.28015	16 <
0.28240- 0.28585	6 <
0.28975- 0.28980	10 <
0.29310- 0.29320	8 <
0.30195- 0.30240	7 <
0.30995- 0.31005	9 <
0.32625- 0.33265	5 <
0.36595- 0.36620	9 <
0.39585- 0.39605	> 9
0.42985- 0.43320	> 5
0.45020- 0.45025	> 9
0.46010- 0.46035	> 7
0.47865- 0.47870	> 8
0.49305- 0.49445	> 6
0.50315- 0.50330	> 10
0.51235- 0.51255	> 12

Table 6.1 Windows embedded in the aperiodic band

< denotes the direction of period-doubling

e.g. 6 < means 6→12→24...

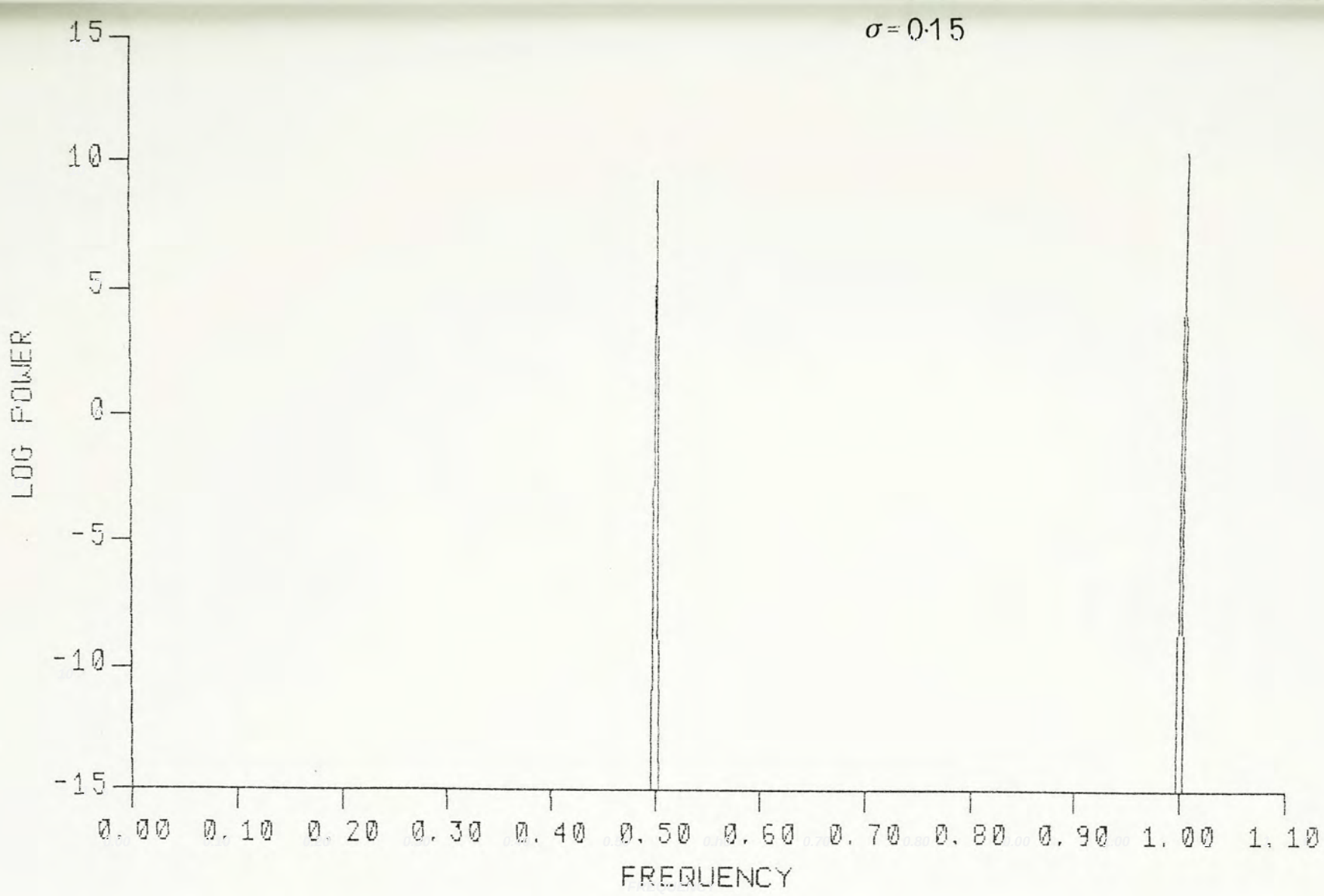

Fig. 6.6a

Fig. 6.6 Power spectra on logarithmic scale for different σ ($\lambda = 1.1$). a) $\sigma = 0.15$, b) $\sigma = 0.5$, c) $\sigma = 0.23$, d) $\sigma = 0.514$, e) $\sigma = 0.256$, f) $\sigma = 0.516$, g) $\sigma = 0.33$, h) $\sigma = 0.338$, i) $\sigma = 0.494$, j) $\sigma = 0.491$, k) $\sigma = 0.3$

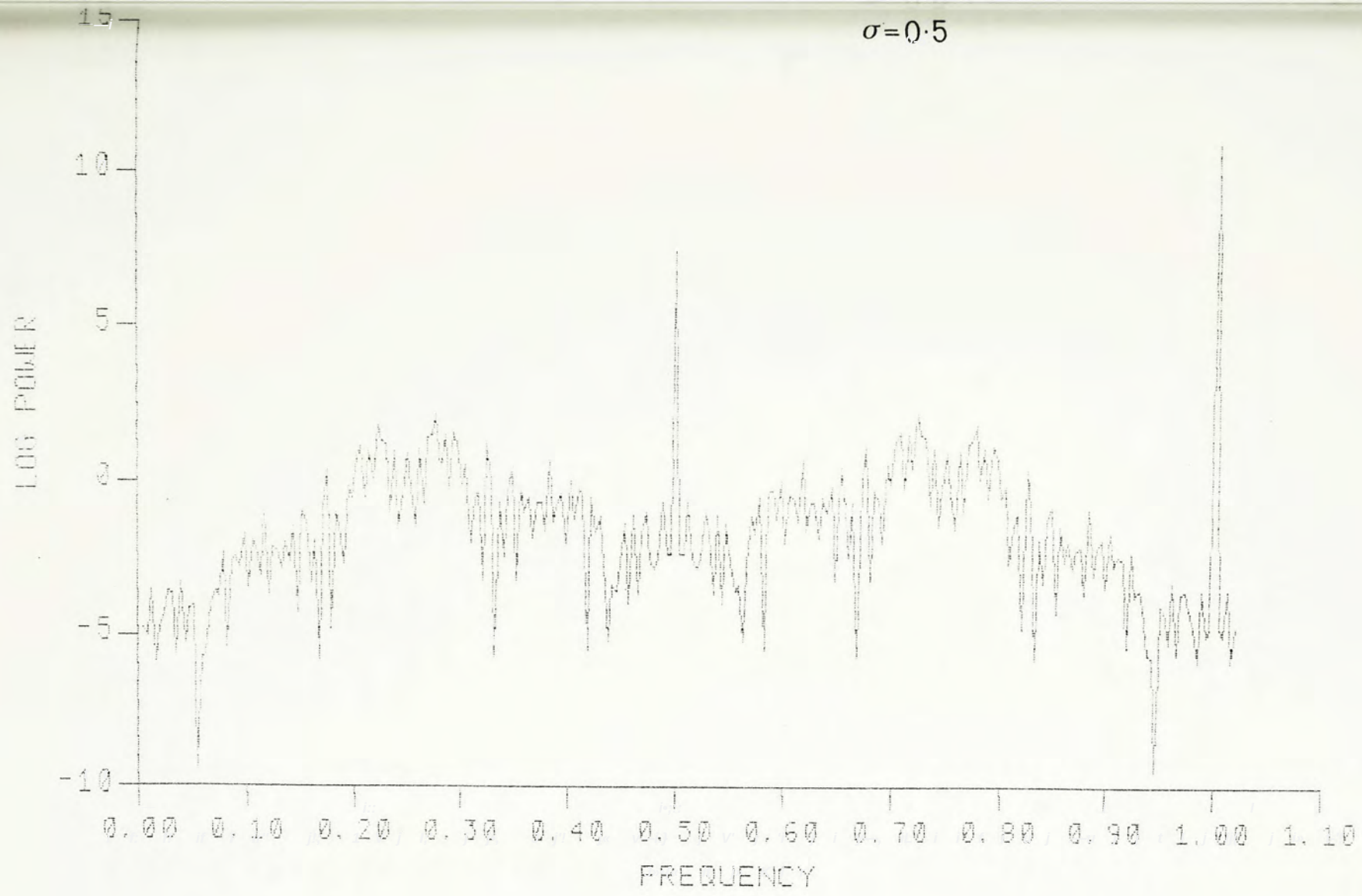
σ=0·5
15
10
5
0
-5
-10
LOG POWER
0.00
0.10
0.20
0.30
0.40
0.50
0.60
0.70
0.80
0.90
1.00
1.10
FREQUENCY

Fig. 6.6b

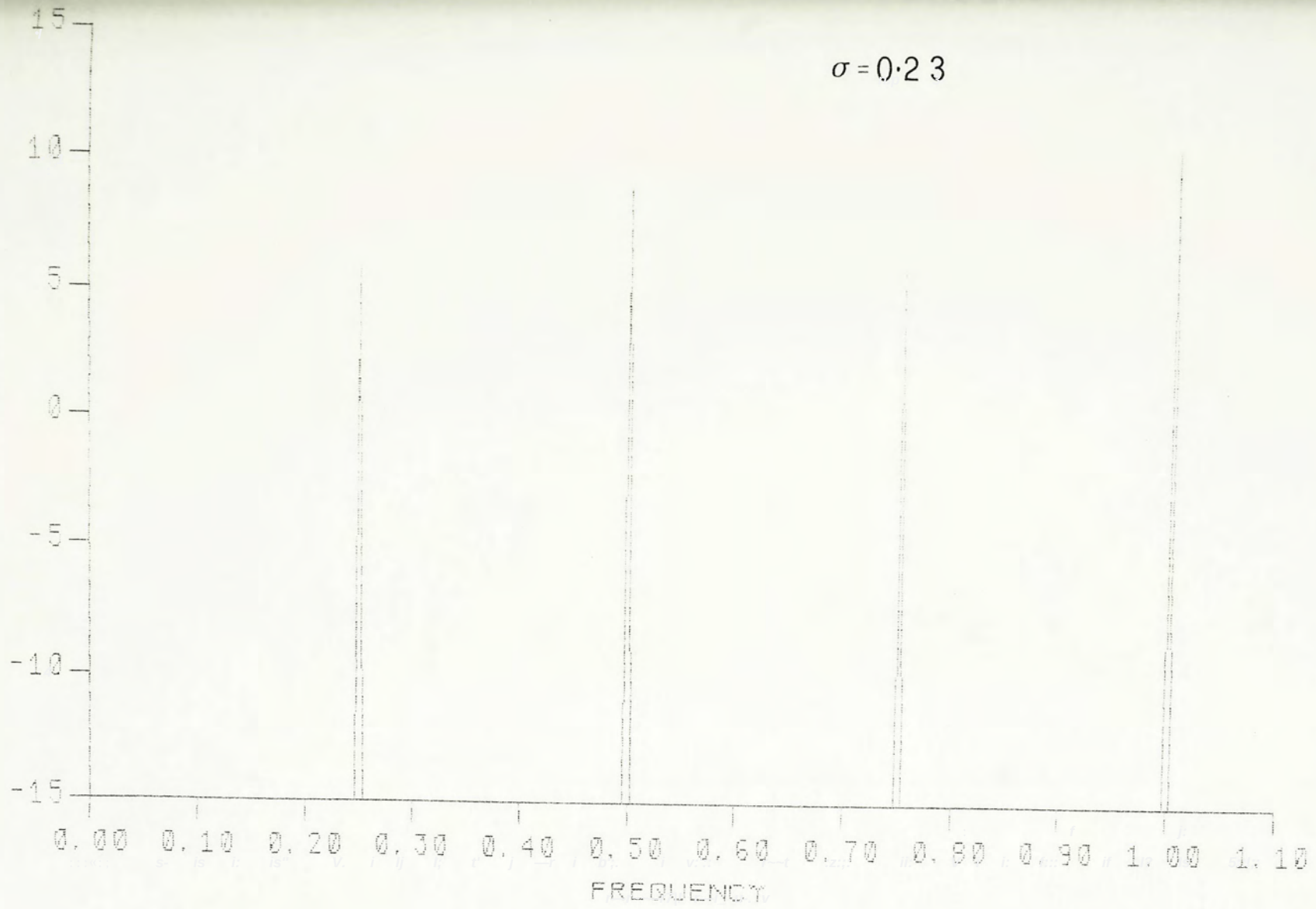
σ = 0·2 3
15
10
5
0
-5
-10
-15
LOG POWER
0.00 0.10 0.20 0.30 0.40 0.50 0.60 0.70 0.80 0.90 1.00 1.10
FREQUENCY

Fig. 6.6c

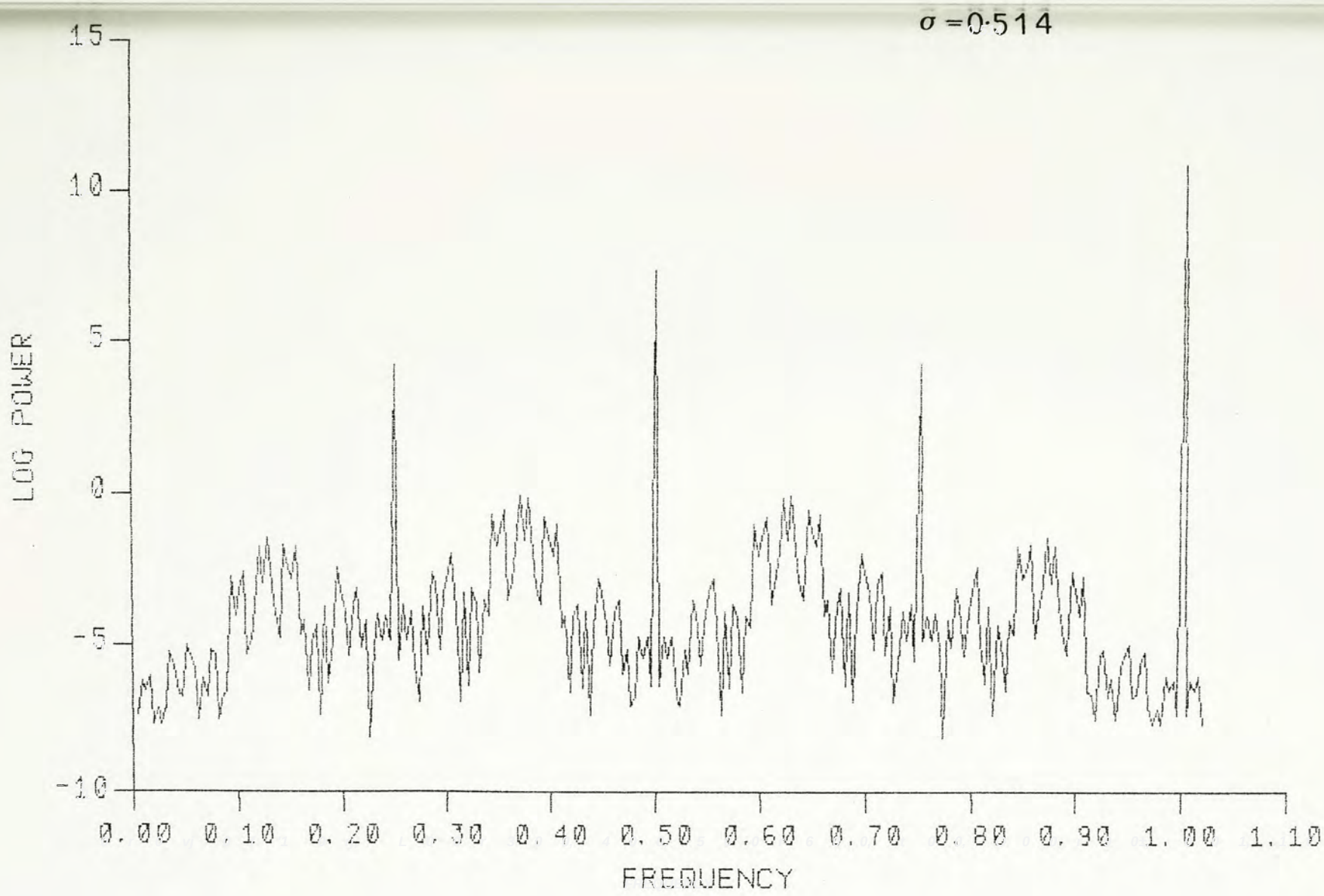
σ =0·514
15
10
5
0
-5
-10
LOG POWER
0.00 0.10 0.20 0.30 0.40 0.50 0.60 0.70 0.80 0.90 1.00 1.10
FREQUENCY

Fig. 6.6d

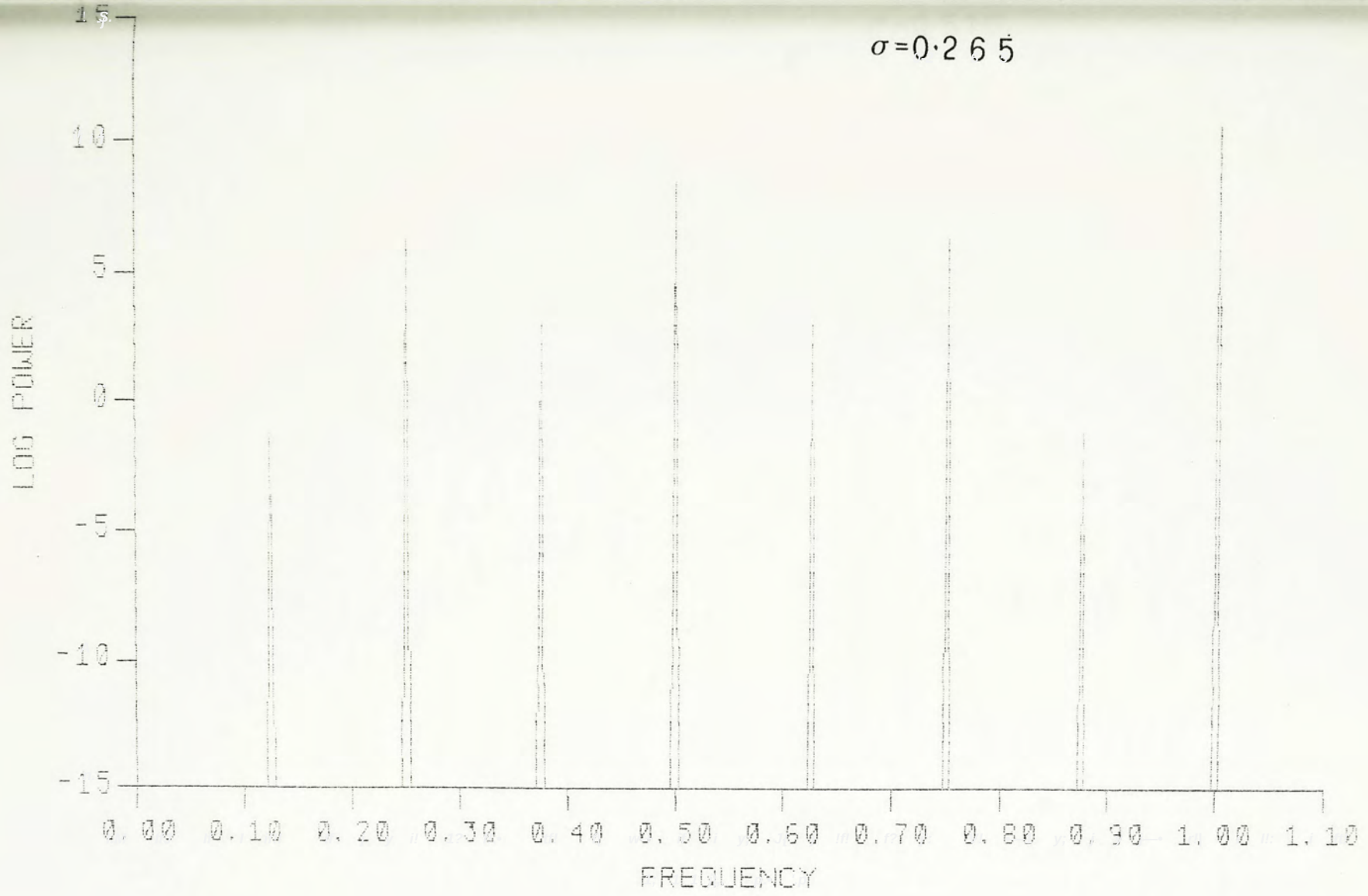
σ=0·265
15
10
5
0
-5
-10
-15
LOG POWER
0.00 0.10 0.20 0.30 0.40 0.50 0.60 0.70 0.80 0.90 1.00 1.10
FREQUENCY

Fig. 6.6e

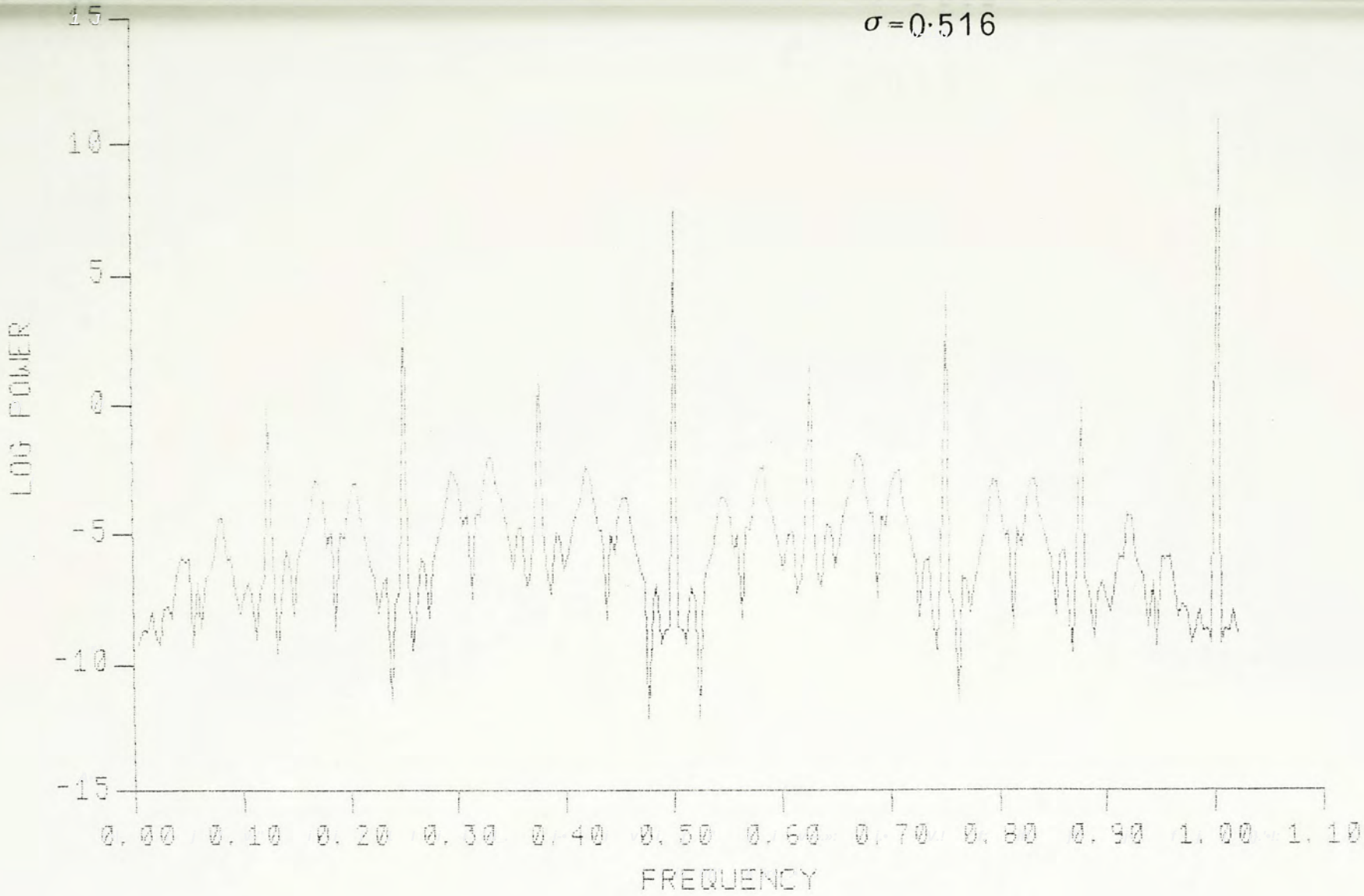
σ=0·516
15
10
5
0
-5
-10
-15
LOG POWER
0.00
0.10
0.20
0.30
0.40
0.50
0.60
0.70
0.80
0.90
1.00
1.10
FREQUENCY

Fig. 6.6f

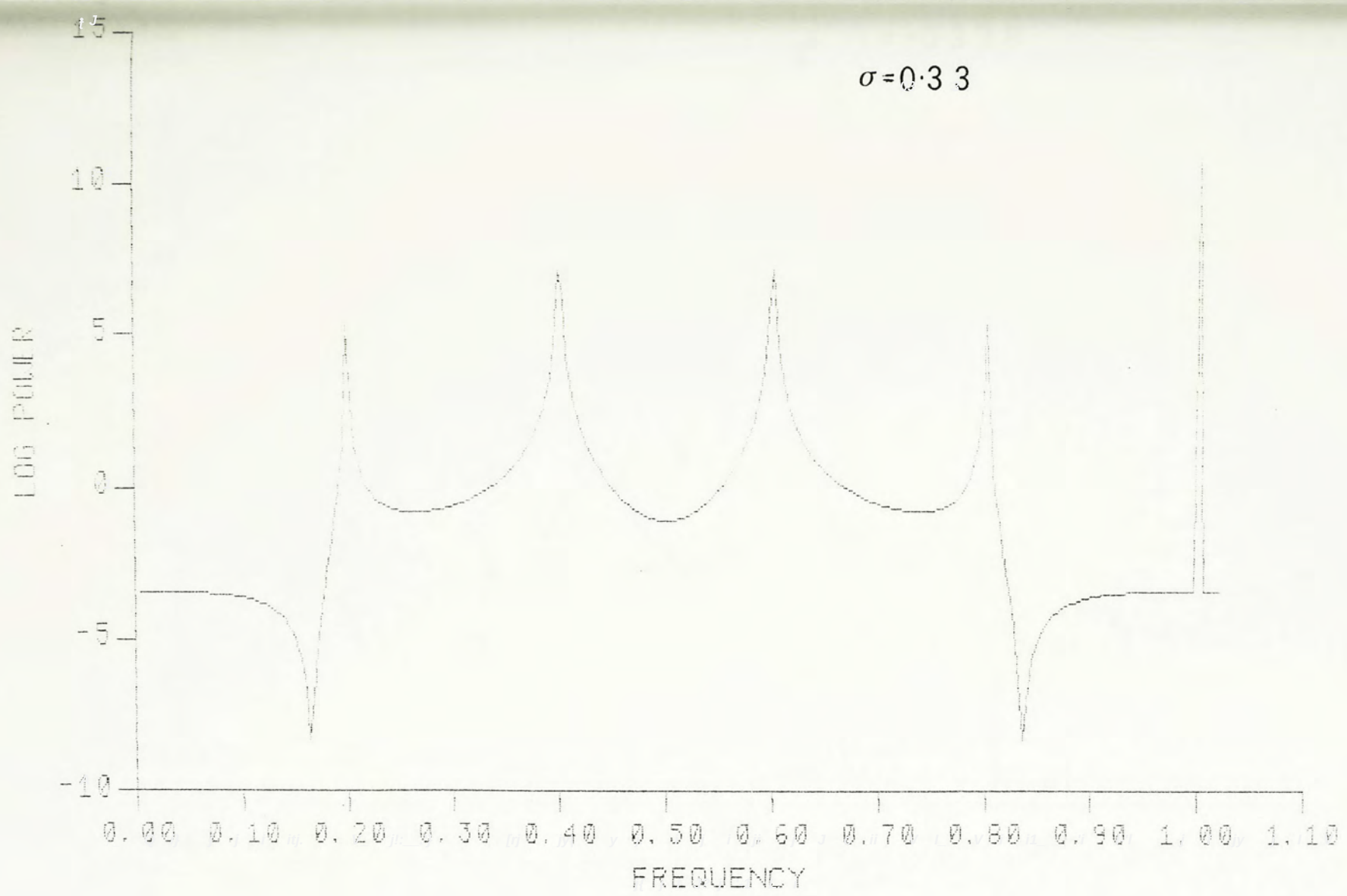
σ=0·33
15
10
5
0
-5
-10
LOG POWER
0.00
0.10
0.20
0.30
0.40
0.50
0.60
0.70
0.80
0.90
1.00
1.10
FREQUENCY

Fig. 6.6g

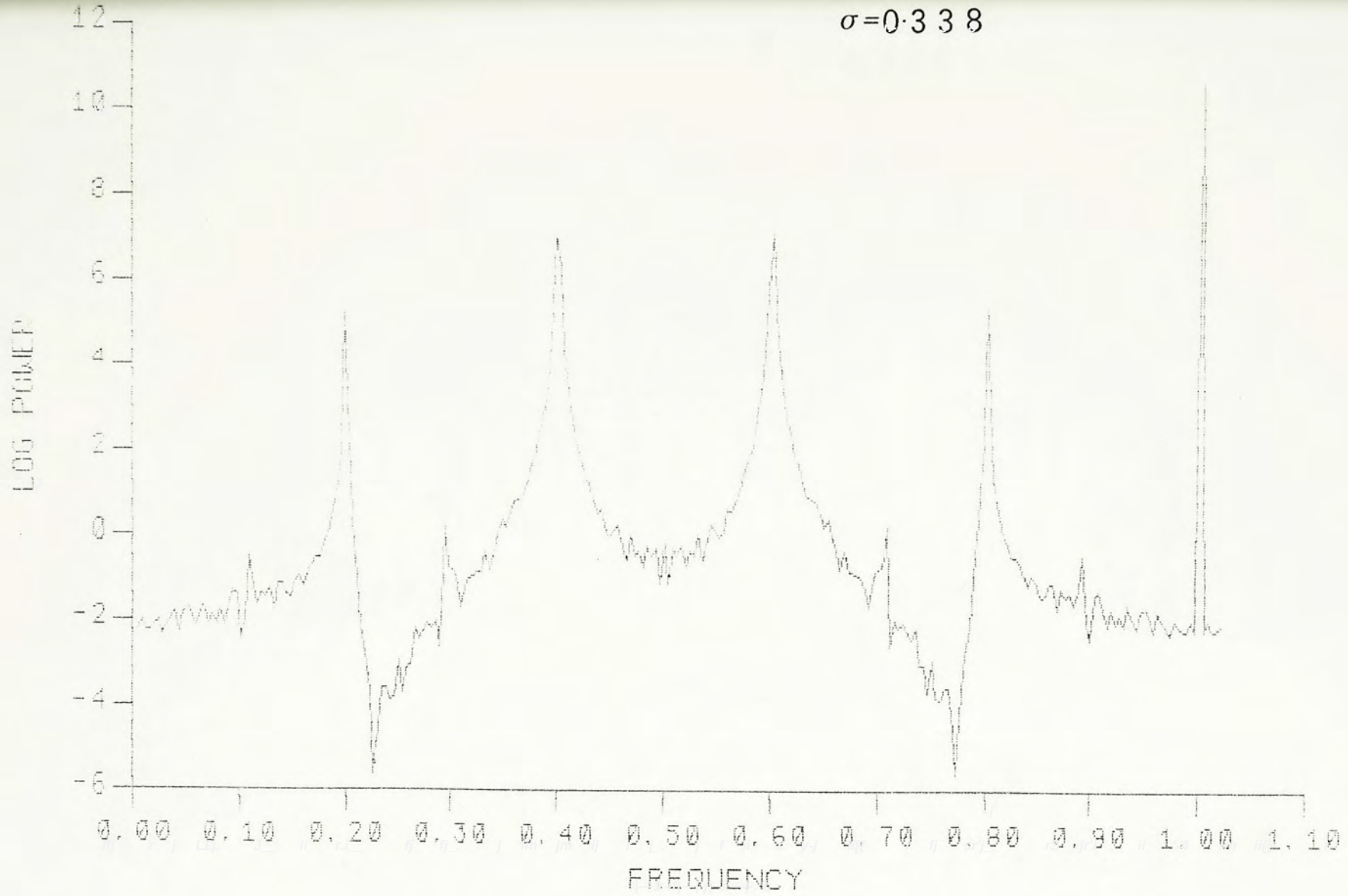
σ=0·338
LOG POWER
12
10
8
6
4
2
0
-2
-4
-6
0.00
0.10
0.20
0.30
0.40
0.50
0.60
0.70
0.80
0.90
1.00
1.10
FREQUENCY

Fig. 6.6h

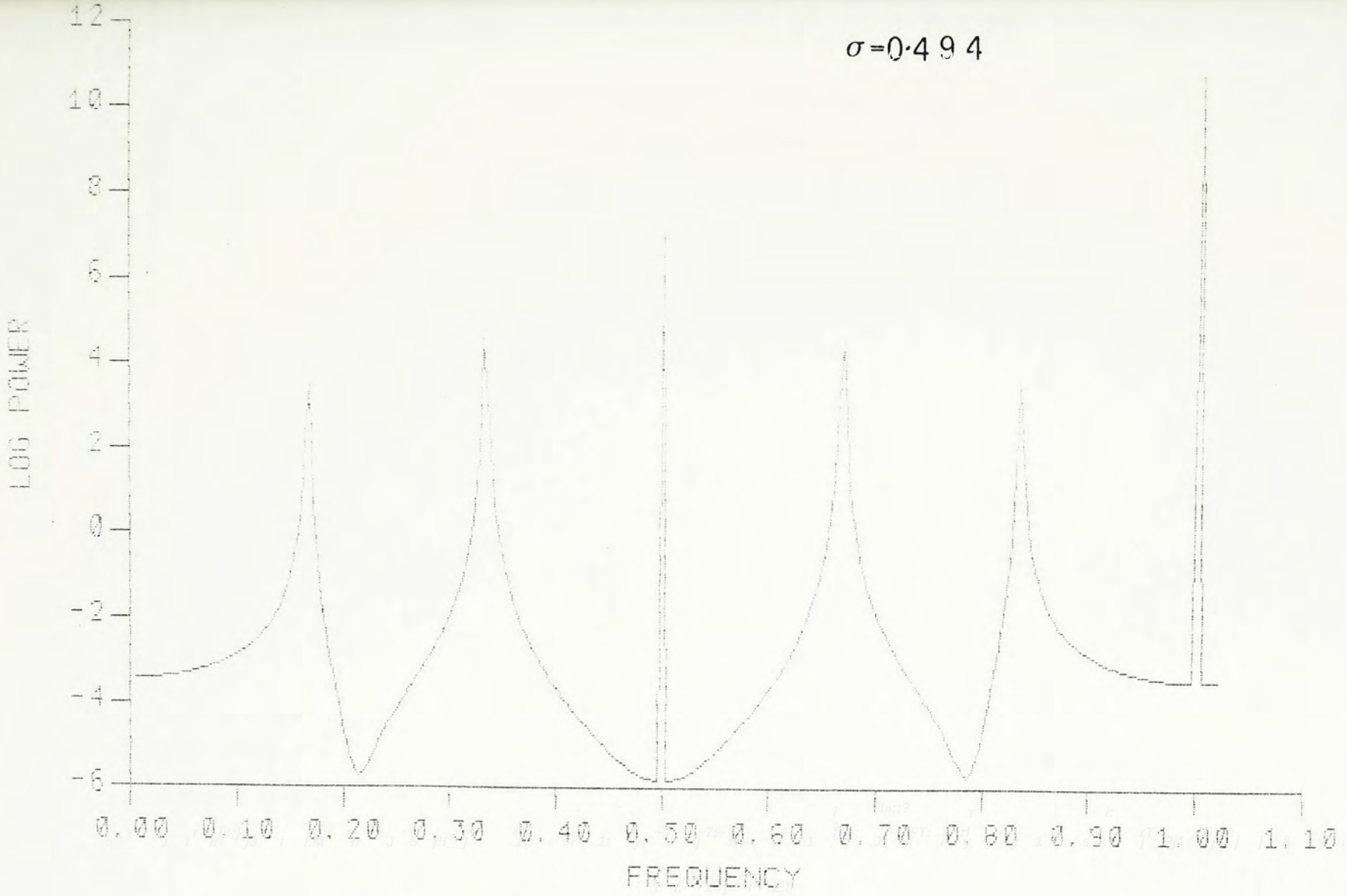
σ=0·494
LOG POWER
12
10
8
6
4
2
0
-2
-4
-6
0.00
0.10
0.20
0.30
0.40
0.50
0.60
0.70
0.80
0.90
1.00
1.10
FREQUENCY

Fig. 6.6i

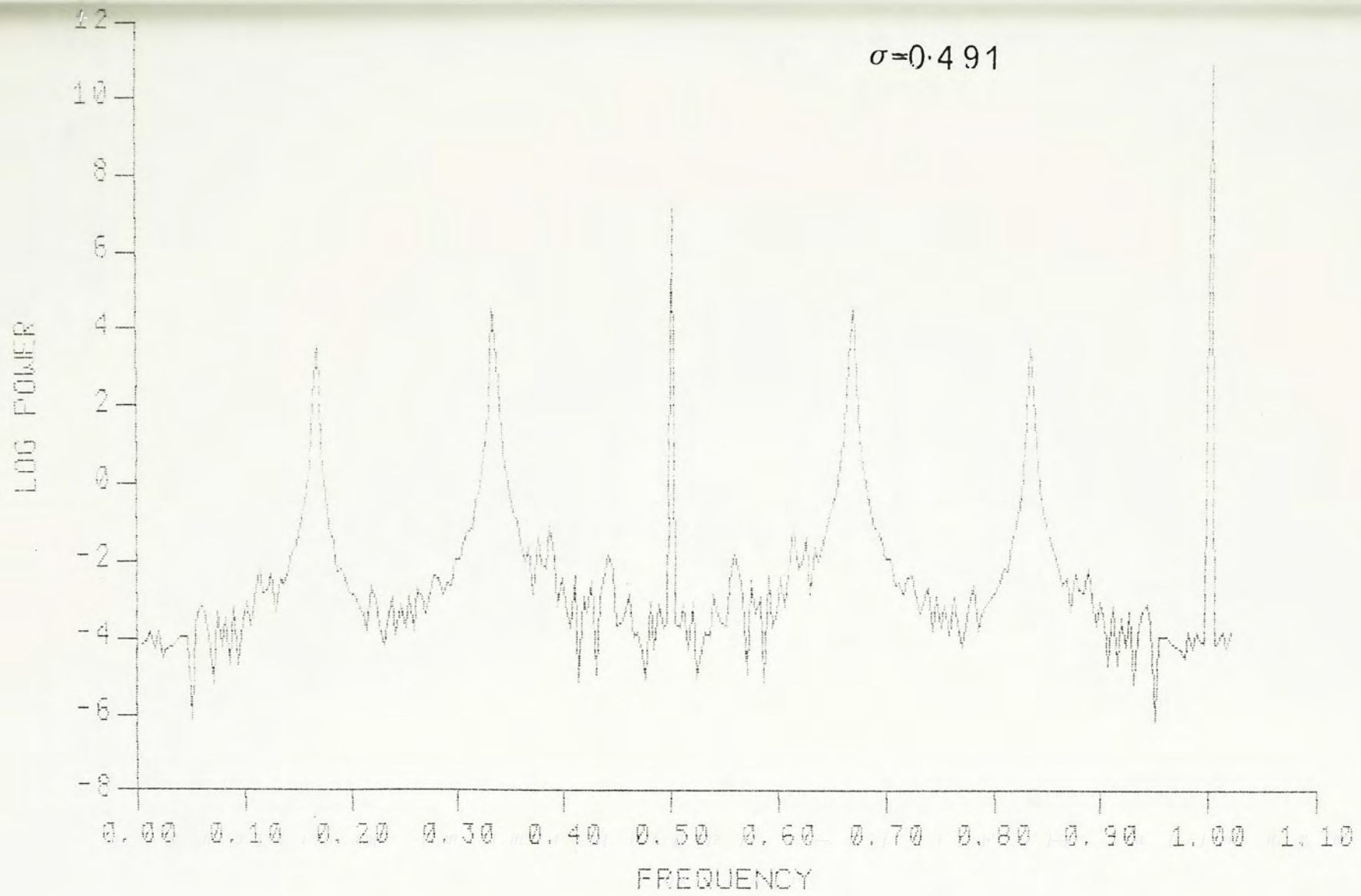
σ=0·491
LOG POWER
12
10
8
6
4
2
0
-2
-4
-6
-8
0.00
0.10
0.20
0.30
0.40
0.50
0.60
0.70
0.80
0.90
1.00
1.10
FREQUENCY

Fig. 6.6j

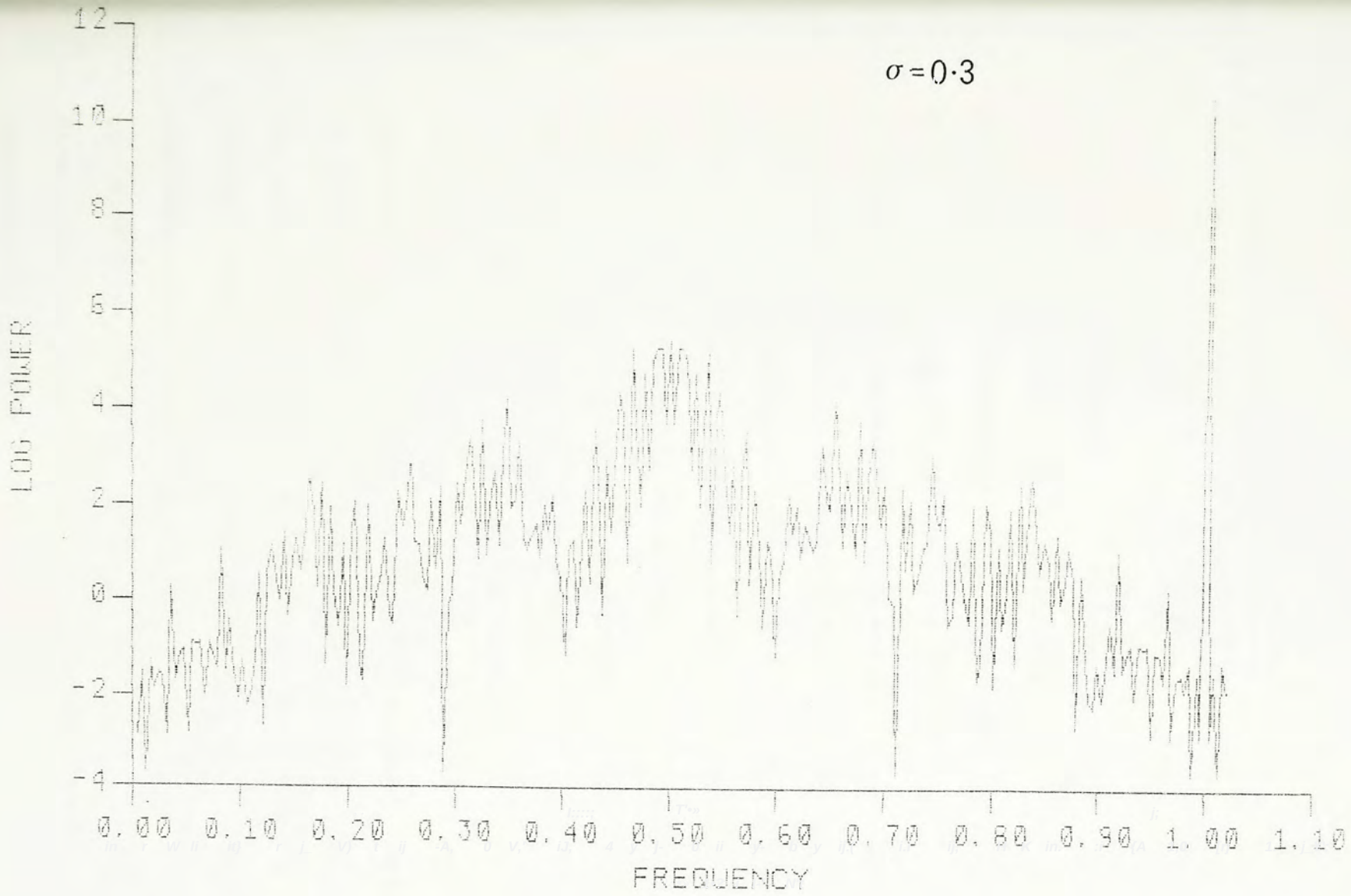
σ = 0·3
LOG POWER
12
10
8
6
4
2
0
-2
-4
0.00
0.10
0.20
0.30
0.40
0.50
0.60
0.70
0.80
0.90
1.00
1.10
FREQUENCY

Fig. 6.6k

6P (σ=0.494), Fig. 6.6i ; 6I (σ=0.491), Fig. 6.6j;

chaos (σ = 0.3), Fig. 6.6k

6.2.3 Large σ region

We now shift our attention to large region ($\sigma \gtrsim 0.7$, different for different λ), where the completely entrained motion will lose stability as σ is further increased. For λ=0.5, the entrained motion loses stability through a series of period doubling, beginning at $\sigma \doteq 2.25$ (Fig. 6.1a). For λ = 0.77, the fully entrained attractor 1P changes rapidly at σ = 0.9 and undergoes the transition 1P $\longrightarrow$ 2P $\longrightarrow$ 4P $\longrightarrow$ 8P $\longrightarrow$ 4P $\longrightarrow$ 2P $\longrightarrow$ period doubling to chaos (Fig. 6.1b). As λ is increased to 0.9, the previous rapidly changing entrained attractor is now separated (Fig. 6.1c).

The fine structure of this region ($\sigma \doteq$ 0.795 to 0.846) is shown in Fig 6.7. Actually there are two tangent bifurcations at σ = 0.795 and at σ = 0.846 between which is an unstable 1P (in y_n) colliding with the stable 1P at the two ends where tangent bifurcations take place. Inside this region, there are 2 sets of stable 1P together with one unstable 1P. Different initial conditions will be attracted to different stable 1P , hence the choice of initial condition is important in this region. We call this sudden discontinuty (the unstable 1P is invisible in the bifurcation diagram) a hysteresis loop. The loop will become

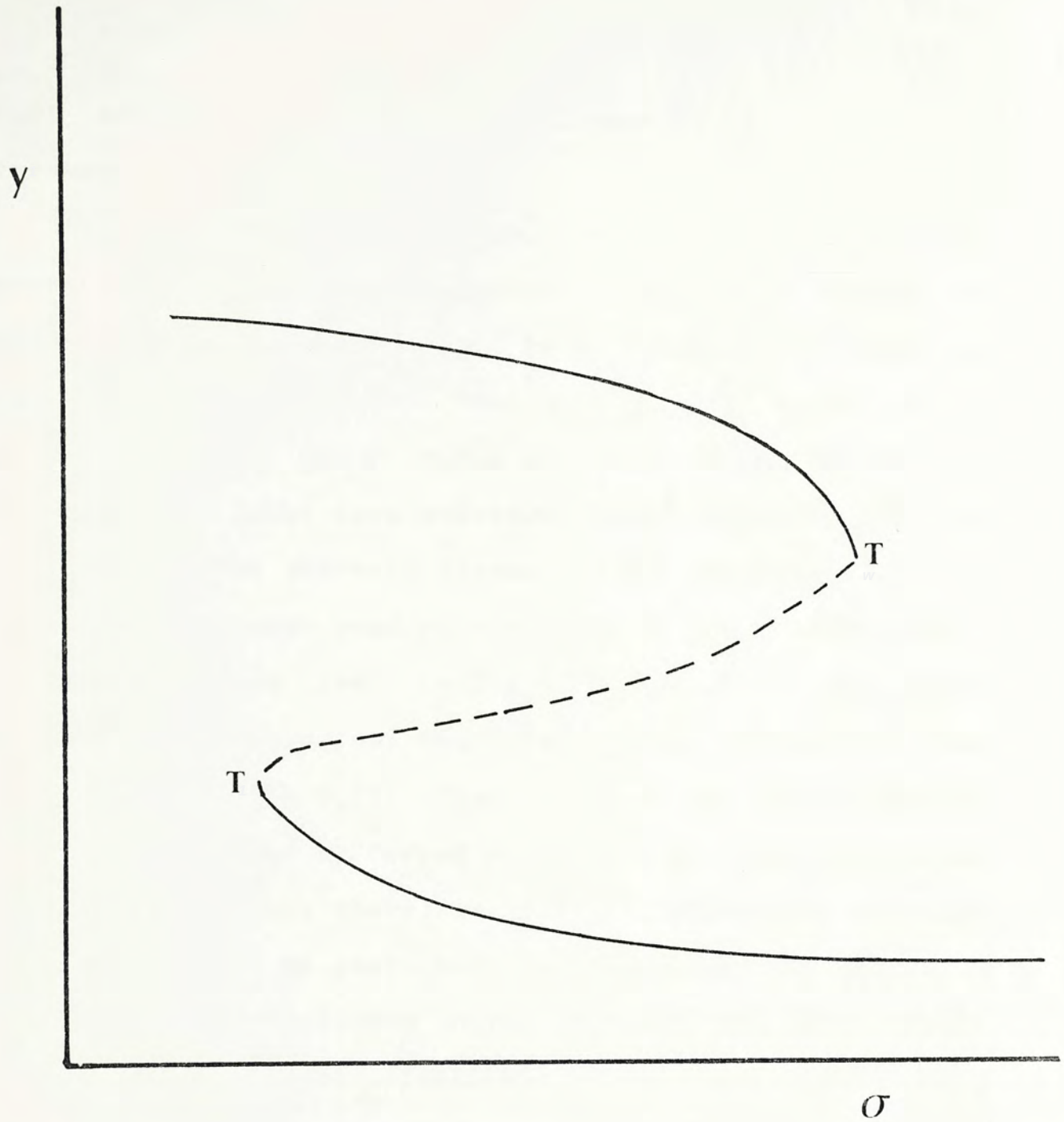

Fig. 6.7 Fine structure of the hysteresis loop. Tangent bifurcations are represented by T and unstable orbits are denoted by - - - - -.

larger and larger in size (larger range of σ) as λ is increased.

As λ is increased to 1.0, the lower part of the hysteresis loop will lose stability through a series of period doubling to chaos, as σ is increased . The loop is larger in size (Fig. 6.1d). For λ = 1.1, the lower part of the loop extends to $\sigma \doteq 0.6$ at which there is 2P co-existing. The lower part undergoes period doubling and the chaotic attractor suddenly disappears due to crisis at $\sigma \doteq 0.7$. There is a large band of chaos for $\sigma \gtrsim 0.8$ (Fig. 6.1e).

To summarize the results for large σ , the fully entrained motion develops into chaos again, either (1) via period doubling (λ= 0.77, Fig. 6.1b) or (2) via a tangent bifurcation followed by period doubling (λ = 1.0, Fig. 6.1d; λ = 1.1, Fig. 6.1e). There is further structure for even larger σ , which we shall not discuss in detail. The two cases are best understood in the λ - σ plane (Fig. 6.8), where the shaded region corresponds to full entrainment. The region of full entrainment is bounded by tangent bifurcations along T_1T_2 and by period doubling bifurcations along D_1 and along D_2. For λ = 0.77 (Fig. 6.1b), the behavior with increasing σ corresponds to first crossing D_2 into full entrainment and then period doubling upon crossing D_1, without touching the line T_1T_2. However for larger λ , say λ=1.0 (Fig. 6.1 d), there is a 1P attractor between D_1 and T_1 (branch 1) and another between T_2 and D_2 (branch 2), as shown in Fig. 6.9a. As λ is increased, the motion is first entrained into branch 1 upon crossing D_1. Between T_1 and T_2

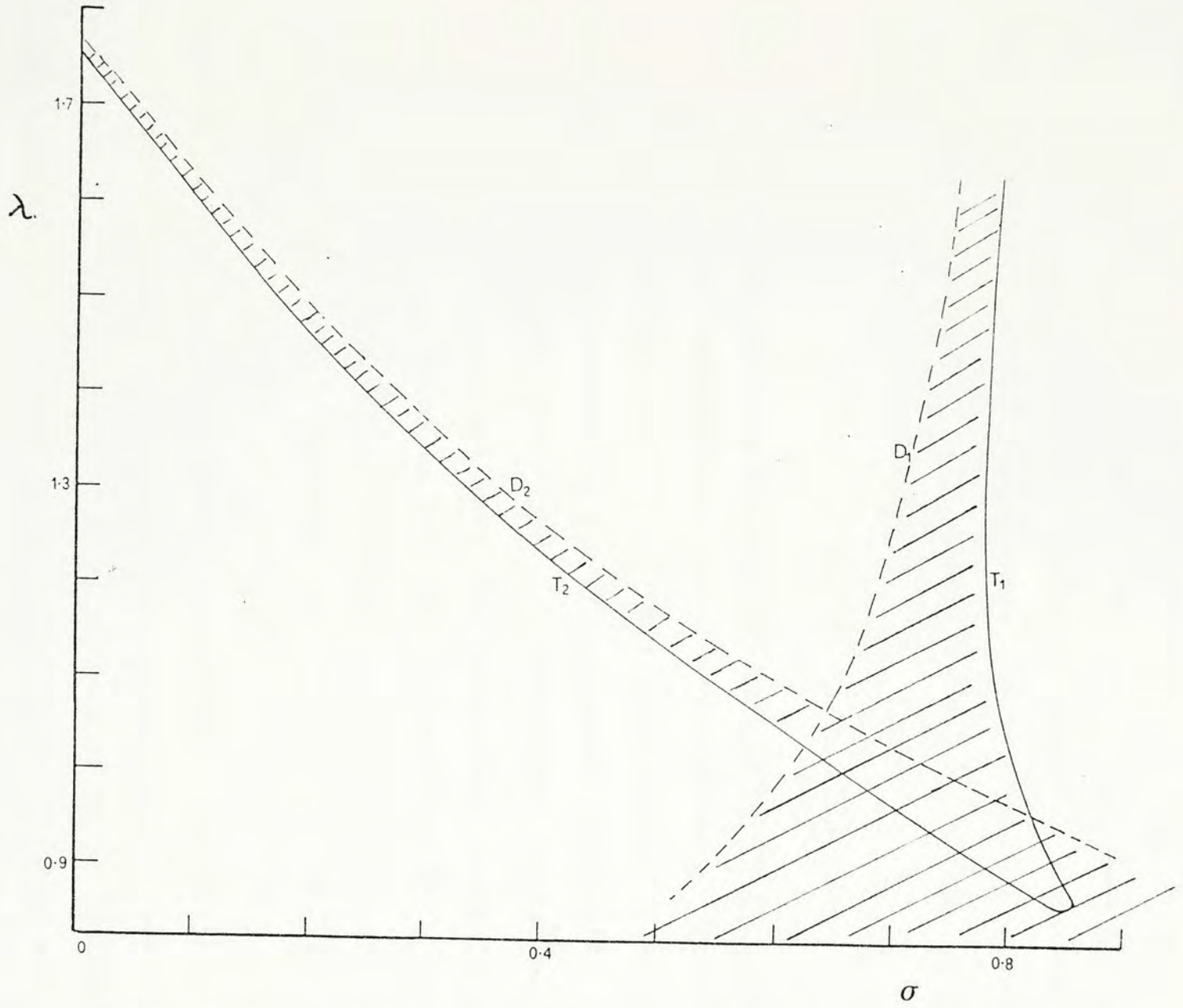

Fig. 6.8 Global connection between full entrainment a pre-existing natural period, showed on $\lambda - \sigma$ plane. The shaded region corresponds to full entrainment (1P).

the 2 attractors co-exist, and depending on the initial condition the motion may become attracted into branch 1. Further increase in λ leads to period doubling when D_2 is crossed. It is clear that the chaotic attractor born out of period doubling from D_2 may undergo a crisis upon collision with the unstable solution linking T_1 and T_2, shown by the broken lines in Fig. 6.9b.

6.2.4 Connection between full entrainment and natural period

The above description delineates the limits of the region of full entrainment. The most interesting result is that the full entrainment by a strong external force with T = 3 (e.g. λ = 0.77, σ = 0.8) is topologically connected to the T_o = 3 motion in the unforced limit cycle (e.g. λ = 1.76, σ = 0), as shown in Fig. 6.8. (Note that the regions shown in Fig. 6.2 and Fig. 6.8 overlap. Because the map $y_n \rightarrow y_{n+1}$ is not unimodal, there may be several attractors at the same value of (λ, σ). For clarity we show the attractor associated with full entrainment separately in Fig. 6.8)

In a sense the external force merely brings out the pre-existing T_o = 3 unforced limit cycle which is resonant with the force. The connection is provided by a band of 1P motion (bounded by T_1 and D_1) cutting across the $\lambda - \sigma$ plane, and for many values of (λ, σ) co-existing with the chaotic attractors. The particular attractor which is reached in each case depends of course on the initial condition.

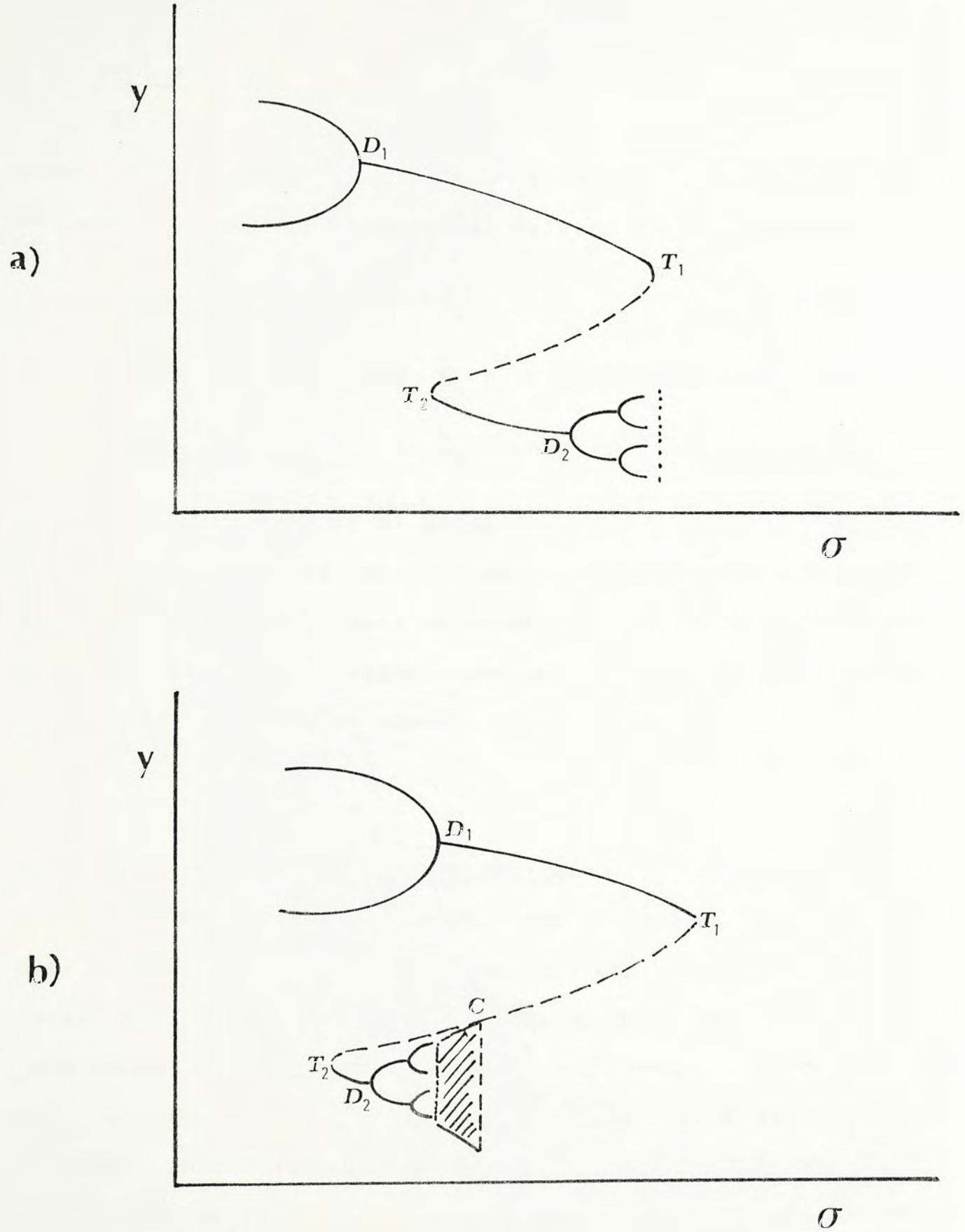

Fig. 6.9 Schematic diagram showing the development to chaos at large σ . There is a crisis in b).

6.3 Period 5 driving force

As comparision, the case for T = 5 is also studied to check whether the results for T = 3 are general. The following three sets of external driving force are used:

(1) $s_1 = 0,\ s_2 = 0.3,\ s_3 = -0.6,\ s_4 = 0.1,\ s_5 = 0.2$

(2) $s_1 = 0,\ s_2 = 0.4,\ s_3 = -0.2,\ s_4 = -0.3,\ s_5 = 0.1$

(3) $s_1 = 0,\ s_2 = 0.6,\ s_3 = -0.2,\ s_4 = -0.1,\ s_5 = -0.3$

For (1) the arrangement of sequence is RLR^2 (zero is taken to be the central point). For (2) and (3) the sequences are RL^2R and RL^3 respectively. Here we study the set $y_n = x_{5n}$ and use the notation nP and nI to represent period n in the direct and inverse sequence of chaotic band in y_n.

6.3.1 Period doubling cascade-anticascade

Similar to the T=3 case, the transition from partial entrainment (2P) for small σ to full entrainment (1P) for large σ is observed. The numbers of bifurcations in the cascade-anticascade $2P \longrightarrow 4P \longrightarrow \ldots\ldots 2^nP \longrightarrow \ldots\ldots 4P \longrightarrow 2P \longrightarrow 1P$ increases as λ is increased. In the y-σ bifurcation diagram, this is manifested as small 'bubbles' embedded inside bubbles (Fig. 6.10a). Here the y-σ bifurcation for T=3 and T=5 are put together for comparision.

For larger λ , the attractors bifurcate to chaos (Fig. 6.10b). For still larger λ , e.g. $\lambda = 1.06$ for T=3 and $\lambda = 1.0638$ for T=5, there are periodic windows of 6P for T=3

and T=5 respectively embedded in the chaotic band for a large range of σ (Fig. 6.10c). The physical situation corresponding to this is that the oscillator suddenly locks to another rational multiple (6 in this case) of T from complete randomness. As σ is increased the entrainment will lose stability and the oscillator will go back to a state of chaos. The two sides of this 6P are bounded by tangent bifurcations. As λ is slightly increased, smaller bubble will again occur inside this 6P, i.e. the transition $6P \longrightarrow 12P \longrightarrow 6P$ is observed. The number of bifurcations in the cascade-anticascade increases for larger λ and the situatuion is similar to the previous one.

We observe there are large 5P , 3P , another 5P and 4P windows for both T=3 and T=5 at larger values of λ (5p , Fig. 6.10d; 3p, Fig. 6.10e). The transitions $5p \longrightarrow 10P \ldots\ldots \longrightarrow 5.2^{n}P \longrightarrow \ldots\ldots 10P \longrightarrow 5P$ and $3P \longrightarrow 6P \longrightarrow \ldots\ldots \longrightarrow 3.2^{n}P \ldots\ldots 6P \longrightarrow 3P$ etc. are also observed. We note that the order of these large periodic windows occurs in the same order: 6P, 5P, 3P, 5P, 4P for both T=3 and T=5 as λ is increased. Combining with the 2P and 4P at smaller λ , the order is the same as the order of the MSS sequence (Fig. 6.2). Although we obtain the above results for T=5 by using the sequence RLR^{2}, it is believed they are universal for other arrangement of sequence s_n. Here the map $y_n \longrightarrow y_{n+1}$ is not unimodal (Fig. 6.11), therefore the occurrence of MSS sequence is quite strange.

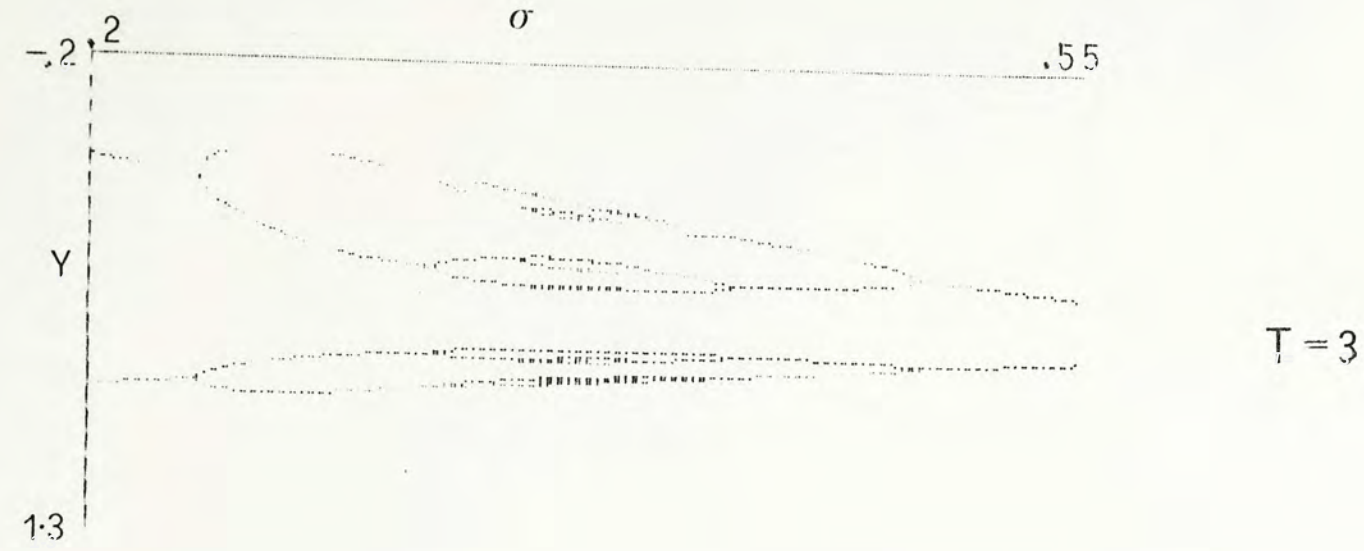

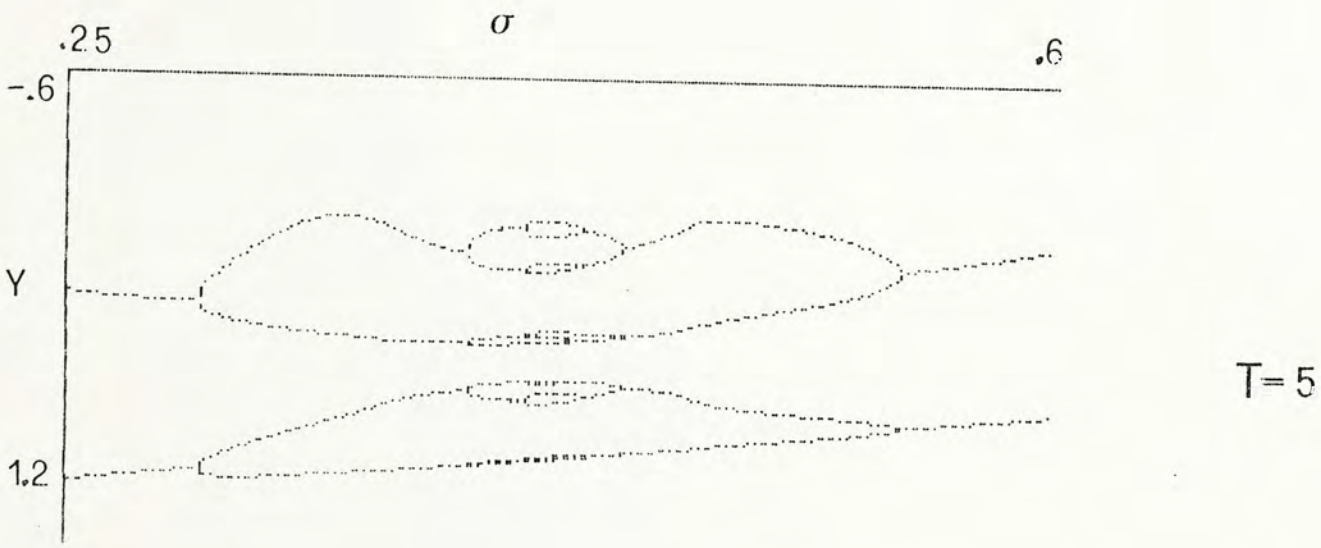

Fig. 6.10a

Fig. 6.10 y - σ bifurcation diagrams for T=3 and T=5.
a) λ =1.0412 for T=3, λ =1.0586 for T=5
b) λ =1.0418 for T=3, λ =1.06 for T=5
c) λ =1.06 for T=3, λ =1.0638 for T=5
d) λ =1.092 for T=3, λ =1.0715 for T=5
e) λ =1.133 for T=3, λ =1.1 for T=5

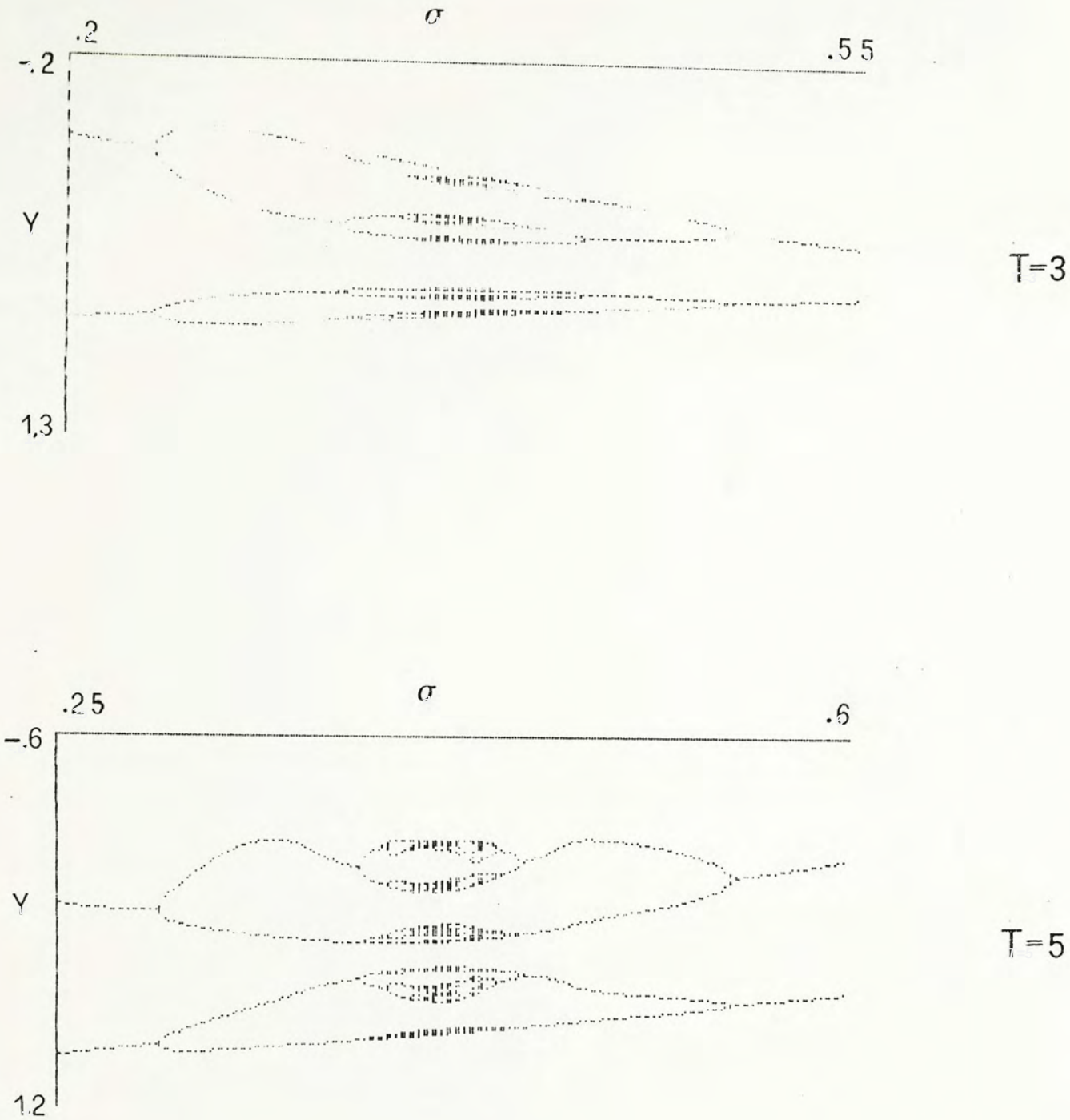

Fig. 6.10b

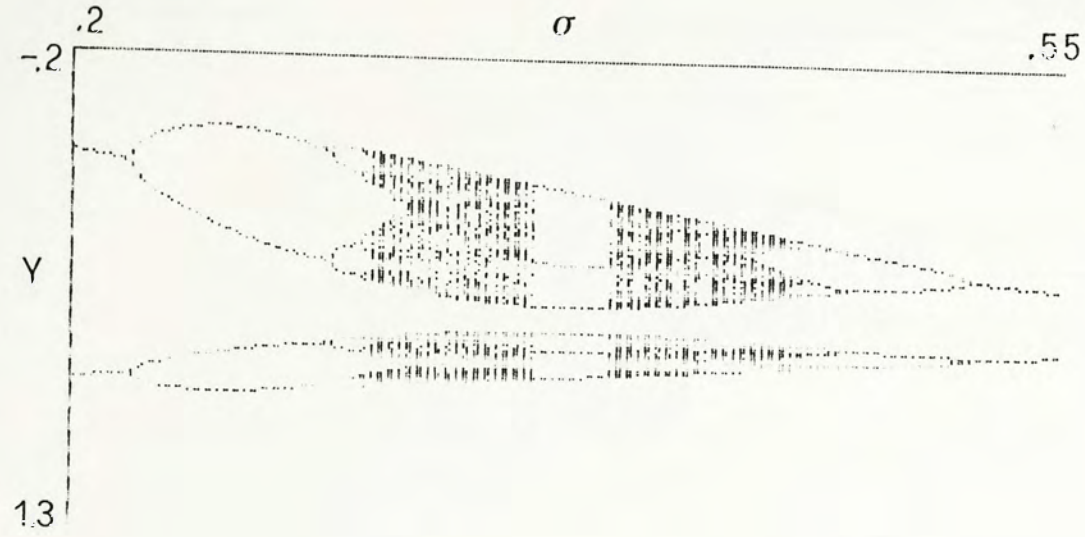

T=3

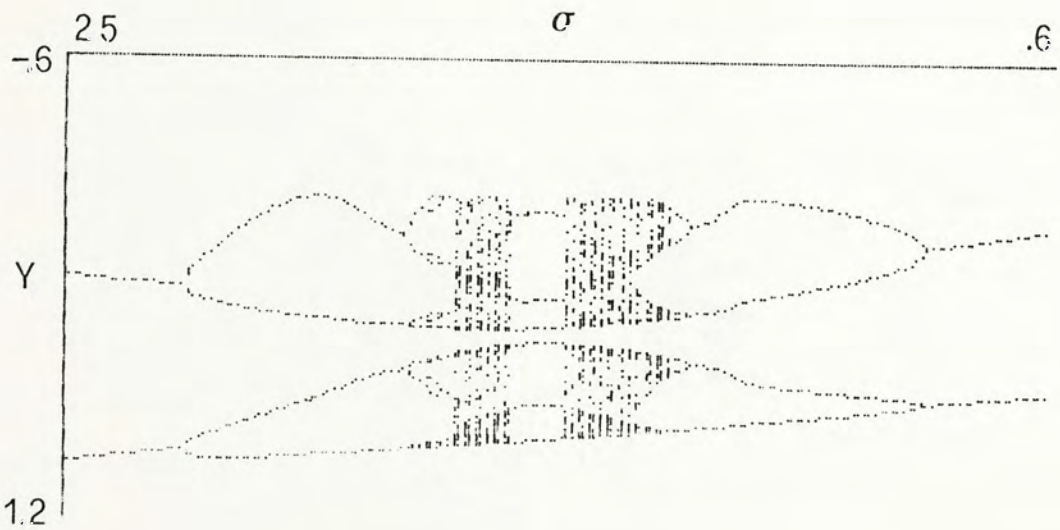

T=5

Fig. 6.10c

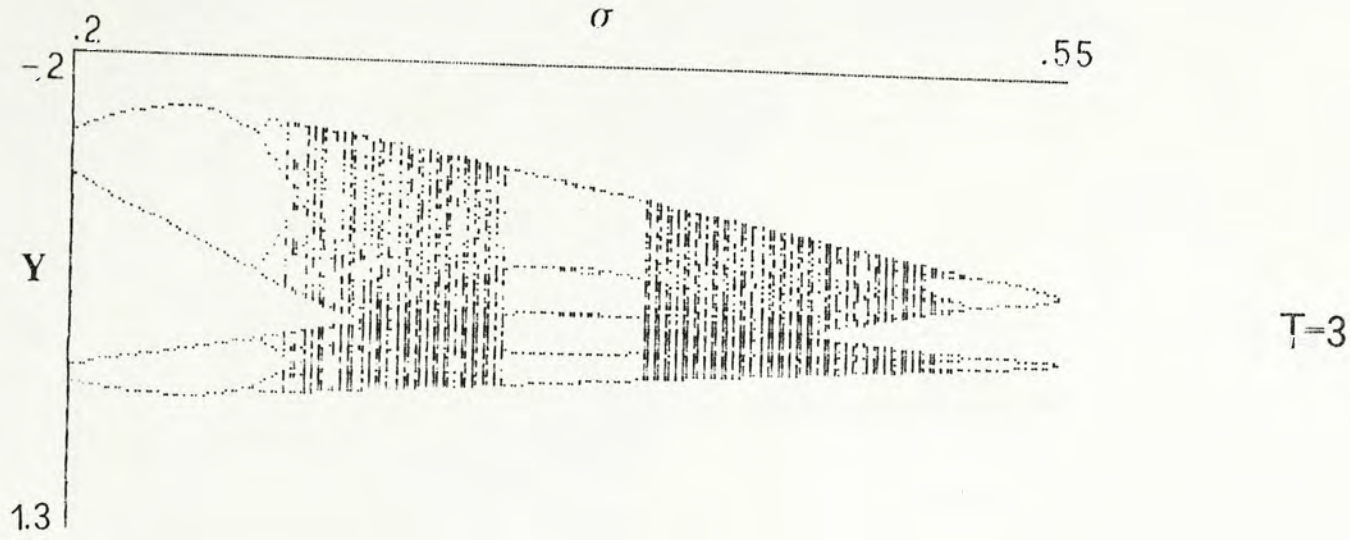

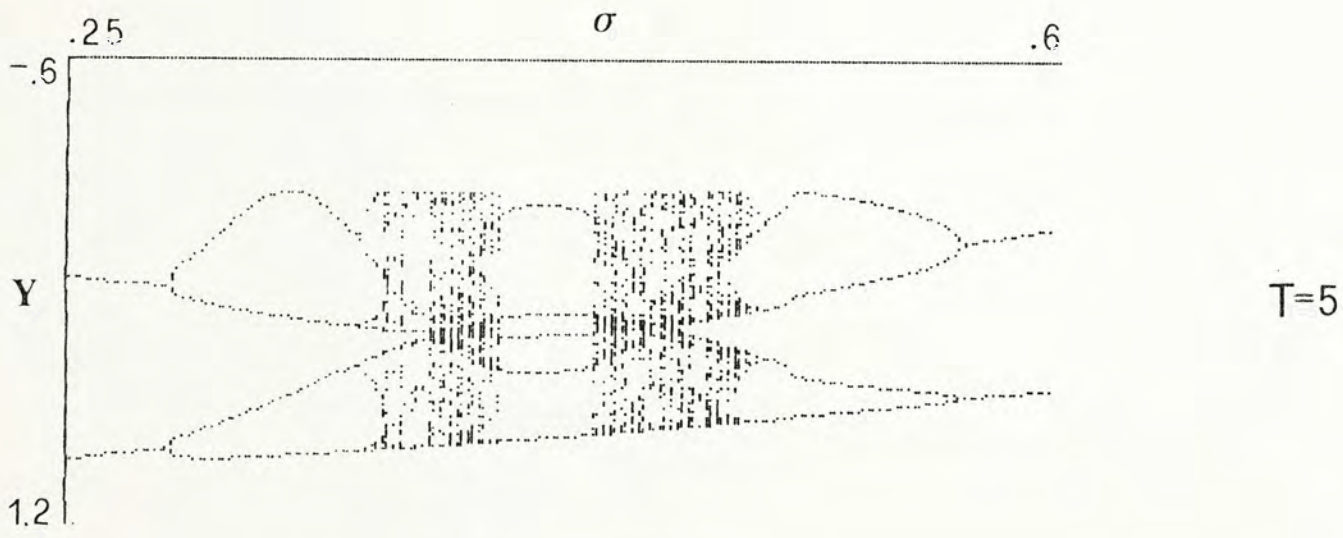

Fig. 6.10d

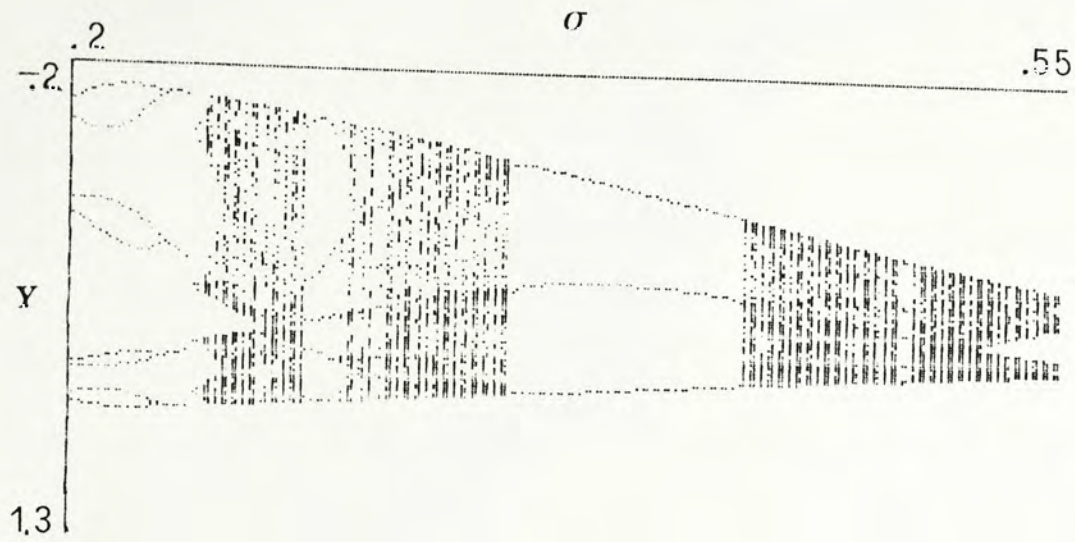

T=3

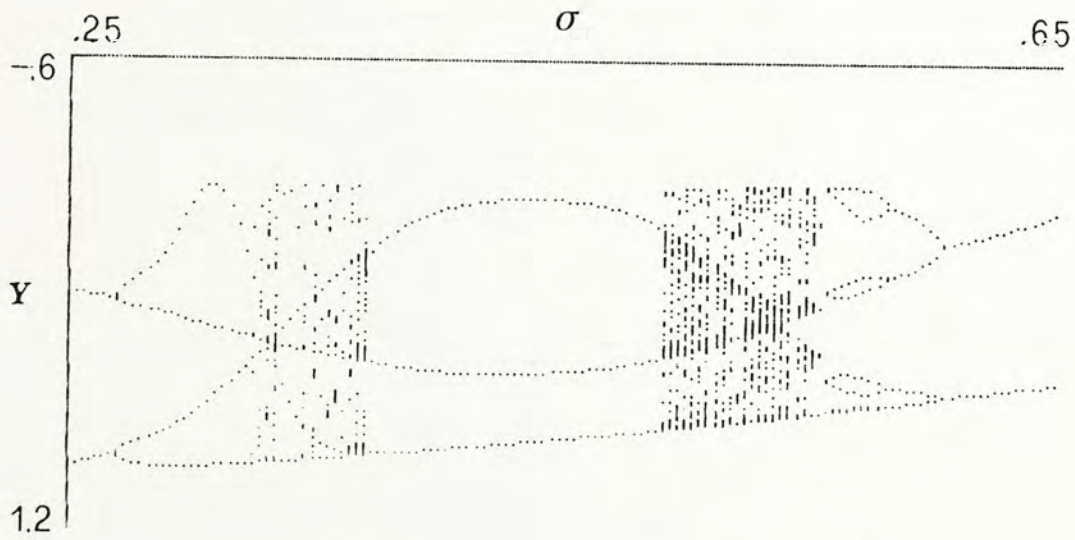

T=5

Fig. 6.10e

a)

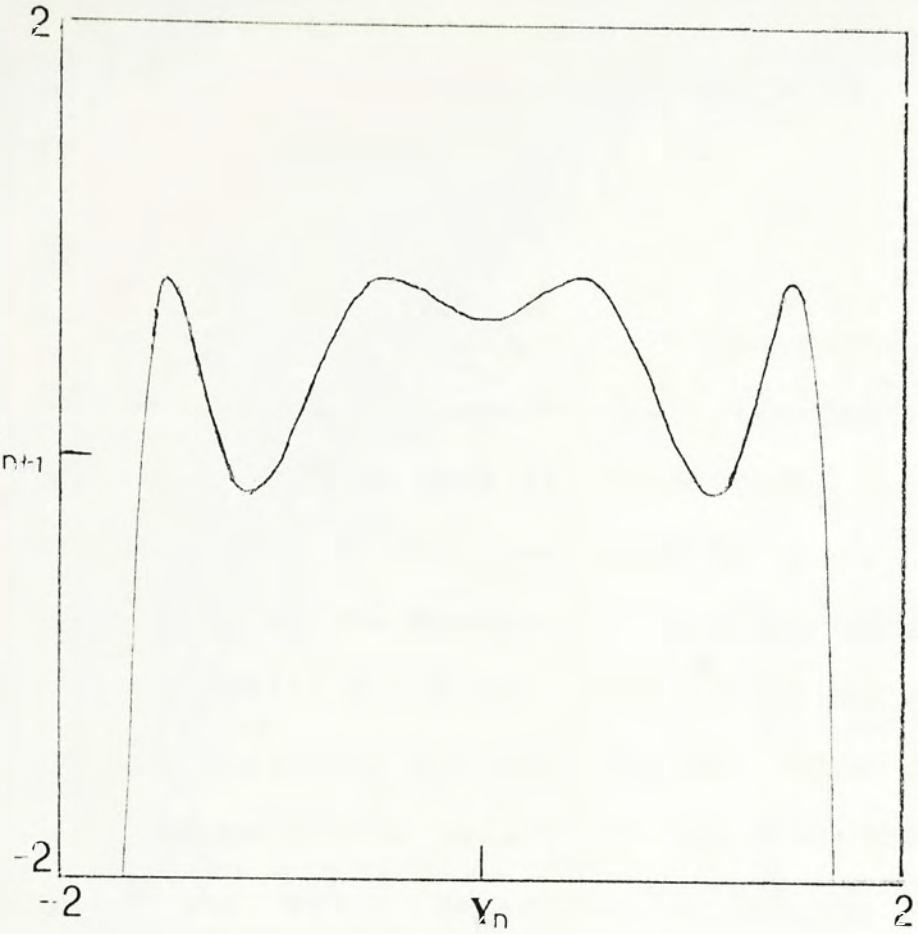

b)

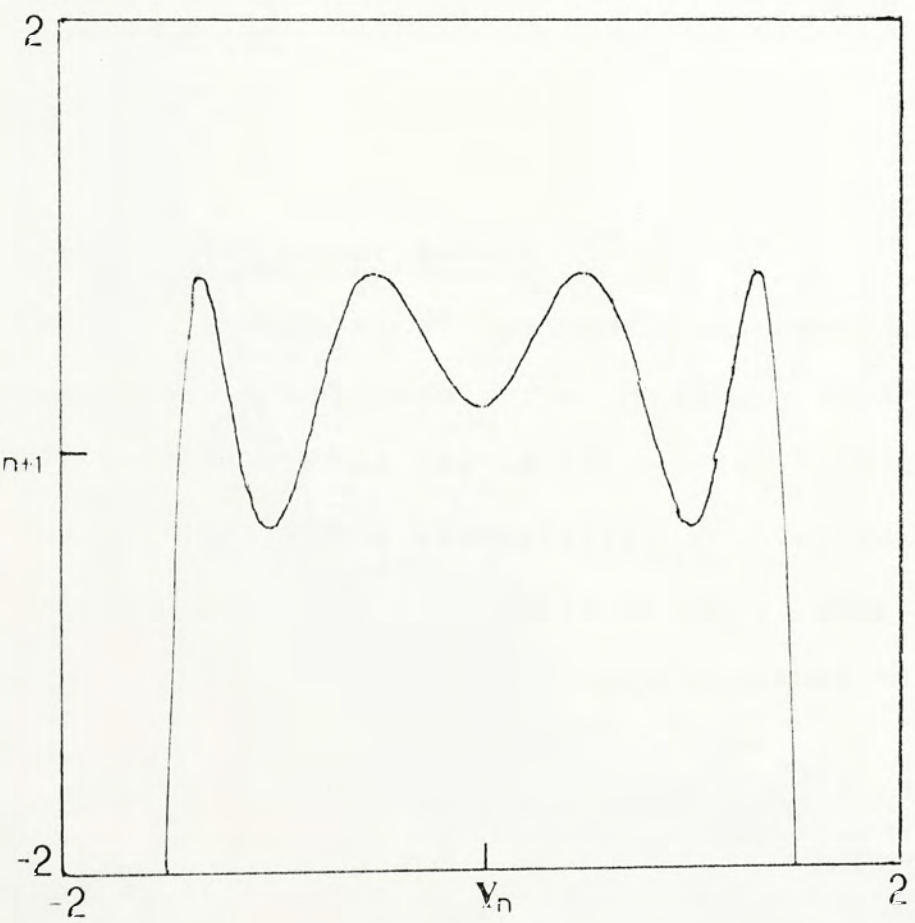

Fig. 6.11 The map $Y_n \longrightarrow Y_{n+1}$ for T=3
a) λ =1.0, σ =0.4
b) λ =1.2, σ =0.4

6.3.2 Global connection for T=5

Same as T=3, a global connection between full entrainment and the natural period 5 for the map $1-\lambda x^2$ is observed for all the three sets of arrangements of s_n. The results for the set RLR^2 are summarized in Fig. 6.12 in which the boundaries of the hysteresis loop (at which tangent bifurcations take place) are drawn. Results for other sets of sequences are topologically similar. In all three cases, the connection is related to one natural period 5 windows.

Therefore the major characteristic are the same for T=3 and T=5. It is believed that they are general results for other value of T.

6.4 Comparision with other models

There are two physical systems that exhibit similar features as those in our case. The first one is the forced Brusselator and the second one is the liquid hybrid optical bistable device. The forced Brusselator is governed by (6.1), a system of ODE, while the bistable device, under certain conditions, can be described by a simple iterated map:

$$x_{n+1} = A \sin^2(x_n - x_B) \qquad (6.4)$$

where A and x_B are two parameters.

6.4.1 The forced Brusselator

The forced Brusselator is a system with complicated

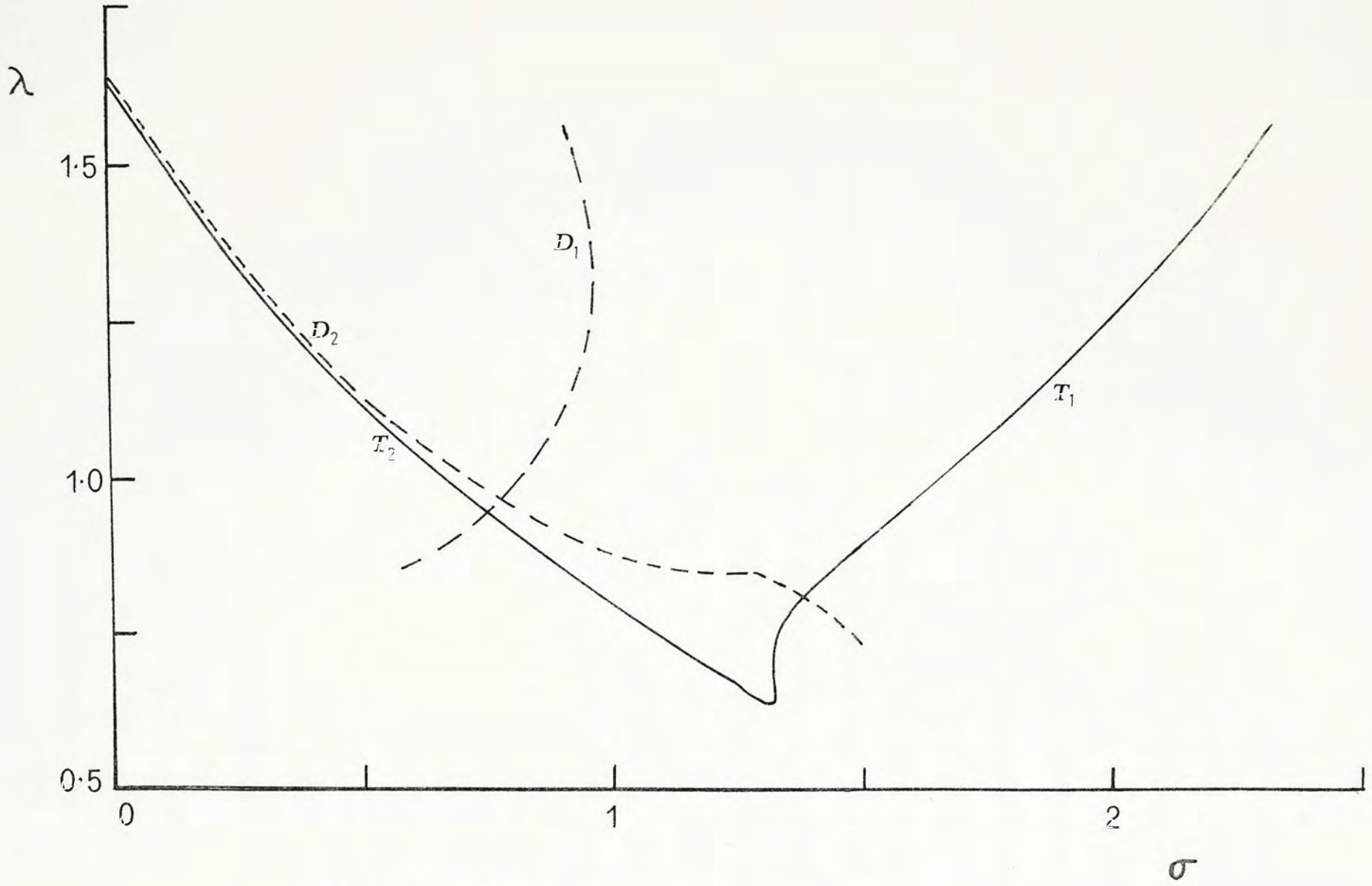

Fig. 6.12 Connection between full entrainment and natural period for T=5 for the set RLRR

bifurcation and chaotic behavior. There are 4 parameters A,B, α and ω and the system is a set of coupled ODE. All well-known routes to chaos are observed in this model. In particular, Hao and Zhang (1982) studied this model and found the hierarchy of period doubling bifurcation sequence. For A=0.4, B=1.2 and ω =0.8 the schematic hierarchy is shown on Fig. 6.13 . For the coupling term α very small, there is the beating region in which there are two independent frequencies, one for the oscillator and one for the the external driving force. At α = 0.008, the oscillator entrains onto the 1/2 harmonics of the external driving frequency. After this is the period doubling cascade-anticascade region, with the chaotic region embedded inside. Finally when α is large enough, the external force dominates the oscillator, so that the system will oscillate with the external frequency. Hao regarded chaos as a new regime of nonlinear oscillation.

This hierarchy of

partial entrainment ⟶ period doubling cascade ⟶ aperiodic motion ⟶ anticascade ⟶ full entrainment

as external force is increased is very similar to our results for the map $x_{n+1}=1-\lambda x_n+\sigma s_n$ except there is no beating region in our model. The mirror image symmetry between (partial entrainment ⟶ chaos) and (chaos ⟶ full entrainment) is observed in both systems and seems peculiar to oscillations with external forcing. Besides, for

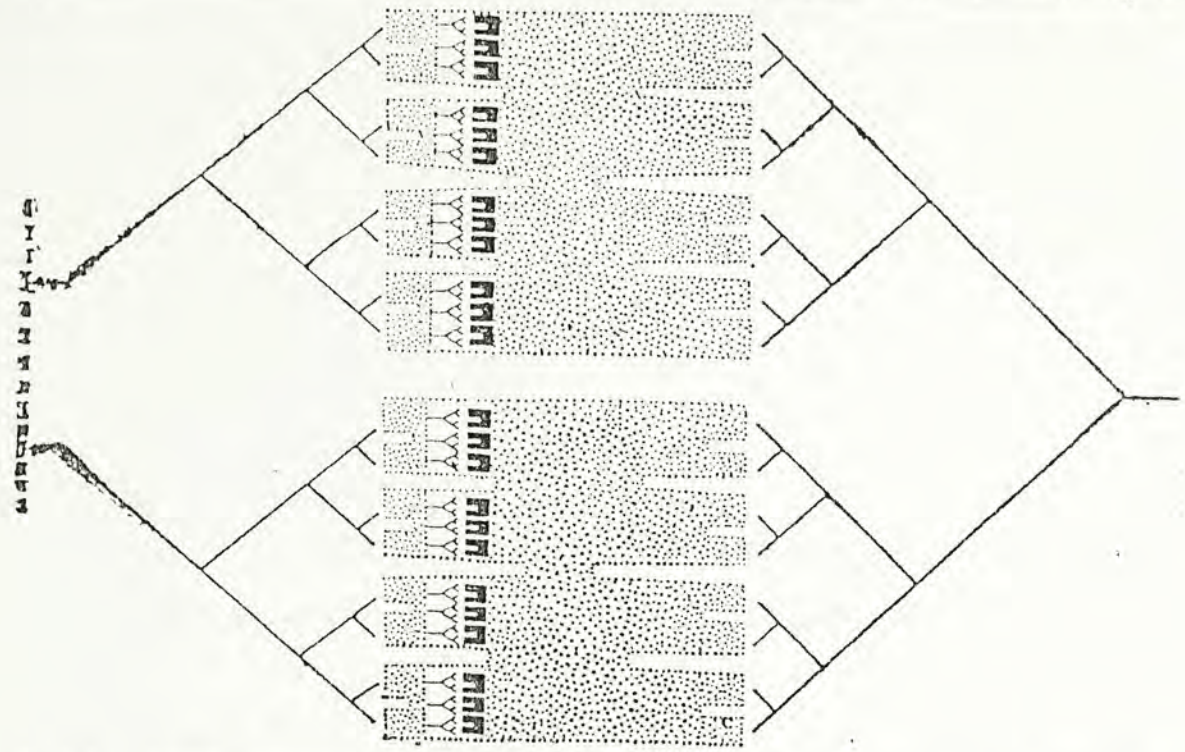

Fig. 6.13 Schematic hierarchy of cascade-anticascade in the forced Brusselator. A=0.4, B=1.2, ω=0.8. (after Hao (1982), p.778)

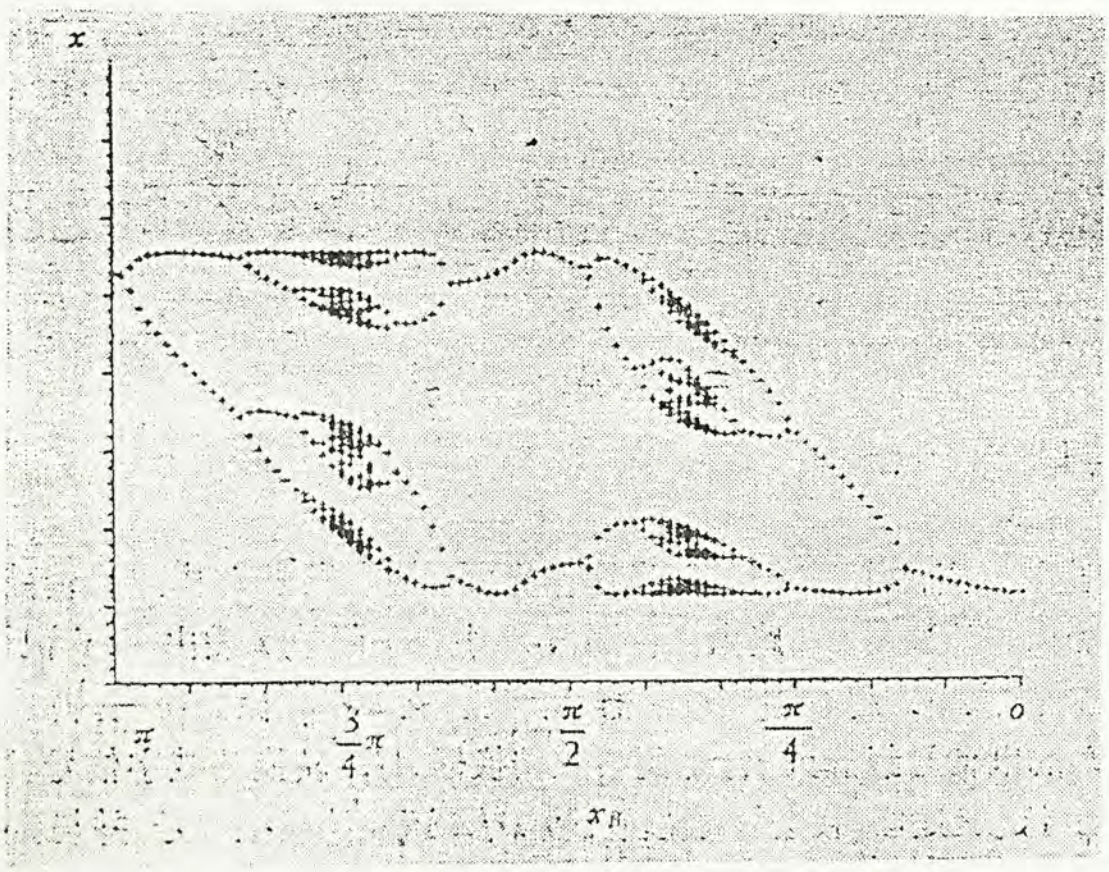

Fig. 6.14 x-x_B bifurcation diagram of (6.4) at A=1.9291. (after Zhang et al. (1984), p.1025)

Brusselator with α = 0.05, B= 1.2 and along the line A = 0.46-0.2ω , MSS-sequence was observed (Hao,1983). In our model, the periods (in y_n) 2, 4, 6, 5, 3, 5, 4 are observed which agree with the MSS-sequence.

6.4.2 The bistable device

Under certain conditions, the bistable device can be described by the one-dimensional map (not unimodal)

$$x_{n+1} = A \sin^2(x_n - x_B)$$

It was studied by Zhang et al. (1983). It was found that for A = 1.9291, the $x-x_B$ bifurcation diagram (Fig. 6.14) has the feature

$$2P \longrightarrow \text{cascade-anticascade} \longrightarrow 2P \longrightarrow \text{cascade-anticascade} \longrightarrow 2p \longrightarrow 1P$$

This feature is quite similar to our cascade-anticascade bifurcations. From the point of view of one-dimensional map, the feature may be common to maps with multiple basins (more than one critical points).

6.5 MSS sequence and Farey sequence

The global connection in parameter space becomes more interesting if we embed (6.3) in a wider class of problems:

$$x_{n+1} = f(\lambda, x_n) + \sigma s(\nu n) \qquad (6.5)$$

where $f(\lambda,x)$ is a unimodal map (e.g. $1-\lambda x^2$) and $s(t)$ is a function of period 1 representing a force of period $1/\nu$.

For γ rational (e.g. $\gamma = 1/3$), we recover the case of commensurate periods discussed so far. However, extend the consideration to irrational γ as well and study the entire three dimensional parameter space (λ , σ , γ). In particular take a small value of σ and consider the (λ , γ) plane (Fig. 6.15). On the λ axis (i.e. $\gamma = 0$), the map is simply

$$\begin{aligned} x_{n+1} &= f(\lambda, x_n) + \sigma s(0) \\ &= \bar{f}(\lambda, x_n) \end{aligned} \tag{6.6}$$

which is again unimodal (and in fact can be brought back to $f(\lambda, x_n)$ by a linear transformation in x). Various periodic windows appear above λ_∞ within a ' chaotic sea', in an MSS sequence, schematically illustrated in Fig. 6.15 . These include for example, the 'natural' period 3 in x_n at λ = 1.76. On the other hand, for small values of λ there are again periodic windows or 'tongues' within the 'quasi-periodic sea' near rational values of γ , in a Farey sequence, again illustrated schematically in Fig. 6.15. For example we know that there is fully entrained periodic motion with period 3 in x_n at $\gamma = 1/3$. A crucial question is whether and how the MSS sequence within the 'chaotic sea' (natural periods) and the Farey sequence within the 'quasi-periodic sea' (full entrainment at Farey period) are related. The model (6.3) studied in this chapter corresponds to a planar section at $\gamma = 1/3$ through the (λ , σ , γ) space, and shows that the two windows are topologically connected. While this result goes some way towards answering the question, the

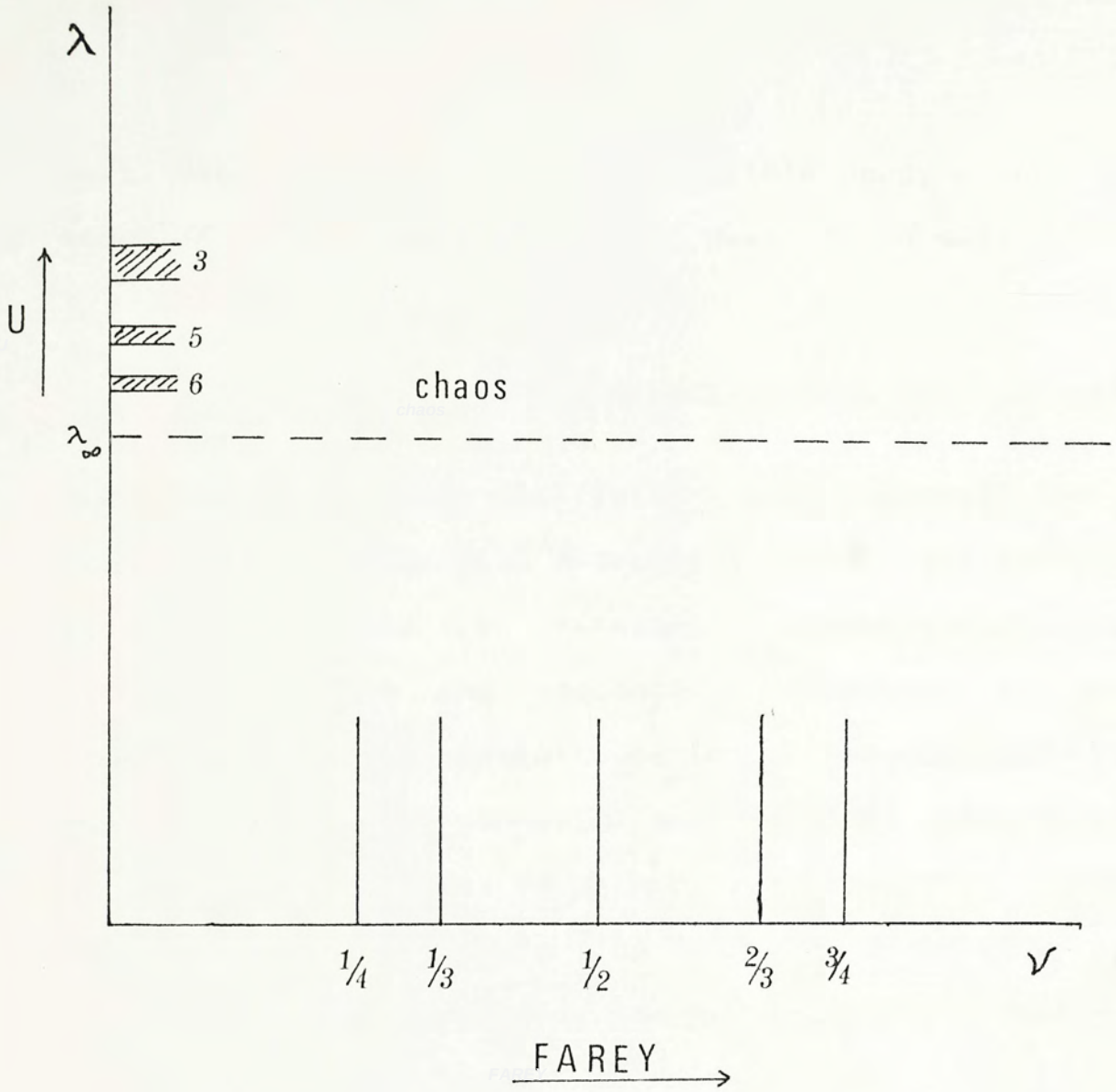

Fig. 6.15 Farey sequence and U-sequence periodic windows at constant σ .

next step is evidently a more complete study of the general model (6.5) with this particular question in mind.

In conclusion, the transition

partial entrainment ⟶ chaos ⟶ full entrainment

seen in limit cycle oscillations with external forcing is found also in maps with external forcing, the latter being more susceptible to numerical investigation. It is conjectured that the topological connection in parameter space between full entrainment and a pre-existing resonant period may be quite general, and that this connection, seen in the wider context of an arbitrary (possibly irrational) forcing period, reveals the connection between the MSS sequence within the chaotic sea and the Farey sequence within the quasi-periodic sea.

References

Collet, P., and J.P. Eckmann, 1980, Iterated Maps on the Interval as Dynamical Systems (Birkhauser, Boston).

Derrida, B., A. Gervois, and Y. Pomeau, 1979, J. Phys. A12, 269.

Eckmann, J.P., 1981, Rev. Mod. Phys. 53, 643.

Farmer, J.D., E. Ott, and J.A. Yorke, 1983, Physica 7D, 153.

Feigenbaum, M.J., 1978, J. Stat. Phys, 19, 25.

Feigenbaum, M.J., L.P., Kadanoff, and S.J. Shenker, 1982, Physica 5D, 370.

Feynman, R.P., R.B. Leighton, and M. Sands, 1964, Lectures on Physics, Vol. 2 (Addison-Wesley).

Grebogi, C., E. Ott, and J.A. Yorke, 1982, Phys. Rev. Lett. 48, 1507.

Grebogi, C., E. Ott, and J.A. Yorke, 1983, Physica 7D, 181.

Guckenheimer, J., G. Oster, and A. Ipaktchi, 1977, J. Math. Biol. 4, 101.

Hansdorf, 1918, Math. Annalen 79, 157.

Hao, B.L., and S.Y. Zhang, 1982, J. Stat. Phys. 28, 769.

Hao, B,L., G.R. Wang, and S.Y. Zhang, 1983, Commun. Theor. Phys. 2, 1075

Hao, B.L., 1984, Chaos (World Scientific).

Hirsh, J.E., B.A. Huberman, and D.J. Scalapino, 1982, Phys. Rev. A25, 519.

Hirsh, J.E., M. Nauenberg, and D.J. Scalapino, Phys. Lett. A87, 391.

Hopf, E., 1948, Commun. on Pure Appl. Math. 1, 303.

Hu, B., 1982, Phys. Rep. 91, 233.

Hu, B., and J.M. Mao, 1982, Phys. Rev. A25, 1196.

Hu, B., and I.I. Satija, 1983, Phys. Lett. A98, 143

Huberman, B.A. and J. Rudnick, 1980, Phys. Rev. Lett. 45, 154.

Landau, L.D., 1944, C.R. Acad, Sci, URSS, 44, 331.

Li, T.Y., and J.A. Yorke, 1975, Am. Math. Monthly 82, 985

Liu, K.L., W.S. Lo, and K. Young, Phys. Lett. A105, 103

Lorenz, E.N., 1963, J. Atoms. Sci. 20, 130.

May, R.M., 1976, Nature 261, 459.

Manneville, P., and Y. Pomeau, 1979, Phys. Lett. A75, 1.

Metropolis, N., M.L. Stein, and P.R. Stein, 1973, J. Comb. Theor. A15,25.

Newhouse, S.E., d. Rulle, and F. Takens, 1978, Commun. Math. Phys. 64, 35

Ott., E., 1981, Rev. Mod. Phys. 53, 655.

Rand, D., S. Ostlund, J. Sethna, and E.D. Siggia, 1982, Phys. Rev. Lett. 49, 132.

Rulle, D., and F. Takens, 1971, Commun. Math. Phys. 20, 167; Added note, Commun. Math. Phys. 23, 343.

Sarkovskii, A.N., 1964, Ukranian Math. J. 16, 61

Sinai, J., 1972, Russ. Math. Surveys 4, 21.

Singer, D., 1978, SIAM J. Appl. Math. 35, 260

Testa, J., and G.A. Held, 1983, Phys. Rev. A28, 3085.

Young, K., and K.L. Liu, 1984, unpublished.

Young, K., 1984, unpublished.

Zhang, H.J. et al., 1984, Acta Physica Sinica 33, 1024